

A THEORETICAL INVESTIGATION OF CONVECTIVE  
PATTERNS IN THE LEE OF THE  
COLORADO ROCKIES

Submitted by  
Richard A. Dirks

In partial fulfillment of the requirements  
for the degree of Doctor of Philosophy  
Colorado State University  
Fort Collins, Colorado

ATMOSPHERIC SCIENCE  
LABORATORY COLLECTION

QC  
880  
.D57  
ATSL

COLORADO STATE UNIVERSITY

March, 1970

WE HEREBY RECOMMEND THAT THE DISSERTATION PREPARED UNDER OUR SUPERVISION BY Richard A. Dirks ENTITLED A Theoretical Investigation of Convective Patterns in the Lee of the Colorado Rockies BE ACCEPTED AS FULFILLING THIS PART OF THE REQUIREMENTS FOR THE DEGREE OF Doctor of Philosophy.

Committee on Graduate Work

William M. Gray  
H. G. Geff  
Adviser

George A. Grant  
Blumhage  
Head of Department

Examination Satisfactory

Committee on Final Examination

George A. Grant  
William M. Gray  
H. G. Geff

Blumhage  
Adviser

Permission to publish this dissertation or any part of it must be obtained from the Dean of the Graduate School

## ABSTRACT

The western Great Plains are observed to be the formation region for many of the summer convective systems in the central United States. Convective activity is greatly reduced in the immediate lee of the Colorado and New Mexico Rockies while it is intensified about a hundred kilometers eastward. An explanation of these observed convective patterns is proposed on the basis of a regional scale Rocky Mountains-Great Plains circulation system.

A two-dimensional numerical model of a large scale mountain-plain circulation is presented which includes the effect of a slightly sloping plain. The equations are integrated over periods of two to eight hours for various initial conditions of thermal stability and ambient wind. An increase in thermal stability is found to suppress the developing circulation while the circulation is enhanced by an ambient shearing wind.

Typical observed stability and ambient wind fields yield an interacting two cell circulation with a strong cell over the mountain slope and a weaker cell over the plain. The resulting airflow is characterized by strong descent ( $m \text{ sec}^{-1}$ ) in the immediate lee of the mountains and weak ascent ( $cm \text{ sec}^{-1}$ ) in a broad region 100 to 300 km leeward. An investigation of contributing factors reveals the effect of the plain slope to be a primary cause of the ascending flow over the plain.

The flow patterns which develop correspond well with observed diurnal oscillations in upper wind profiles over the plains with regard to velocity magnitude, time of reversal, and depth of flow. The dynamic effects of the circulation are found to be of sufficient magnitude to control convective activity. The spatial distribution of the dynamic effects is also in general agreement with observations of related convective activity. Nocturnal cooling reverses the circulation around "sunset"

and results in ascending flow in the near lee of the mountains. This compares favorably with observed convective activity in that region.

An examination of orographic waves and other plausible mechanisms finds that these are not generally applicable over the wide range of observed conditions. This restriction does not apply to the Rocky Mountains-Great Plains circulation system.

Richard A. Dirks  
Department of Atmospheric Science  
Colorado State University  
December 1969

## ACKNOWLEDGEMENTS

The author expresses his sincere appreciation to Professor Elmar R. Reiter for his valuable suggestions and encouragement throughout the various aspects of this work. The author is also indebted to Michael Fosberg for his helpful discussions and to Professors Lewis Grant, William Gray, and Hubert Morel-Seytoux for their services on the candidate's committee.

Special thanks go to Paul Lissauer who assisted in much of the data reduction and programming and to Sandra Olson who typed the many revisions of the manuscript. Tom Kochneff also contributed to the data reduction and programming. Finally the author wishes to thank his wife, Stephanie, for her continuous faith and encouragement throughout the duration of this research.

This research was sponsored by the Environmental Science Services Administration under Grant E-10-68G.

## TABLE OF CONTENTS

<u>Chapter</u>		<u>Page</u>
I.	Introduction. . . . .	1
II.	Variability of Mesoscale Convection on the Great Plains . . . . .	5
III.	Review of Slope Wind Observations and Theory . . . . .	22
IV.	Theoretical Slope Circulation Model . . . . .	33
V.	Model Results . . . . .	51
VI.	A Comparison of Observed and Model Winds. . . . .	78
VII.	An Examination of Atmospheric Waves and Other Mechanisms for Controlling Convection . . . . .	93
VIII.	Summary and Conclusions . . . . .	102
	LITERATURE CITED . . . . .	106
	Appendix: Mesoscale Wave Application. . . . .	121

LIST OF TABLES

<u>Table</u>		<u>Page</u>
5.1	Summary of main conditions and results of various cases. Principal feature is underlined . . . . .	77
A.1	Estimated theoretical and observed mesoscale wavelengths (in kilometers) for select days during summer 1966. . . . .	122

## LIST OF FIGURES

<u>Figure</u>		<u>Page</u>
1. 1	Map of the central Rocky Mountains and central Great Plains. (A) Front Range and (B) Sangre de Cristo Range. . . . .	3
2. 1	Percentage of summer thunderstorm occurrences per quarter-day. . . . .	6
2. 2	Percentage of precipitation occurring at night (12 hours ending at 8 a. m., 75th meridian time, April to September) . . . . .	6
2. 3	(Above) Six groups of stations with north-south orientations used in the timing analysis of convective shower activity. (Right) Timing of major convective activity for ten-year summary of hourly precipitation $\geq .10$ inch for the six groups of stations . . . . .	7
2. 4	Colorado map showing normal May-September precipitation (1931-1960) east of longitude $106^{\circ}$ W. Isolines are in inches. Note regions of reduced rainfall leeward of both the Front Range and Sangre de Cristo Range. . . . .	8
2. 5	Average number of days with hail, annual. . . . .	9
2. 6	Temporal distribution of radar observations of mesoscale convective systems, May-August 1966; (X) = 1300 CST, X = 1500 CST, [X] = 1700 CST . . . . .	13
2. 7	Spatial distribution of mesoscale convective systems as observed by satellite photos May-August 1966 (ESSA I and Nimbus II, incomplete), May-July 1968 (ESSA V). 1966 alone given in parentheses . . . . .	14
2. 8	ATS III, 30 May 1968, 170349 GMT, frame 30G. The Gulf Coast and Baja Peninsula are visible in the lower part of the picture and the Florida Peninsula at the right-center. Colorado is shown in outline. . . . .	15
2. 9	ATS III, 30 May 1968, 191038 GMT, frame 39G. Colorado is shown in outline . . . . .	16

## List of Figures Continued

<u>Figure</u>		<u>Page</u>
2.10	ATS III, 30 May 1968, 211808 GMT, frame 48G. Colorado is shown in outline. . . . .	17
2.11	ATS III, 30 May 1968, 233042 GMT, frame 57G. Colorado is shown in outline. . . . .	18
3.1	Profiles, normal to the slope, of observed upslope (solid) and downslope (dashed) wind speeds . . . . .	25
3.2	Schematic illustration of the daytime circulation in a cross section through the Alps . . . . .	25
4.1	Scheme for computing diffusion at lower boundary grid points. $\phi_0$ represents the actual grid point. $\phi_1$ and $\phi_2$ are located on the surface. . . . .	44
4.2	Computational grid mesh. . . . .	50
4.3	Flow chart of the numerical program. Symbols are defined in Preface . . . . .	50
5.1	Evolution of the stream function (solid lines in $10^{+2} \text{ m}^2$ $\text{sec}^{-1}$ ) and potential temperature deviation (dashed lines, in C deg) fields for Case A. Real time in minutes is given in the upper right-hand corner . . . . .	52
5.2	Trajectory of the stream function center for Case A shown at 15 minute positions . . . . .	53
5.3	Evolution of the stream function (solid lines in $10^2 \text{ m}^2$ $\text{sec}^{-1}$ ) and potential temperature deviation (dashed lines in C deg) fields for Case B. Top of superadiabatic region is shown by heavy dashed line (A) . . . . .	55
5.4	Trajectory of the stream function center for Case B shown at 15 minute positions . . . . .	56
5.5	The computed wind field after 60 minutes of real time for Case B . . . . .	58

List of Figures Continued

<u>Figure</u>		<u>Page</u>
5. 6	Characteristic vertical motion components ( $m \text{ sec}^{-1}$ , scaled by order of magnitude) in the lower troposphere for Case B. Vectors in parentheses indicate ascent at lowest levels with subsidence above. . . . .	59
5. 7	Evolution of the vorticity field (in $10^2 \text{ sec}^{-1}$ ) for Case B. . . . .	60
5. 8	Time variation of kinetic energy as generated by the circulation for Case B. . . . .	61
5. 9	Trajectory of the stream function center for Case C shown at 15 minute positions . . . . .	62
5. 10	Evolution of the deviation stream function (solid lines in $10^2 \text{ m}^2 \text{ sec}^{-1}$ ) and potential temperature deviation (dashed lines in C deg) fields for Case D. Top of superadiabatic region is shown by heavy dashed line (A). . . . .	63
5. 11	Trajectory of the solenoidal cell center for Case D shown at 15 minute intervals . . . . .	65
5. 12	Characteristic vertical motion components ( $m \text{ sec}^{-1}$ ) scaled by order of magnitude) in the lower troposphere for Case D. Vectors in parentheses indicate ascent at lowest levels with subsidence above. . . . .	66
5. 13	The total wind field after 120 minutes of real time for Case D. . . . .	67
5. 14	Evolution of the deviation stream function (solid lines in $10^2 \text{ m}^2 \text{ sec}^{-1}$ ) and potential temperature deviation (dashed lines in C deg) fields for Case E. Time is in hours past start of diurnal sine wave . . . . .	69
5. 15	Characteristic vertical motion components ( $m \text{ sec}^{-1}$ , scaled by order of magnitude) in the lower troposphere for Case E . . . . .	72
5. 16	Streamline patterns for reduced vertical grid (stream function in $10^2 \text{ m}^2 \text{ sec}^{-1}$ ) and potential temperature deviation field (dashed lines in C deg) . . . . .	73

List of Figures Continued

<u>Figure</u>		<u>Page</u>
5.17	Characteristic vertical motion components ( $\text{m sec}^{-1}$ ), scaled by order of magnitude) in the lower troposphere after 60 minutes real time. Conditions correspond to Case D with an extended grid in the x direction, with (upper) and without (lower) plain slope . . . . .	75
6.1	Average divergence (in $\text{sec}^{-1}$ ) at 3 km for 0600 GMT (upper) and 1800 GMT (lower), 1 to 5 July 1966 . . . . .	80
6.2	Westerly (upper) and southerly (lower) components of the mean departure vector as a function of altitude and time for July 1958 at Fort Worth, Texas. Values are in $\text{m sec}^{-1}$ . . . . .	81
6.3	Westerly (upper) and southerly (lower) components of the mean departure vector as a function of altitude and time for July 1958 at Shreveport, Louisiana. Values are in $\text{m sec}^{-1}$ . . . . .	82
6.4	Westerly component of the mean departure vector as a function of altitude and time for 28 days selected during summer 1966 at Amarillo, Texas. Values are in $\text{m sec}^{-1}$ . . . . .	84
6.5	Westerly component of the mean departure vector as a function of altitude and time for 28 days selected during summer 1966 at Dodge City, Kansas. Values are in $\text{m sec}^{-1}$ . . . . .	84
6.6	Westerly component of the mean departure vector as a function of altitude and time for 28 days selected during summer 1966 at Albuquerque, New Mexico. Values are in $\text{m sec}^{-1}$ . . . . .	85
6.7	Westerly component of the mean departure vector as a function of altitude and time for 28 days selected during summer 1966 at Denver, Colorado. Values are in $\text{m sec}^{-1}$ . . . . .	85
6.8	Westerly component of the perturbation flow of the model as a function of altitude and time, taken at a point 35 km from the base of the mountain slope. Values are in $\text{m sec}^{-1}$ . . . . .	87

List of Figures Continued

<u>Figure</u>		<u>Page</u>
8.1	Schematic illustration of the idealized Rocky Mountains-Great Plains daytime circulation. . . . .	103

## DEFINITION OF SYMBOLS

### English Letters

A	kinematic eddy viscosity coefficient
c	wave speed
$c_p$	specific heat for air at constant pressure
C	centigrade degrees
C(z)	amplitude of surface temperature oscillation
$\frac{d}{dt}$	total derivative following the motion of a parcel
$D_\phi$	heat diffusion term
f	Coriolis parameter
$F_x, F_y, F_z$	frictional force components
g	acceleration due to gravity
H	depth of an adiabatic atmosphere
k	friction coefficient
K, K'	eddy exchange coefficient
$K_H$	eddy coefficient for heat
$K_m$	eddy coefficient for momentum
$\ell$	grid spacing
L	right-hand grid boundary; also horizontal wave length
M	upper grid boundary
n	vertical damping coefficient; also coordinate axis normal (vertical) to a slope
p	atmospheric pressure
$p_0$	reference pressure (1000 mb)

## Definition of Symbols Continued

### English Letters

R	gas constant for dry air
t	time
T	temperature (degrees Kelvin)
u, v, w	wind velocity components along w, y, and z axes, respectively
$V_s$	wind velocity parallel to a slope
$w_o$	vertical wind velocity at top of planetary boundary layer
x, y	distances along mutually perpendicular coordinate axes in the horizontal plane
z	distance along the vertical coordinate axis

### Greek Letters

$\alpha$	specific volume of the atmosphere
$\beta$	coefficient of expansion of air
$\Gamma$	rate of temperature change
$\frac{\partial}{\partial t}, \frac{\partial}{\partial x}, \frac{\partial}{\partial y}, \frac{\partial}{\partial z}$	partial derivative with t, x, y, and z, respectively variable
$\frac{\partial}{\partial n}$	partial derivative with n, vertical normal to the slope, variable only
$\Delta$	finite increment operator
$\epsilon$	angle (degrees)
$\zeta_g$	vorticity of the geostrophic wind
$\eta$	component of vorticity along y axis

## Definition of Symbols Continued

### Greek Letters

$\theta$	potential temperature for dry air
$\theta'_s$	surface potential temperature change
$\overline{\theta'(z)}$	initial average thermal stratification
$\kappa$	$R/c_p = 0.286$
$\nu$	coefficient of turbulent friction
$\pi$	non-dimensional pressure variable = $\left(\frac{p}{p_0}\right)^\kappa$
$\rho$	atmospheric density
$\tau$	temperature difference
$\phi$	non-dimensional potential temperature variable = $\frac{\theta'}{\overline{\theta}}$
$\psi$	stream function

## I. INTRODUCTION

### Statement of Problem

The presence of the Rocky Mountain barrier in the western United States dominates the weather throughout the western and central plains during all seasons of the year. As a result, well-defined climatic and bioclimatic zones are evident. Mean annual conditions such as temperature, moisture, precipitation, wind direction, and cloud cover generally reflect this orographic control. In winter the anchoring of the planetary wave pattern by the mountain barrier controls the storm tracks over the eastern half of the nation. The vertical stretching of air columns moving over the mountain barrier has further been shown to result in the leeward generation of cyclones.

Summertime conditions do not generally show the synoptic and planetary scale control observed during winter. Flow patterns are much weaker and storm systems are found on a smaller scale. A number of mesoscale phenomena are especially prominent during this season. Intense convective systems and squall lines show a preference for formation over the western Great Plains. A unique combination of conditions in the upper and lower troposphere cause frequent outbreaks of severe weather and tornadoes, unparalleled in any other region of the world. An intense low-level jet stream is also observed with unusual frequency. To the immediate lee of the mountains, surface and radar observations, and especially satellite pictures reveal a zone of suppressed convection and minimal cloud cover. The manner in which the orography induces these mesoscale phenomena is not yet well understood.

### Purpose of this Study

The purpose of this investigation is to determine the role of the Rocky Mountains in producing the observed summertime convective patterns over the western plains, i. e., suppressed convection in the lee and enhanced convection one hundred to several hundred kilometers to the east. Attention is focused on the region to the lee of the Front Range and Sangre de Cristo Range of the Colorado Rockies where the mountain-plain boundary is clearly defined and the mountains present a continuous north-south barrier (see Figure 1.1).

### Approach

In general the dynamic effects of a large mountain range on the general circulation may be treated in two major categories: (1) modification of an existing general circulation current due to flow over or around the mountain barrier, and (2) generation of local and regional circulation systems. A thorough investigation of the mechanisms responsible for the convective patterns in the lee of the Colorado Rockies requires a consideration of both categories of effects.

A previous investigation (Dirks et al., 1967) proposed a mesoscale wave as the mechanism which initiates the formation of mesoscale convective systems and accounts for suppressed development in the near lee. This and other wave approaches to this problem were found to be somewhat restrictive in their applicability as will be seen in Chapter VII. On the other hand, the pattern of convective development persists through highly varying atmospheric conditions (Dirks, 1969). It is then proposed that the regional circulation mechanism is a more generally applicable approach.

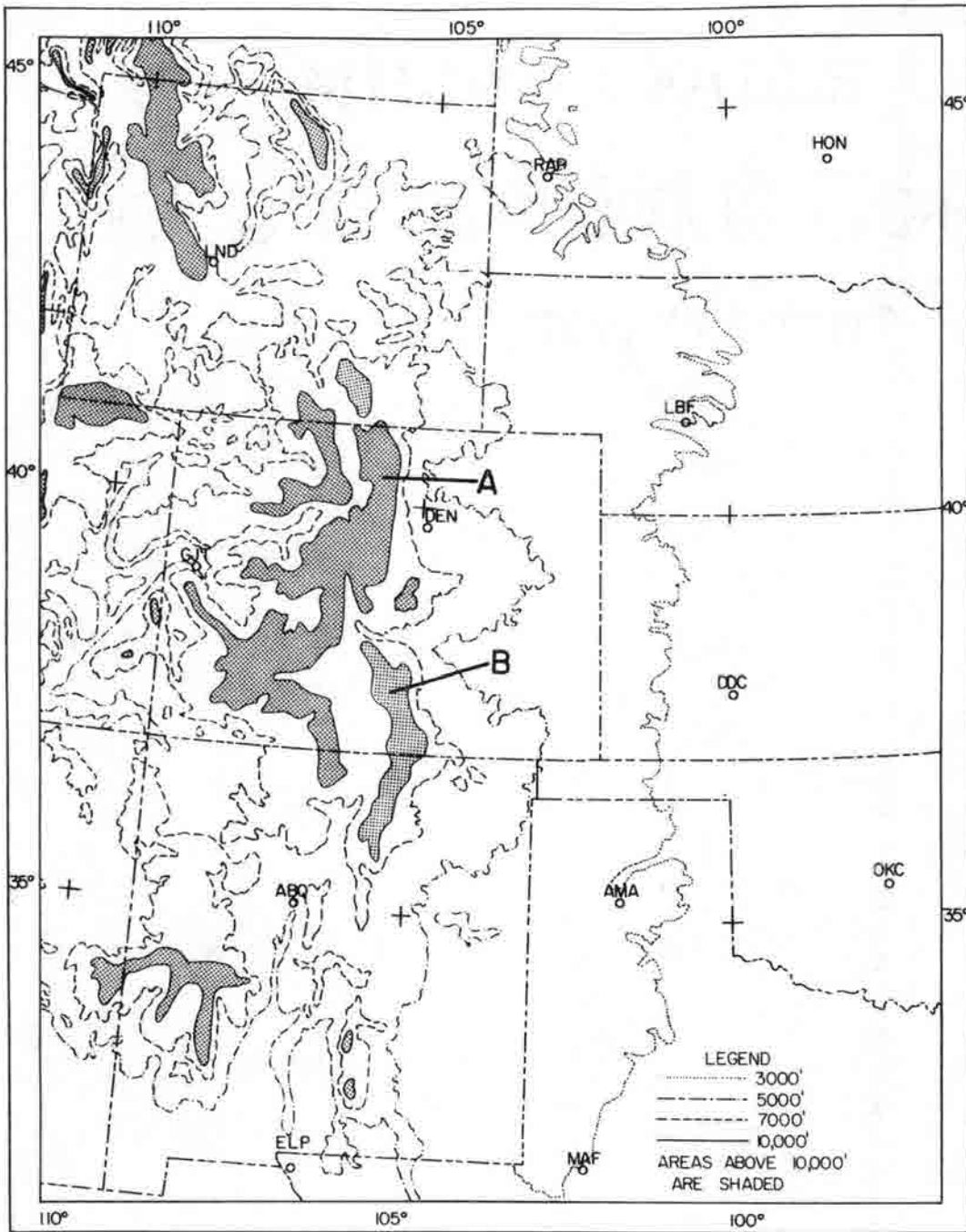


Figure 1.1. Map of the central Rocky Mountains and central Great Plains. (A) Front Range and (B) Sangre de Cristo Range.

The orographic features of the Front Range and the Sangre de Cristo Range of the Rocky Mountains are shown in Figure 1.1. The mountains present an abrupt and nearly continuous barrier from about 5,000 ft MSL to above 10,000 ft MSL extending from southern Wyoming to central New Mexico. The ridge line lies nearly north-south along longitude 105.5W. The central Great Plains slope slightly eastward from an elevation near 5,000 ft MSL at the western edge to below 1,000 ft MSL at longitude 95W. The problem is examined in terms of this mountain barrier and the adjacent plain.

A two-dimensional model in vertical cross-section is developed and characteristics of the flow are examined under various ambient conditions. Results are compared with vertical profiles of summertime diurnal wind oscillations. The magnitude of the slope circulation effects are compared with similar effects produced by both synoptic and thunderstorm systems; from this evaluation the control of the slope circulation on the formation and development of convective systems is inferred.

## II. VARIABILITY OF MESOSCALE CONVECTION ON THE GREAT PLAINS

Mesoscale convective systems are a common summertime feature of the Great Plains area. These systems commonly develop in the afternoon (Brunk, 1953) and travel eastward moving about  $20^{\circ}$  to the right of the lower tropospheric winds (Newton and Newton, 1959). They frequently persist well into the night and early morning, sometimes diminishing during the next day and reintensifying in the late afternoon and evening (Porter et al., 1955).

Bonner (1963) points out that the nocturnal thunderstorms of Kansas and Oklahoma form along the slopes of the Rocky Mountains in the afternoon and move into that region at night. The diurnal distributions of summer thunderstorms and precipitation (Figures 2.1 and 2.2) also support the concept of an eastward migration of convective systems with a nocturnal maximum in Oklahoma, Kansas, and Nebraska. Crow (1969) examined hourly precipitation amounts along north-south lines of stations extending from Denver eastward to Wichita, Kansas. Figure 2.3 shows the resulting diurnal variability of major convective activity over a distance of about  $7^{\circ}$  longitude ( $\sim 600$  km) showing an approximate ten hour lag at stations farthest east. Comparable diurnal patterns in hail are also evident (Musil and Dennis, 1968; Crow, 1969).

In addition to the diurnal variability of precipitation and convective activity the magnitude of convective summer precipitation is greatly reduced in the immediate lee of the mountains as shown in Figure 2.4. The pronounced maximum in hail frequency in the lee of the central Rockies (Figure 2.5) emphasizes the spatial variation of severe convective activity in that region.

The first occurrence of convective clouds over mountain slopes is well-known and is readily explained by high level heating and slope

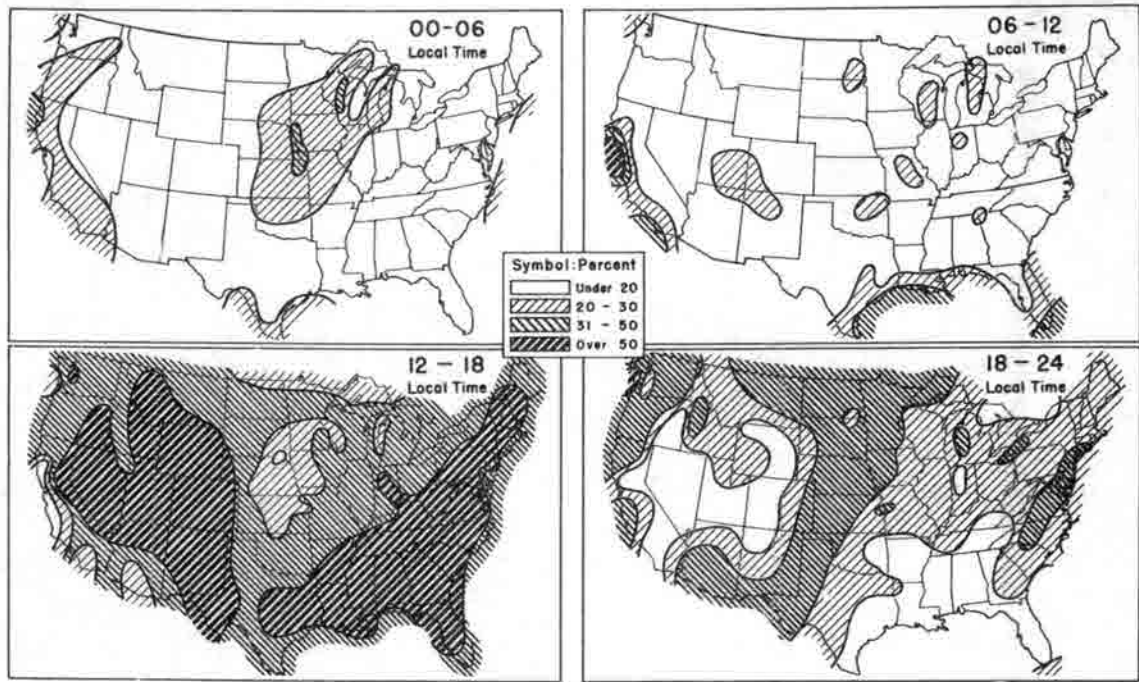


Figure 2.1. Percentage of summer thunderstorm occurrences per quarter-day (from Hydrometeorological Report, 1947).

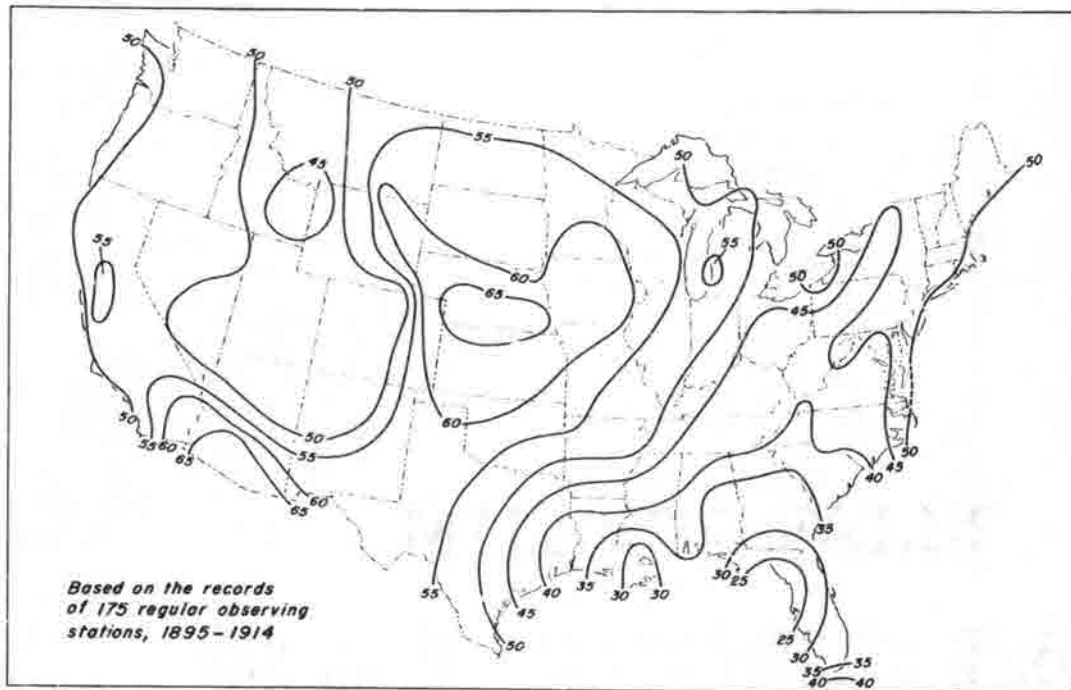


Figure 2.2. Percentage of precipitation occurring at night (12 hours ending at 8 a.m., 75th meridian time, April to September) (from Hydrometeorological Report, 1947).

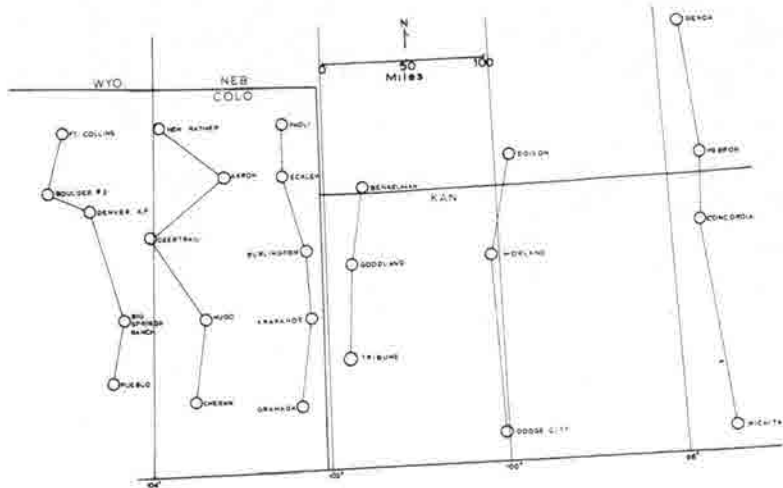
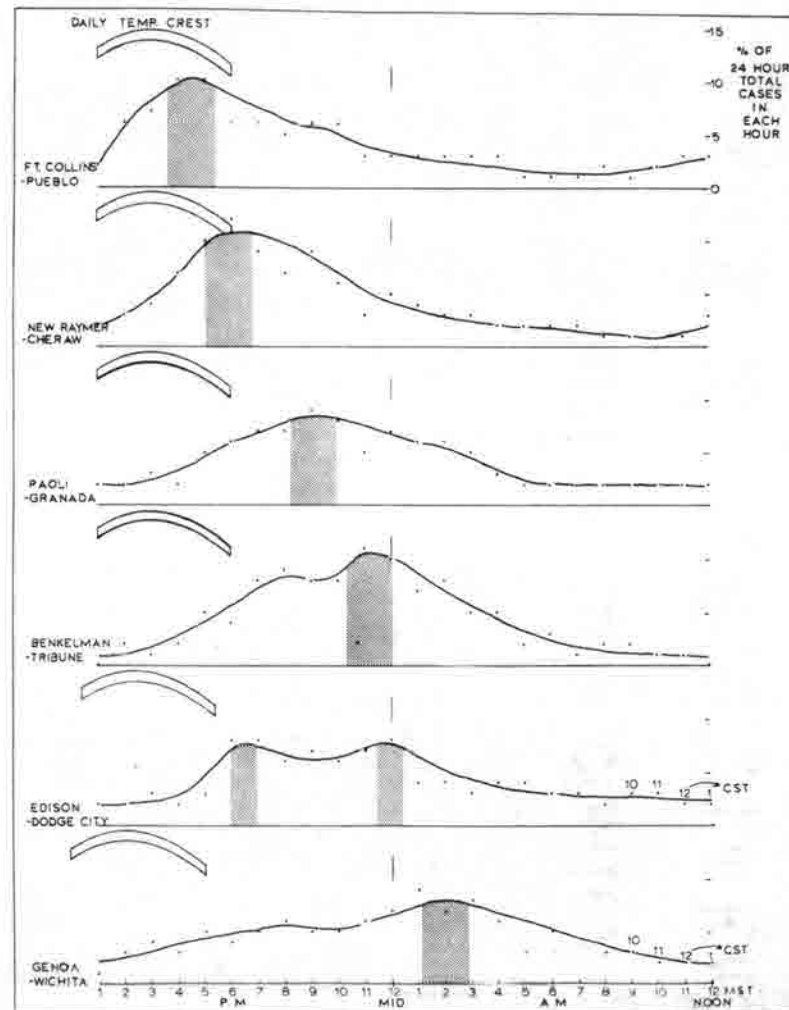


Figure 2.3. (Above) Six groups of stations with north-south orientations used in the timing analysis of convective shower activity. (Right) Timing of major convective activity for ten-year summary of hourly precipitation  $\geq .10$  inch for the six groups of stations (from Crow, 1969).



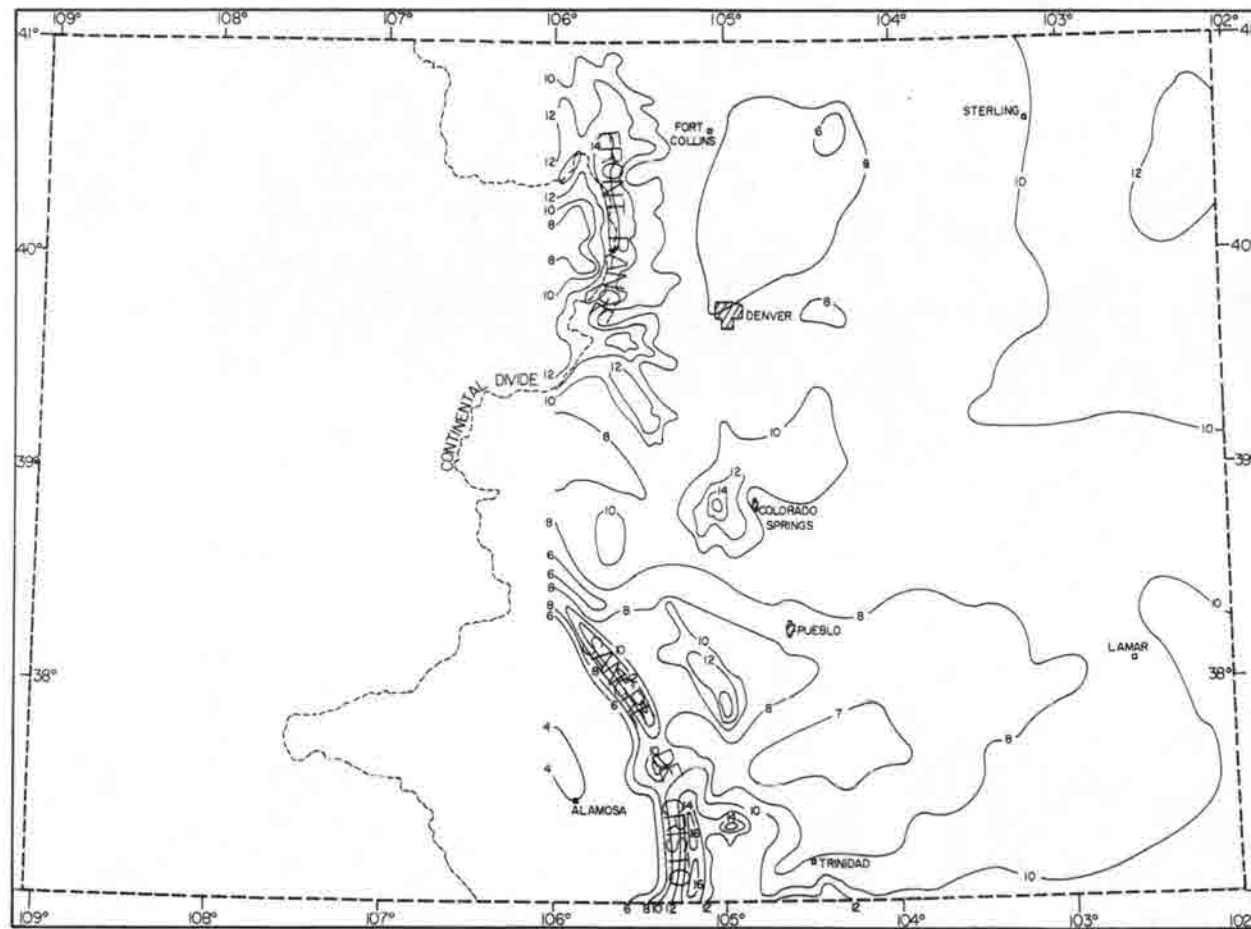


Figure 2. 4. Colorado map showing normal May-September precipitation (1931-1960) east of longitude 106°W. Isolines are in inches. Note regions of reduced rainfall leeward of both the Front Range and Sangre de Cristo Range. (Analysis from U. S. Department of Commerce Map)

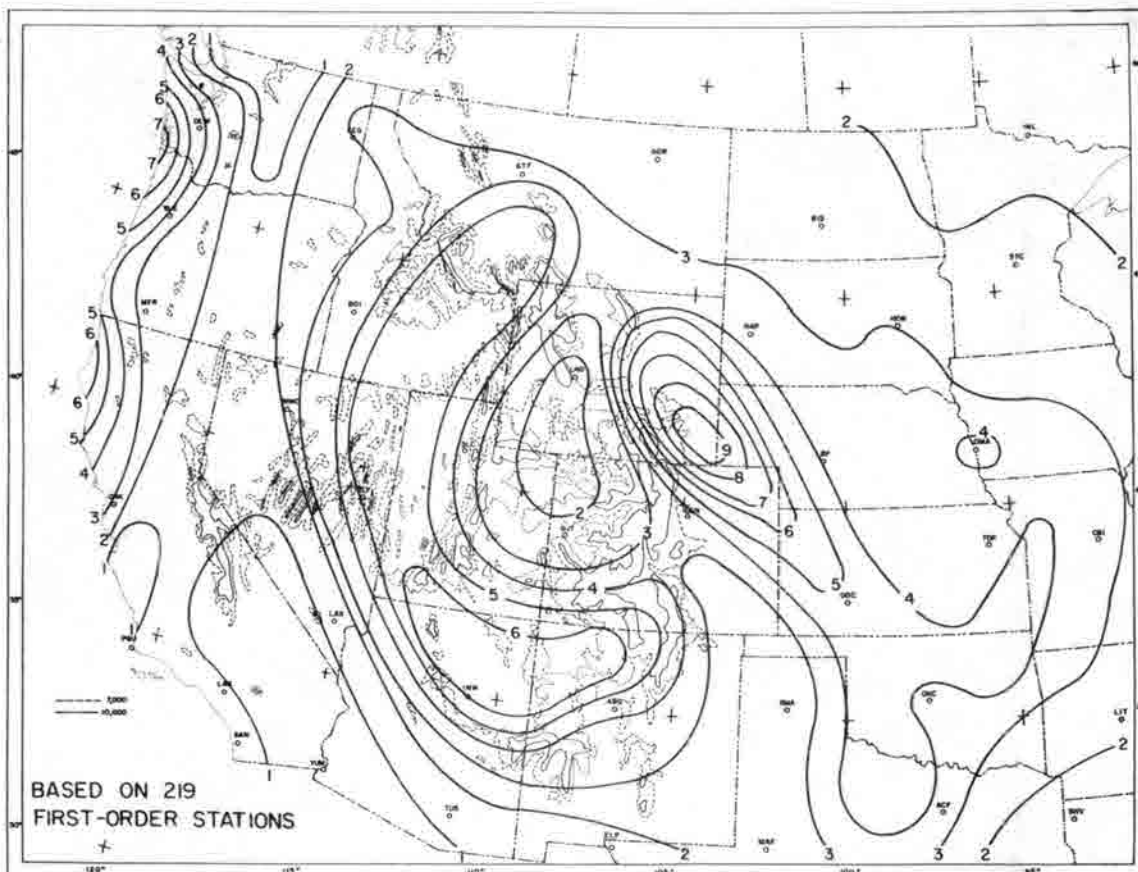


Figure 2.5. Average number of days with hail, annual (after Hydrometeorological Report, 1947).

heating which initiate upslope motions and result in localized chimney effects over mountain peaks (Braham and Draginis, 1960). The convective region to the lee of the mountains and the organization into meso-systems are not as easily explained although an association with certain features has been noted and several triggering mechanisms have been proposed.

Both dynamic and thermodynamic factors have been associated with the enhanced convection somewhat to the lee of the mountains. Development has in general been observed in regions of low thermal stability (e. g. , Showalter Index < 0) but no correlation is evident

with regions of greatest instability (Means, 1952; Porter et al., 1955; Breiland, 1958; Bonner, 1963).

Warm, moist Gulf air advected by a southerly flow at about 850 mb is a common feature associated with summer convection over the Great Plains. The role of the low-level jet (LLJ) in this advection has been emphasized in several studies (Means, 1952; Bonner, 1963). The lower layer of moist air is often capped by an inversion and overlain by a layer of cold, dry air (Breiland, 1958). The "cap" damps thunderstorm development and permits a build-up of moisture and convective instability until the inversion is penetrated and "explosive" development takes place (Fulks, 1951; Means, 1952). Although the warming at low levels is usually of a larger magnitude than the cooling aloft, Fulks (1951) points out that the cooling is important since it permits vertical motions to extend to higher levels so that more intense convection results.

The role of topography is paramount in developing the favorable thermal structure described above. The north-south barrier at low levels favors a southward flow of cold air and northward flow of warm, moist air which may be overridden by westerly flow off the mountain plateau.

In addition to its role in the advection of heat and moisture, the LLJ (low-level jet) has been examined with regard to its dynamic properties. Bonner (1963) found that the associated vertical motions played a significant role in the maintenance of nocturnal squall lines in Oklahoma, while a dying out of moisture advection did not appear to damp convective activity. Pitchford and London (1962) discovered a high correlation between the occurrence of summer nocturnal thunderstorms over the Great Plains and the convergence produced by the low-level jet. They observed a rapid ascent of air downstream from the LLJ maximum, also observed by Bonner (1963) and linked with squall line formation. The association of the LLJ with pre-frontal squall line

formation has also been found to be significant, e. g., Porter et al. (1955) found the LLJ present 75% of the time.

Beebe and Bates (1955) present a mechanism produced by the crossing of the upper jet stream and the LLJ which would affect the release of convective instability through the inversion "cap" by vertical stretching or lifting. The superimposed fields of upper divergence and lower convergence have been shown to occur in some cases of tornado activity, however, such occurrences are not frequent enough to account for the general formation of mesoscale convective systems.

A theory which has received considerable attention as a mechanism for squall line formation is the "pressure jump line". The theory originally proposed by Freeman (1948) is an analogy to waves produced by motion of a piston in a gas initially at rest with an inversion at a constant height. Tepper (1950, 1952) assigned a cold front to the role of the piston with the initiated pressure jump taking the form of a gravity wave. The latter paper suggested meteorological conditions which might produce a pressure jump without a cold front which included any situation producing either an acceleration of the air below the inversion or an elevation of the inversion surface. The effect of the breaking of the gravity wave is to aid in convective penetration of the inversion commonly observed prior to squall line formation.

The line formation and frequent meridional growth of squall lines is evident when viewed over broad time and space scales (cf. Brunk, 1953; Fujita and Brown, 1958). The apparent irregular shapes and erratic movements observed on a small time scale may be attributed to the sporadic formation of new cells as the squall system undergoes continuous evolution.

Newton (1963) summarizes the conditions favorable for the occurrence of severe convective storms (cf. Fawbush et al., 1951):

- a) conditional and convective instability;
- b) availability of abundant moisture in lower levels;

- c) generally, bands of strong winds in lower and upper levels, usually veering with height;
- d) some dynamic mechanism which can cause the release of instability.

In the preceding discussion some of the conditions necessary, but not sufficient, for the formation of mesoscale convective systems have been described. This study does not propose to re-evaluate each of the previous concepts but seeks a basic mechanism to account for the formation of mesoscale systems several hundred kilometers leeward of the Colorado Rockies and the presence of a near lee-side divergence zone. Only the pressure jump theory has proposed a really basic mechanism which may be present in all cases of development.

A recent climatological study (Dirks, 1969) based on satellite and radar data has given further evidence to both the west to east motion of maximum convective activity and the enhancement of convection one hundred to several hundred kilometers to the lee of the mountains. An evaluation of radar echo patterns (Figure 2.6) indicates that except in grid box 15, most strong echoes are not observed until 1400 MST. An eastward migration of systems may be noted from the time sequence of echoes in grid boxes 2, 3, 7 and 11. It is evident that convective systems show a preference for earlier occurrence in more westerly regions, in reverse of the solar path. Thus, the temporal distribution of convective development in the central Great Plains does not follow from local maxima of solar heating, but rather indicates that other factors play a dominant role.

The spatial distribution of meso-system development was evaluated from satellite photos (Figure 2.7). There is definite evidence of a non-development zone in the eastern half of grid boxes 1, 5, 9, 13, 17 as well as in the western half of grid box 6. Preferred development areas are found in grid boxes 2, 3, 6, 7, 10, 11, 12, 14, 15, 19

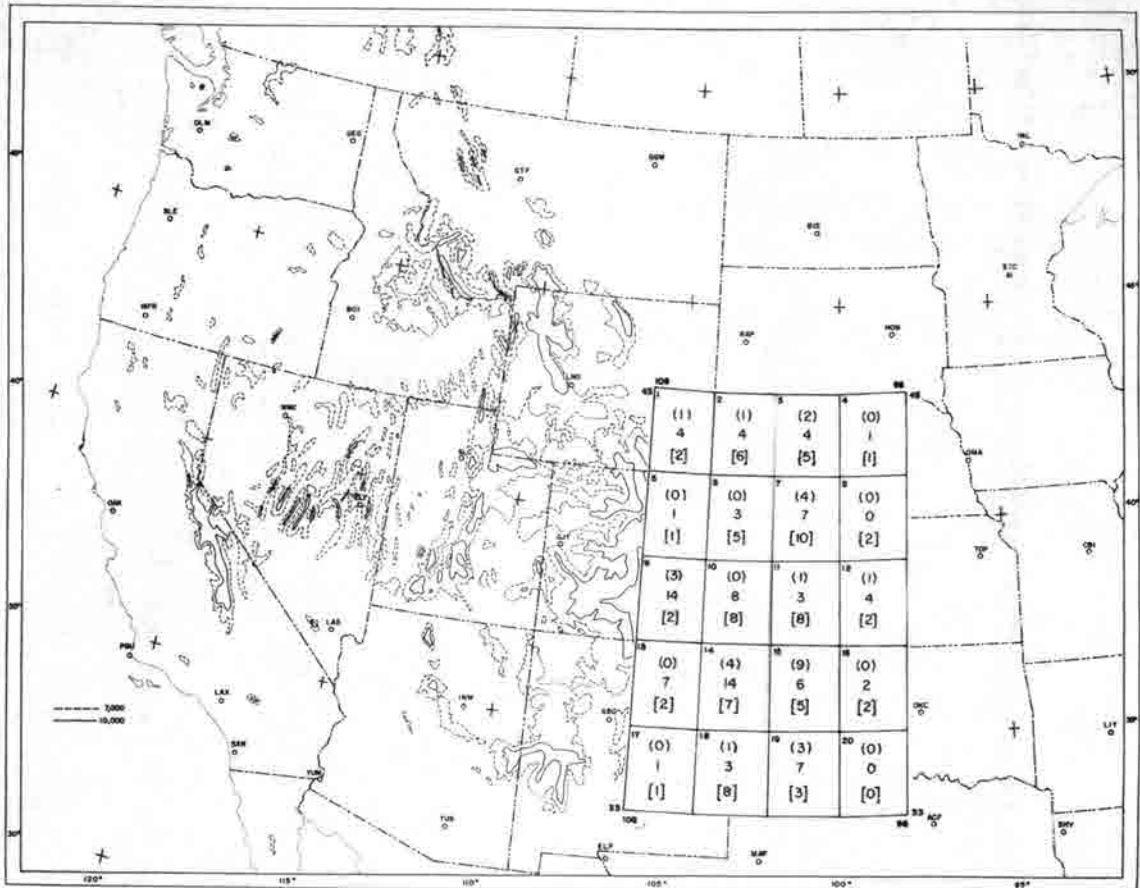


Figure 2. 6. Temporal distribution of radar observations of mesoscale convective systems, May-August 1966; (X) = 1300 CST, X = 1500 CST, [X] = 1700 CST.

but not in grids to the east. Even from the limited amount of data evaluated, the variation appears to be quite significant.

An example of the eastward migration of convective activity is shown in a stationary satellite (ATS-III) picture sequence for 30 May 1968. Figures 2. 8 to 2. 11 show development over a six-hour interval beginning at 1004 MST (1704 GMT), Colorado is seen in outline. Initial development can be observed over the mountains of central and western Colorado and New Mexico, and a cold front is visible north-west of Colorado (Figure 2. 8). By 1211 MST (Figure 2. 9) widespread convection is evident over the mountains and faint development is

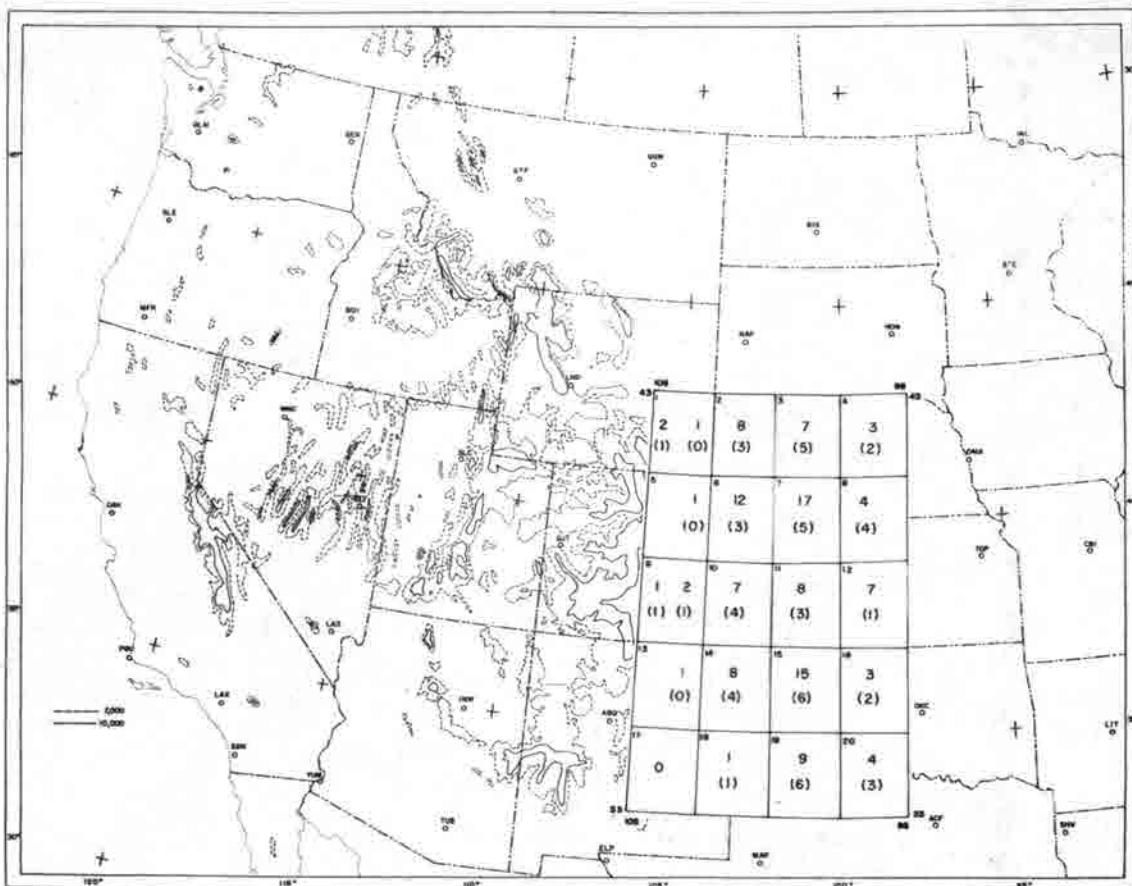


Figure 2.7. Spatial distribution of mesoscale convective systems as observed by satellite photos May-August 1966 (ESSA I and Nimbus II, incomplete), May-July 1968 (ESSA V). 1966 alone given in parentheses.

visible in northeast Colorado and southwest Nebraska with a clear region in the immediate lee of the mountains. Two hours later (Figure 2.10) strong development can be seen throughout eastern Colorado and northeastern New Mexico, with continued evidence of a divergence zone in north-central New Mexico and central Colorado. By 1631 MST (Figure 2.11) intense meso-systems have moved eastward especially into southwestern Kansas, western Oklahoma, and the Texas Panhandle. A divergence zone remains well defined in both Colorado and New Mexico. Thus, meso-system development in this case took place in eastern Colorado and northeast New Mexico and then traveled eastward steered by westerly and northwesterly flow aloft.

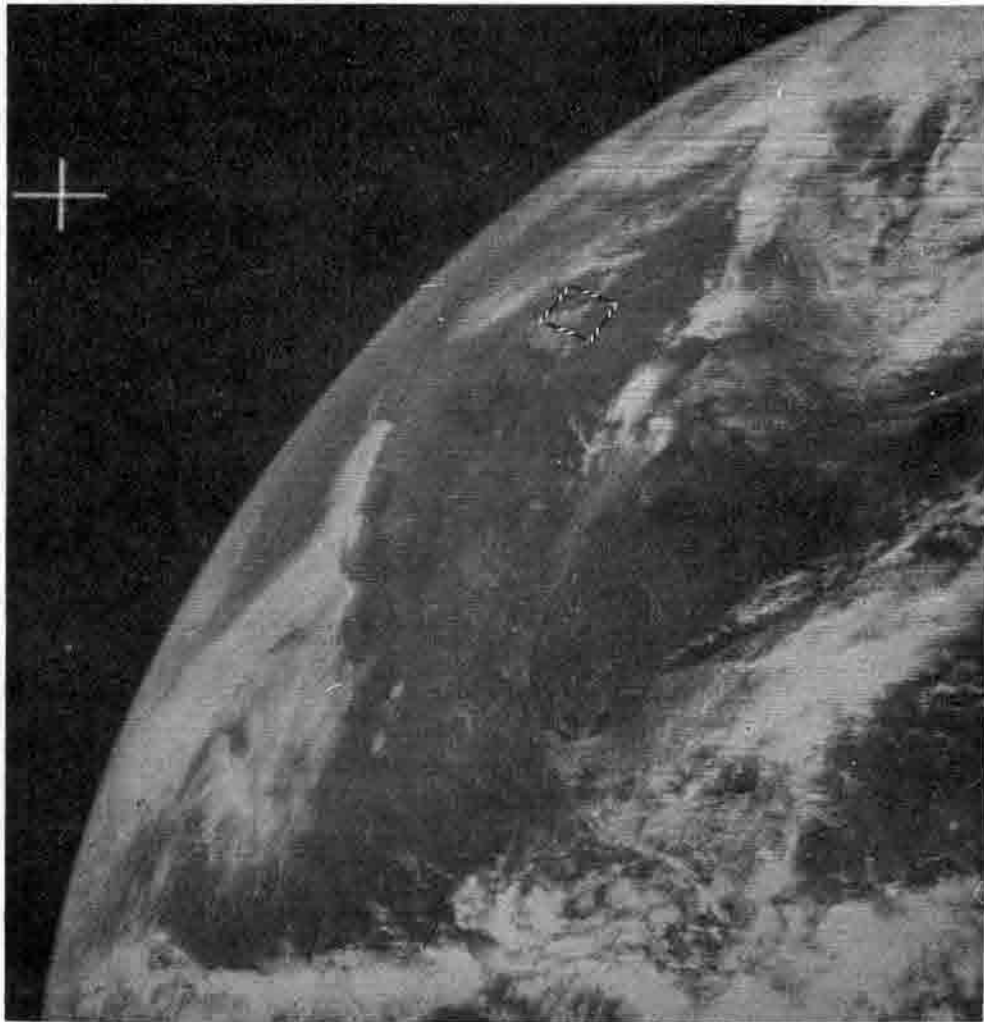


Figure 2. 8. ATTS III, 30 May 1968, 170349 GMT, frame 30G.  
The Gulf Coast and Baja Peninsula are visible in the lower part of the picture and the Florida Peninsula at the right-center. Colorado is shown in outline.

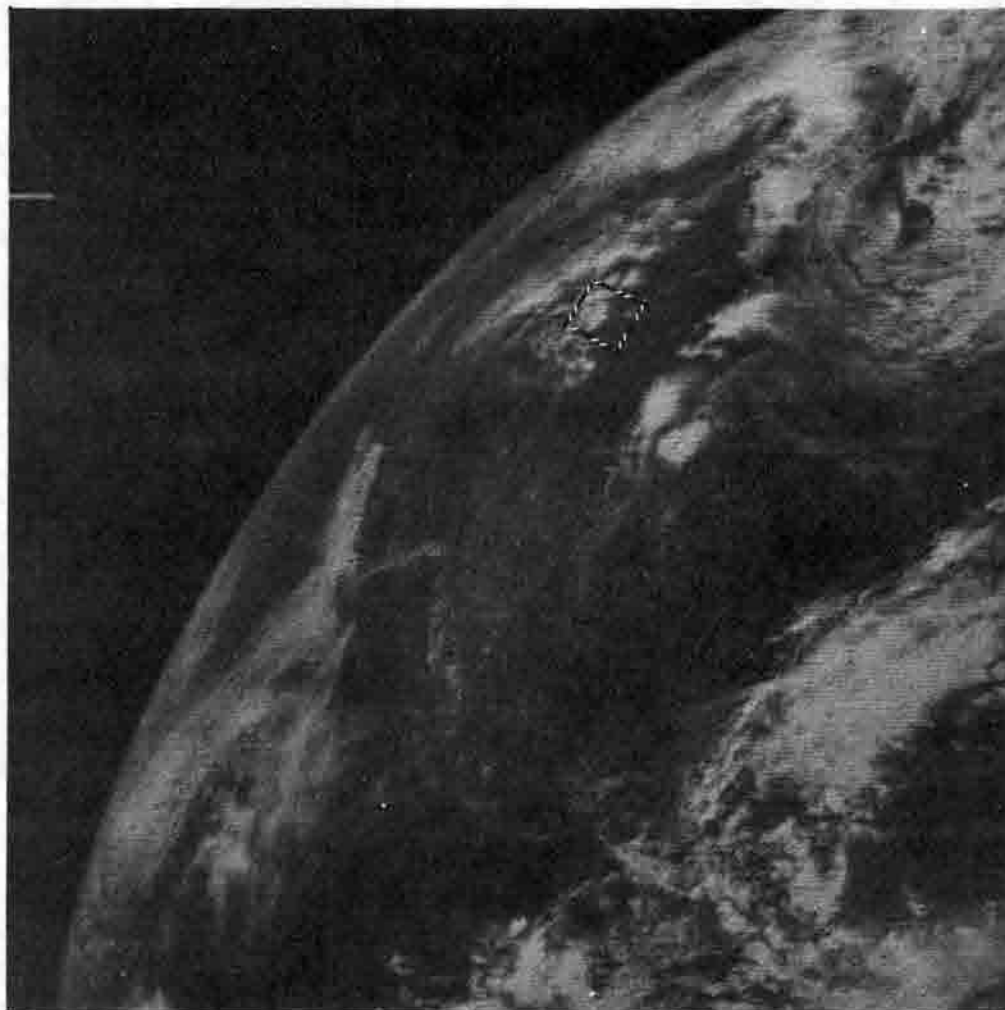


Figure 2.9. ATS III, 30 May 1968, 191038 GMT, frame 39G.  
Colorado is shown in outline.

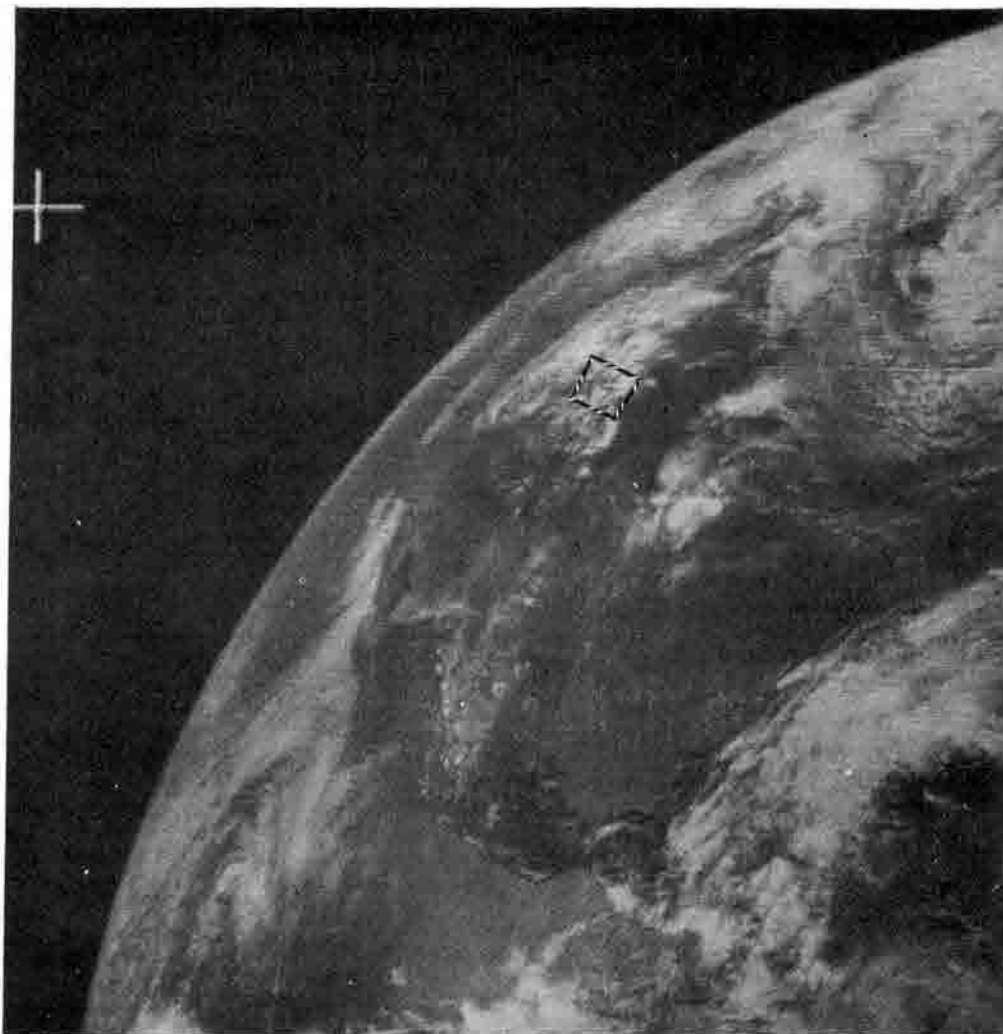


Figure 2.10. ATS III, 30 May 1968, 211808 GMT, frame 48G.  
Colorado is shown in outline.

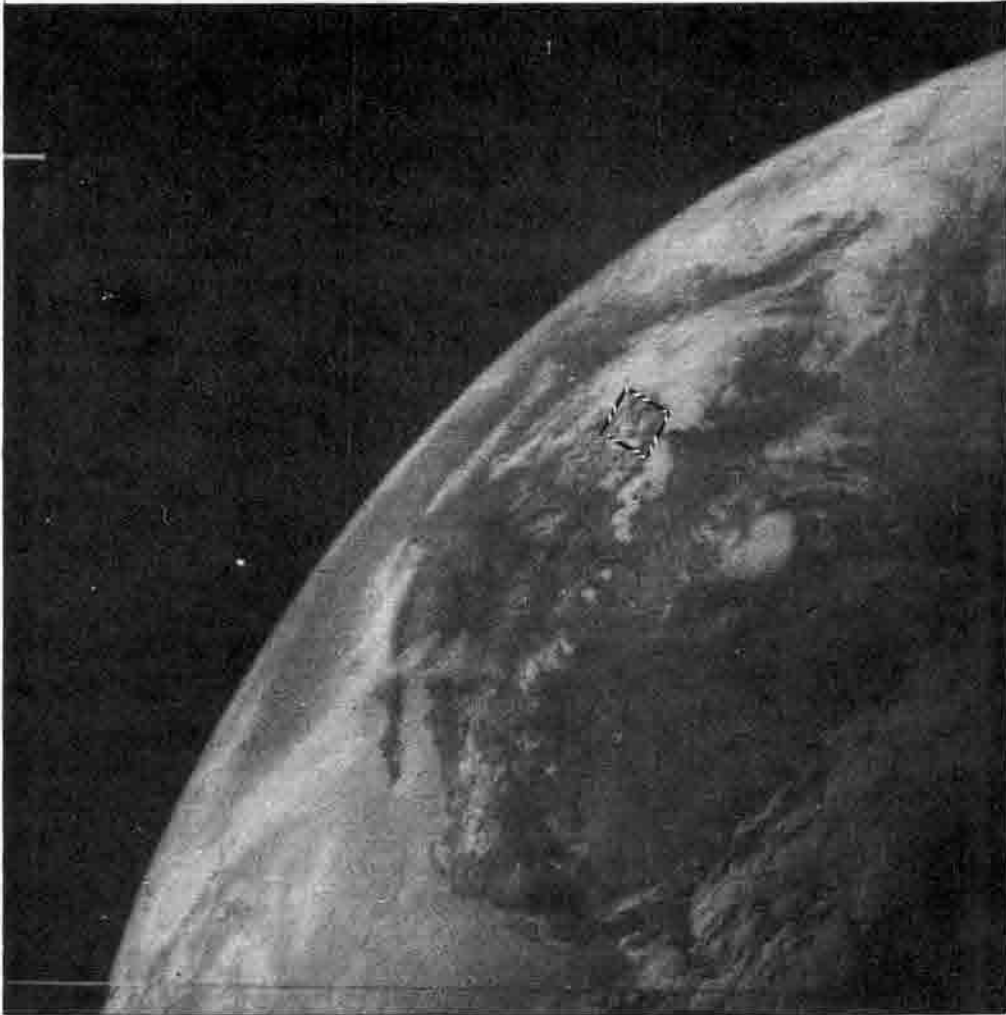


Figure 2.11. ATS III, 30 May 1968, 233042 GMT, frame 57G.  
Colorado is shown in outline.

The climatological study also examined various dynamic and thermodynamic features of the atmosphere in order to distinguish those conditions necessary for development to take place. The dynamic properties of the large-scale upper level flow indicated that in somewhat more than 50 per cent of the cases the flow at 500 mb was weak (5-10 m/s) and anticyclonic and thus did not appear to be a significant factor. However, when a fairly strong flow pattern ( $> 15$  m/s) existed at upper levels, development of meso-systems occurred only under conditions of cyclonic curvature. The dynamics of upper level wind maxima played a corresponding role. Under strong cyclonic flow conditions, especially in association with dynamically induced fronts, there was evidence of a dynamic role of the "jet stream". Thus the role of the upper-level jet stream in forming meso-scale systems of all types is of much less significance than its role in specifically tornadic storm systems (Bates, 1962; Skaggs, 1967).

A strong positive vertical wind shear was evident in 50 per cent of all cases with the remainder showing only weak to moderate wind speeds (5-15 m/s) throughout the vertical. Strong vertical shears have been suggested as a necessary "evacuation" mechanism in the development of large cumulonimbus clouds (Dessens, 1960; Newton, 1963; Bates and Newton, 1965). Others have noted that strong vertical shears are not a critical feature, e. g. , they do not on the average differ for thunderstorms with and without accompanying hail (Ratner, 1961).

Convective instability has often been measured in terms of the Showalter Index (SI) and was evaluated in this way here. A good correlation of meso-system development with regions of low thermal stability was found--SI  $< 0$ , 35 per cent; SI 0-3, 55 per cent; SI  $> + 3$ , 10 per cent. However, meso-systems did not necessarily develop in regions of maximum instability and a number of non-development days showed regions in which the Showalter Index was negative.

The presence of a stable layer or inversion in the lower to middle troposphere has been postulated to play two roles in localized release of convective development; it acts as a "lid" on the development which when penetrated permits "explosive growth" to occur and, secondly, the interface provides a surface on which gravity waves may travel in the pressure jump theory. Observations of temperature profiles in the Great Plains area indicated the presence of an inversion layer about 50 per cent of the time in the region where development took place. In most of these cases the inversion was weak and shallow; strong, deep inversions tended to suppress development as might be expected. The apparent absence of a well-defined inversion layer in such a large number of cases places in doubt the general application of the "pressure jump theory" as an initiating mechanism.

This brief climatic study has shown that mesoscale convective systems develop under a great variety of synoptic conditions and are associated with various features under different conditions. The features common to all cases were the presence of a warm, moist tongue at low levels (850 mb) and a certain amount of convective instability ( $SI < +4$ ). The apparent presence of an upper level short wave was revealed in most cases. Certain features including the low-level jet, jet streams aloft, cold air advection aloft, and a mid-tropospheric stable layer were found to be included in a high percentage of the cases.

The results of this climatological study gave quantitative support to the observation that strong convective patterns favor development in the western Great Plains one hundred to several hundred kilometers to the lee of the Colorado Rockies. In the region immediately to the lee of the mountains convection is largely suppressed until late afternoon when cells and thunderstorms move off the mountain slopes.

Development of the convective systems has been shown to occur over a wide range of atmospheric conditions so any theoretical explanation of the observed patterns should be applicable under the variety of conditions described. This will provide a basis for evaluation of the theoretical considerations which are to follow.

### III. REVIEW OF SLOPE WIND OBSERVATIONS AND THEORY

Descriptions of slope winds appeared in scientific literature as early as 1840 (Fournet, 1840) and theoretical explanations may be found back to 1879 (Hann, 1879). The first comprehensive studies of slope wind systems were carried out in the Alps in the late 19th Century and early theoretical deductions were made by Hann (1879, 1919). After V. Bjerknes presented his fundamental circulation theories, Wenger (1923) produced a new circulation theory for mountain and valley winds. In the 1930's numerous aerological studies were made in the Alps, particularly in the vicinity of Innsbruck (for references, see Defant, 1951). As a result of these studies, a revised version of Wenger's theory was proposed by Wagner (1932, 1938). From a careful examination of the daily pressure and temperature variations in the free atmosphere within the valley Wagner found that diurnal pressure variations were completely equalized at a level about twice the ridge height. It was also observed that diurnal temperature variations in valleys were more than twice as large as variations in a similar layer over the plain. Therefore, a pressure gradient from plain to valley must exist during the daytime with the reverse gradient at night. A descriptive discussion of Wagner's theory is given by Defant (1949, 1951). The slope wind theory by Wenger and Wagner finds the acceleration by applying the circulation theorem to a triangular path in a vertical plane. The path leads up the slope, then along an isobaric surface, and vertically back down to the plain.

#### Small Scale Observations of Slope Winds

Most of the early observations of slope winds have been summarized by Defant (1951). In general the thickness of the layer is not over

200 m, being somewhat less for the nocturnal downslope flow. The intensity of the slope wind shows a great variability with locality, exposure, time of day, and synoptic conditions. Velocities of 2 to 5 m sec<sup>-1</sup> are common, while the nocturnal drainage flow is usually weaker. Wind profiles for both upslope and downslope flow as given by Defant (1949) in Figure 3.1 show a maximum velocity at a height of about 30 m above the slope. Large vertical velocities in excess of 10 m sec<sup>-1</sup> have been measured in the updrafts over the ridges. Wind systems which are channeled through valleys (i. e., mountain and valley winds) show extreme variations from the profiles by Defant and may have a depth up to 1000 m with maximum velocities occurring at heights of several hundred meters (e. g., Davidson and Rao, 1958).

The compensating flow which overlies the slope wind is generally weak and is frequently disguised by the prevailing winds. The presence of this return flow has been noted in a number of observational studies (e. g., Davidson and Jaffe, 1960; Buettner and Thyer, 1965; Fosberg, 1967); however, due to the weakness of this component and its combination with a much stronger gradient wind field, little is known about its detailed vertical structure. Fosberg has estimated a 200 m deep return flow in his case study. Buettner and Thyer indicate that the "anti-wind" usually has a definite upper limit.

The reversal in direction of slope flow is normally found to take place 1/4 to 3/4 hours after sunrise or sunset (Defant, 1951; Sterten and Knudsen, 1961), however, Davidson and Jaffe (1960) in a study of valley winds in Vermont found the flow reversal to vary several hours before and after sunrise or sunset depending on the particular valley under study. This periodicity is probably dependent on the duration of sunshine, cloud cover, slope angle, and roughness of the terrain. Buettner and Thyer remark that the flow reversal occurs nearly simultaneously at all heights.

Sterten and Knudsen (1961) in a combined field program and synoptic study found that an interdiurnal variation in atmospheric pressure accompanied the mountain and valley wind system. The forecasting of mountain and valley winds required taking into account cloud cover and strength of the prevailing wind.

Characteristics of the thermal stability over heated slopes are available from studies by Braham and Draginis (1960), Vul'fson (1964) and Fosberg (1967). These reveal superadiabatic lapse rates adjacent to the slope in a layer several hundred meters deep. Hot superadiabatic caps form over ridge lines and cold cores may be found over mountain slopes. Analyses of aircraft flights in Arizona by Braham and Draginis reveal that the convective columns originate in the slope wind circulation which ascends the mountain slopes, converging into a "massive column" at the mountain top. The potential temperature "dip" in upper regions of this column suggests that forced ascent carries the column to higher levels. Vul'fson also associates the initiation of convective activity over mountain peaks with the slope wind system. He points out further that the ascending branch of the circulation tends to intensify the instability while the descending branch has a stabilizing effect on the atmosphere. The field observations by Braham and Draginis and by Silverman (1960) provide some of the few data on the distribution of moisture. These data show considerable moisture enrichment downwind over heated slopes with most of the enrichment occurring in narrow cores ~ 2 km in diameter.

#### Evidence of Mountain-Plain Scale Circulations

There is also evidence of a slope circulation on a much larger scale existing between a mountain range and the surrounding plains. Burger and Ekhardt (1937) were able to deduce a daytime circulation scheme in the Alps with a low level flow towards the mountains and an upper level compensating current flowing radially away from the

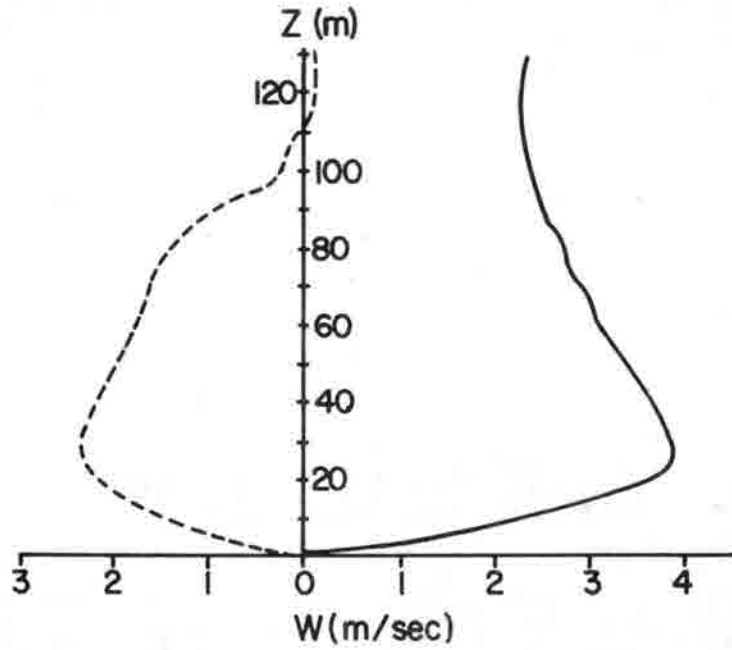


Figure 3.1. Profiles, normal to the slope, of observed upslope (solid) and downslope (dashed) wind speeds. After Defant (1949).

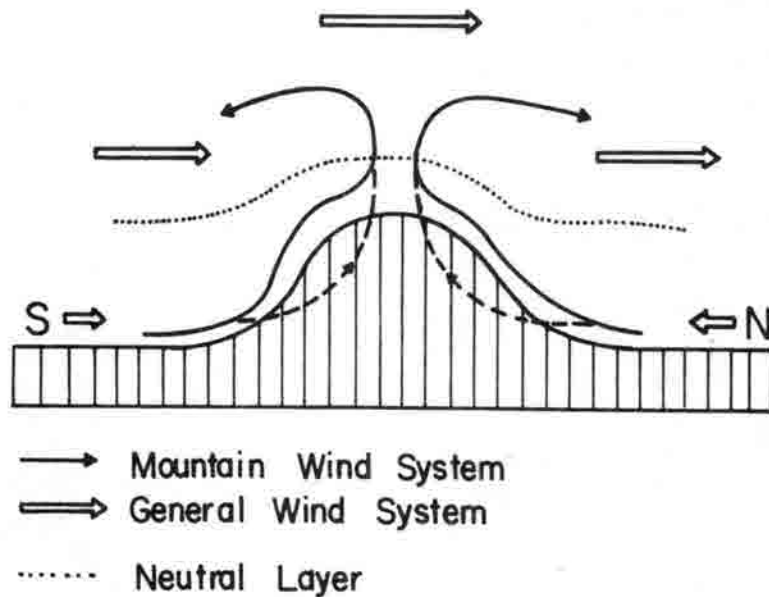


Figure 3.2. Schematic illustration of the daytime circulation in a cross section through the Alps. After Burger and Ekhardt (1937).

mountains toward the plains (see Figure 3.2). Wagner (1939) and Ekhart (1940) found a similar flow pattern on the eastern slope of the Rockies, with a neutral level near 2500 m. The compensatory upper level flow was found to be comparatively weak with velocities on the order of  $15 \text{ cm sec}^{-1}$ . This flow is also affected more strongly by the ambient wind field than is the low level flow.

Flohn (1968) made a similar estimate for the daytime branch of the diurnal circulation between the Tibetan plateau and the surrounding plains. He finds an upslope component of about  $360 \text{ cm sec}^{-1}$  and a return flow of  $120 \text{ cm sec}^{-1}$ . It should be noted that in this case the flow cannot be attributed to the slope alone but also includes the effect of the heating of a broad plateau. Such diurnal circulation systems are also evidenced for the Bolivian high plains (Flohn, 1955). Bleeker and Andre (1951) proposed a large scale circulation cell over the central United States to account for the suppression of thunderstorms during the day and a maximum of nocturnal thunderstorm activity over the Great Plains. They examined the diurnal change in the horizontal divergence and found these to be consistent with such a large-scale circulation pattern.

Knudsen (Sterten and Knudsen, 1961) has considered a large scale mountain and valley wind system ("monsoon circulation") which extends over the whole of southern Norway. The system is somewhat obscured by its interaction with the coastal sea breeze. Malkus (1955) has also described an orographic-convection system over Puerto Rico in which sea-land effects interact with orographic effects to produce a convective circulation on the scale of 100's of km.

An investigation of the diurnal variation of the surface geostrophic wind over the Great Plains by Sangster (1967) revealed an appreciable diurnal cycle with a night to day range of around 20 knots under clear sky conditions. The maximum variation occurred near the ground with a minimum wind at 0600 CST and a maximum at 1800 CST. The

effect of the diurnal temperature cycle was determined from the component of surface geostrophic wind normal to an east-west line extending from Albuquerque to Nashville.

### Analytical Theories of Slope Winds

The driving mechanism of slope winds is the heating (or cooling) of air above an inclined surface resulting in a horizontal temperature gradient between two points at the same altitude along different parts of the slope. A complete theory of slope wind must take this generating mechanism and couple it with the various modifying influences in a mathematically tractable form. The effects of surface friction, eddy diffusion, coriolis forces, and advection must all be considered if they apply to the particular scale of motion under study. Furthermore, latent heat release and cloud cover may often play an important role. The theoretical problem then becomes one of simplifying the equations so that solutions may be determined and at the same time retaining the important physical properties of the fluid and the flow field.

A more quantitative model than the early circulation theorems was presented by Prandtl (1942; Defant, 1949) in which he arrived at a steady state wind parallel to the slope ( $V_s$ ) given in terms of gravity, turbulent heat conduction, and turbulent friction in a compressible atmosphere. The model assumed a uniform slope of infinite extent and heat conduction normal to the slope only. The equation of motion for flow along the slope,  $V_s$ , may thus be given by

$$\frac{dV_s}{dt} = g\beta\theta' \sin\epsilon + \nu \frac{\partial^2 V_s}{\partial n^2}$$

where  $\beta$  is the coefficient of expansion of air,  $\epsilon$  is the angle of the slope,

$\theta'$  is the variation in potential temperature due to heat conduction in the direction  $n$  (normal to the slope),  $g\beta\theta'\sin\epsilon$  represents the buoyant acceleration, and  $\nu$  is the coefficient of turbulent friction. A steady state temperature field is possible when there is a balance between potential temperature advection along the slope and heat loss or gain due to eddy diffusion normal to the slope. The resulting steady state wind is derived from a balance between buoyancy force (pressure gradient) and frictional force. The velocity expression which is derived shows that the slope wind speed is directly proportional to the temperature deviation at the slope surface. Also near the ground the slope wind is nearly independent of the slope angle and the horizontal component is approximately proportional to the cosine of the slope angle. Defant (1949) found "splendid agreement" of the above profiles with observed winds at a single location.

In an earlier but somewhat similar derivation Jeffreys (1922) arrived at an expression for a stationary wind in which the wind speed varied directly with the horizontal temperature gradient and the slope of the ground. He assumed an incompressible atmosphere and an equilibrium between pressure gradient, gravitational, and frictional forces. Fleagle (1950) examined the problem of drainage wind for a compressible fluid being cooled from below by a radiating slope surface. The resulting expression for the drainage velocity predicted that the mean velocity of the layer being cooled (a) is proportional to the net outgoing radiation from the ground, (b) is inversely proportional to the height to which cooling extends, (c) has the form of a damped periodic oscillation, and (d) is inversely proportional to the slope of the ground. The periodic oscillations in drainage winds are at least partially confirmed by observations although the observed amplitudes of the surges are much smaller than theory predicts.

Fleagle concludes that the results (c) and (d) are due to the compressibility and inertia of the air and the contradiction with the results obtained by Jeffreys (1922), who found a direct variation of slope velocity with angle, is attributed to Jeffreys' use of an incompressible atmosphere.

Recently several studies have investigated the influence of a large-scale terrain slope on the flow within the boundary layer above such a slope. Holton (1967) considered a coupling of thermal forcing, due to the diurnal insolation cycle, with the viscous (Ekman) boundary layer. A set of three second order differential equations was derived which described the dynamics of the boundary layer. These are the usual time dependent Ekman equations with gravitational terms added for the sloping terrain and a thermodynamic equation containing the diurnal heating function. In the case of a stably stratified atmosphere the effect of potential temperature advection opposes the buoyancy force so that the diurnal boundary layer wind oscillation along the slope is largely suppressed. Solutions to these equations are obtained by standard methods and for conditions of neutral stability or level ground the wind field reduces to that of the usual Ekman spiral formula. The solutions show further that thermal effects over sloping terrain may contribute substantially to the diurnal wind oscillation. The use of constant coefficients of eddy viscosity and heat diffusion was felt to be a major weakness of the theory. However, including time and height variation of these coefficients would require a numerical integration of the equations.

Lettau (1966; Lettau and Schwerdtfeger, 1967) has discussed the mechanisms of a large-scale drainage flow over the interior of Antarctica. He found that when the large-scale terrain slope is gentle and a strong surface temperature inversion persists, the thermal "inversion wind" prevails rather than katabatic flow. A more quantitative development of a phenomenon entitled the thermo-tidal wind has

also been given by Lettau (1967), which has more general application to all large-scale terrain slopes. This theory encompasses the coupling of the viscous and thermal boundary layers as examined by Holton and further includes a quasi-tidal solar forcing function. By analogy to tidal theory the dynamic response of the atmospheric boundary layer to the harmonic forcing function is considered. The dynamical impedance of the boundary layer is a function of the Coriolis parameter so that the phase lag or lead between forcing and response functions is dependent on latitude. A qualitative application of the theory to observations shows that it can account for the latitudinal variation in the phase angle of thermal slope winds.

Neither of the above boundary layer approaches to slope winds present a complete theory in that the return flow is not considered. However, the basic principles of these developments are important when considering the properties of the flow above an extended sloping surface.

The interaction of the thermodynamic slope circulation with the large-scale gradient flow has not been treated in any of these analytic models. Effects of atmospheric stability, upwind terrain, and shape of the mountain ridge should determine the penetration of prevailing flow into leeward slope regions. Only a qualitative treatment of flow separation from mountain surfaces by Scorer (1955) has been offered.

#### Numerical Slope Wind Experiments

The advent of high speed computer technology in recent years has made possible the solution of equations by numerical means. Thyer and Buettner (1962; also Thyer, 1966) presented one of the first numerical experiments of valley winds. They experimented with various forms of the equations and grid networks having different densities, finally arriving at a stream function representation of the two-dimensional flow, incorporating eddy viscosity effects by the

Fickian equation. A ground to air heat input was defined. Computational stability difficulties limited the numerical integrations to only two minutes so time variations of the slope circulation could not be investigated. Nevertheless, the early computations revealed flow fields with striking similarity to those given by observations.

Orville (1964) carried out a numerical study of mountain upslope winds which were initiated by a diurnal potential temperature oscillation at the surface. A mountain one kilometer high with a 45 degree slope was used. The Boussinesq system of equations was employed. (If the conclusions made previously by Fleagle (1950) are correct, such an incompressible system may not be realistic for studying the case of downslope flow.) Diffusion was again given by the Fickian equation. The circulation which developed originated near the bottom of the slope, strengthened with time, and moved up and away from the surface. The advection of isentropes by the circulation resulted in a packing of isentropes in the cap over the ridge. In its early stages the upslope flow extended only about 100 m above the surface but increased with time, particularly increasing with distance up the slope. Velocities of about  $3 \text{ m sec}^{-1}$  were attained after about one hour and a countercurrent also appeared. These results generally conform to the observations given by Defant (see Figure 3.1). Under stable conditions, using a potential temperature lapse rate of  $1^\circ \text{C km}^{-1}$ , the circulation was found to develop only half as fast with a decrease in potential temperature gradients near the mountain surface. Later forms of the model (Orville, 1965, 1968a) included moisture effects and were particularly directed towards a study of the formation of cumulus clouds over mountain slopes.

A comparable numerical procedure was used by Fosberg (1967) except for the form of the viscous and diffusive terms. Comparisons of the developing solenoidal cell and energy integrals were made with a two-day field study. The simulation was found to reproduce the major features and processes of the slope wind and its convective chimney.

All of the above models have been on the scale of only a few kilometers so that Coriolis effects were neglected. Lettau (1967) points out that Coriolis effects cannot be ignored in realistic slope models if the horizontal extent is at least of meso-scale. A recent paper by Magata and Ogura (1967) examined air flow over mountains on a scale of 10's of km under the influence of heating or cooling from below. The effect of heating along the mountain slope and the details of the flow along the mountain slope were not resolved by the grid scheme used. An interesting result of the experiment was the formation of a series of convective cells in the unstable layer to the lee of the mountains.

A numerical procedure developed by Haurwitz (1962) is of interest even though it has not been applied to a case of sloping terrain. The model is based on the Bjerknes circulation theorem and retains both Coriolis and frictional forces. The resulting non-linear equation is

$$\frac{d}{dt} \left( \frac{u^2 + v^2}{2} \right) = -k(u^2 + v^2) + \frac{gz}{4T} \left( \Gamma - \frac{d\tau}{dt} \right)$$

where  $k$  is the friction coefficient,  $\Gamma$  is the rate of temperature change, and  $\tau$  is the temperature difference between ascending and descending branches of the flow. The change in kinetic energy is thus partly due to friction and partly due to temperature advection. The important advantage of this formulation over the simpler circulation theorems discussed earlier is that the atmospheric motions which develop are able to modify the temperature field which drives the circulation.

#### IV. THEORETICAL SLOPE CIRCULATION MODEL

Analytic solutions to the general hydrodynamic equations are difficult to obtain because the advection terms render the equations nonlinear, therefore, most of the analytic treatments have been linearized to varying degrees so that in general horizontal advection terms have been omitted and temperature profiles have been arbitrarily specified. The initial organization of a convective circulation is basically a non-linear process and is thus difficult to treat analytically. The primary advantage of the numerical approach is in the retention of the non-linear advective terms in the equations. In this way the feedback effect of the wind field itself on the original temperature field may be considered and the coupled alterations between wind field and temperature field are retained as the motion develops. Linearization of the equations to analytically tractable form decouples this interaction and much of the basic physics of the process is lost.

The complexity of three-dimensional flow, computer storage limitations, and computation time demands generally restrict the application of a three-dimensional modeling approach to simple fluid phenomena--e. g. , Deardorff (1965). Furthermore, two-dimensional models in vertical cross-section have been found to reveal significant features of orographically controlled circulations on both the meso-scale--e. g. , slope winds, Orville (1964, 1967)--and on the planetary-synoptic scale--e. g. , Asian monsoon, Murakami et al. (1969). The longitudinal uniformity of the Rocky Mountains-Great Plains latitudinal cross-section permits the introduction of such an idealized two-dimensional numerical model. It is felt that this type of model experiment is warranted and that the actual situation may be represented adequately by the system of equations and conditions derived

in this chapter so as to describe the general characteristics of the Rocky Mountains-Great Plains circulation in the real atmosphere.

Although numerical solutions are readily obtained in principle, the solutions are also limited in extent by the non-linear advection, or transport terms. Finite difference approximations of the advective terms can introduce both phase and amplitude errors. The accuracy of various finite-differencing schemes applied to advective equations has recently been investigated by Crowley (1968) and Molenkamp (1968).

The basic hydrodynamic equations may be treated in either advective or flux forms. For the advective form, e. g. ,  $\frac{\partial \xi}{\partial t} + \mathbf{w} \cdot \nabla \xi = 0$  (where  $\xi$  is any arbitrary quantity), the finite difference approximations to the advection term are not necessarily momentum conserving. In the so-called flux or conservation form, e. g. ,  $\frac{\partial \xi}{\partial t} + \nabla \cdot \xi \mathbf{w} - \xi \nabla \cdot \mathbf{w} = 0$ , transports appear as flux divergence which by Green's theorem may be transformed to surface integrals. Finite difference approximations of these terms are mass and momentum conserving if the equations are properly compared with respect to accuracy, numerical stability, and conservation (Crowley, 1968).

The disadvantage of the flux form is that proper evaluation of the transport terms may be quite time consuming while the advective form may give simpler equations to be solved. Thus from practical considerations the advective form of the equations is often invoked. Although the advective form of the equations may not be conservative, it is still possible that the significant quantities are approximately conserved and the exchange of accuracy for efficiency does not necessarily imply that the results are unreliable (Crowley, 1968). Various numerical experiments have found the advective formulation suitable in local circulation problems (e. g. , Pearce, 1955; Malkus and Witt, 1959; Fisher, 1961; Ogura, 1963); in fact, Orville (1964) found the flux form of the equations produced very irregular

unrealistic temperature fields which did not appear in the advective system. Based on these considerations the advective formulation of the equations was deemed most expedient in treating the problem at hand.

### Derivation of Model Equations

General equations of motion:

$$1) \frac{du}{dt} = -\alpha \frac{\partial p}{\partial x} + fv + F_x$$

$$2) \frac{dv}{dt} = -\alpha \frac{\partial p}{\partial y} - fu + F_y$$

$$3) \frac{dw}{dt} = -\alpha \frac{\partial p}{\partial z} - g + F_z$$

State conditions:  $p\alpha = RT$  and  $T = \theta \left( \frac{p}{p_0} \right)^\kappa$ , where  $\kappa = R/c_p$ . For convenience the non-dimensional variable  $\pi$  is defined to replace pressure,

$$\pi = \left( \frac{p}{p_0} \right)^\kappa$$

then,

$$\alpha \nabla p = \frac{RT}{p} \nabla p = R\theta \frac{p^{\kappa-1}}{p_0^\kappa} \nabla p = \frac{R\theta}{\kappa} \nabla \left( \frac{p}{p_0} \right)^\kappa = c_p \theta \nabla \pi$$

The mountain slope is treated as extending infinitely in the  $y$  direction and it is assumed that there are no changes in variables parallel to the slope:

$$1a) \frac{\partial u}{\partial t} = -u \frac{\partial u}{\partial x} - w \frac{\partial u}{\partial z} - c_p \theta \frac{\partial \pi}{\partial x} + fv + F_x$$

$$2a) \quad \frac{\partial v}{\partial t} = -u \frac{\partial v}{\partial x} - w \frac{\partial v}{\partial z} - fu + F_y$$

$$3a) \quad \frac{\partial w}{\partial t} = -u \frac{\partial w}{\partial x} - w \frac{\partial w}{\partial z} - c_p \theta \frac{\partial \pi}{\partial z} - g + F_z$$

Next the  $\theta$  and  $\pi$  variables are expanded in terms of a reference-state equilibrium value (adiabatic) and a deviation from this reference state,

$$\theta = \bar{\theta} + \theta' \quad , \quad \pi = \bar{\pi}(z) + \pi'$$

where the primed quantities are assumed to be at least one order of magnitude smaller than the corresponding reference-state values.

Substitution of the expanded terms into equations 1a) and 3a) gives:

$$1b) \quad \frac{\partial u}{\partial t} = -u \frac{\partial u}{\partial x} - w \frac{\partial u}{\partial z} - c_p \bar{\theta} \frac{\partial \bar{\pi}}{\partial x} - c_p \theta \frac{\partial \pi'}{\partial x} + fv + F_x$$

$$3b) \quad \frac{\partial w}{\partial t} = -u \frac{\partial w}{\partial x} - w \frac{\partial w}{\partial z} - c_p \bar{\theta} \frac{\partial \bar{\pi}}{\partial z} - c_p \theta \frac{\partial \pi'}{\partial z} - g + F_z$$

If it is assumed that the reference-state is in hydrostatic equilibrium:

$$c_p \bar{\theta} \frac{\partial \bar{\pi}}{\partial z} = -g$$

and assuming  $\theta \sim \bar{\theta}$ ,

$$\text{then, } c_p \theta \frac{\partial \pi}{\partial x} = c_p \theta \frac{\partial \pi'}{\partial x} \approx c_p \bar{\theta} \frac{\partial \pi'}{\partial x}$$

$$\text{and, } c_p \theta \frac{\partial \pi}{\partial z} = c_p \theta \frac{\partial \pi'}{\partial z} - g \frac{\theta}{\bar{\theta}} \approx c_p \bar{\theta} \frac{\partial \pi'}{\partial z} - \left(1 + \frac{\theta'}{\bar{\theta}}\right) g$$

This gives:

$$1c) \quad \frac{\partial u}{\partial t} = -u \frac{\partial u}{\partial x} - w \frac{\partial u}{\partial z} - c_p \bar{\theta} \frac{\partial \pi'}{\partial x} + fv + F_x$$

$$3c) \quad \frac{\partial w}{\partial t} = -u \frac{\partial w}{\partial x} - w \frac{\partial w}{\partial z} + \frac{g}{\theta} \theta' - c_p \bar{\theta} \frac{\partial \pi'}{\partial z} + F_z$$

For an incompressible fluid the equation of continuity becomes

$$4) \quad \frac{\partial u}{\partial x} + \frac{\partial w}{\partial z} = 0$$

The assumption of incompressibility is confined to the equation of continuity since changes in density due to non-adiabatic heating are essential to the theory. The incompressibility assumption eliminates sound waves and allows longer time steps to be used in the numerical integration.

Elimination of  $\pi'$  from 1c) and 3c) by cross differentiation yields a vorticity equation which is convenient for computational purposes:

$$5) \quad \frac{\partial \eta}{\partial t} = -u \frac{\partial \eta}{\partial x} - w \frac{\partial \eta}{\partial z} - f \frac{\partial v}{\partial z} + \frac{g}{\theta} \frac{\partial \theta'}{\partial x} + \frac{\partial}{\partial x} F_z - \frac{\partial}{\partial z} F_x$$

where

$$6) \quad \eta = \frac{\partial w}{\partial x} - \frac{\partial u}{\partial z}$$

Since incompressible flow has been assumed, a stream function may be defined, where

$$7) \quad u = -\frac{\partial \psi}{\partial z}, \quad w = \frac{\partial \psi}{\partial x}$$

thus,

$$6a) \nabla^2 \psi = \eta .$$

For convenience in the numerical analysis, numerical integrations will be performed in terms of the stream function.

The first law of thermodynamics is represented as the equation for specific entropy of air:

$$8) \frac{\partial \phi}{\partial t} = -u \frac{\partial \phi}{\partial x} - w \frac{\partial \phi}{\partial z} + D_{\phi} \quad \text{where}$$

$$9) \phi = \frac{\theta'}{\theta} , \quad \text{and } D_{\phi} \text{ is the heat diffusion term.}$$

The basic set of equations for the model includes three prognostic equations 2a), 5), and 8), one diagnostic equation 6a), and the defining relationships 7) and 9).

According to Ogura and Phillips (1962) (cf. Spiegel and Veronis, 1960; Dutton and Fichtl, 1969), this system of equations is suitable for describing the motion where the potential temperature is almost constant and "shallow convection" is considered, i. e.,  $z/H \ll 1$  where  $H \sim 30$  km ( $H$  = depth of an adiabatic atmosphere). Phillips (1967) suggests a somewhat less restrictive condition,  $z/H < 1$ , thus including all convective phenomena.

The restrictions of the application of the Boussinesq approximations to "shallow convection" has generally led to the use of a domain 5 km or less in depth (cf. Asai, 1964; Ogura and Charney, 1962), although in his sea-breeze model Fisher (1961) used a depth of nearly 8 km. Certainly in the upper regions the uniform density assumption is not valid since  $\rho_0(z = 10 \text{ km}) \sim 0.4\rho_0(z = 1.5 \text{ km})$ ;

however, the character of the flow at lower levels (< 6.5 km) should not be strongly affected and the absence of an upper boundary at a physically unrealistic level in a motion on this scale would seem to be an important consideration. While the magnitude of the wind components at upper levels may not be realistic in terms of momentum conservation, the general pattern of the flow should not be affected and the important features of this circulation should still appear.

Treatment of Friction and Diffusion Terms

$$\begin{aligned} \text{In general, } F_{x,y,z} &= f(K_m, V), & K_m &= \text{eddy viscosity} \\ D_\phi &= f(K_H, \phi), & K_H &= \text{eddy thermal conductivity} \end{aligned}$$

As a first approximation let:

$$K_{(x,y,z)} = K_m \nabla^2 V; \text{ i. e., } F_x = K_m \nabla^2 u, F_y = K_m \nabla^2 v, F_z = K_m \nabla^2 w$$

$$D_\phi = K_H \nabla^2 \phi$$

where  $\nabla^2 = \frac{\partial^2}{\partial x^2} + \frac{\partial^2}{\partial z^2}$  .

Assuming  $K_m$  is a constant (i. e., Fickian diffusion), equation 5) becomes

$$5a) \quad \frac{\partial \eta}{\partial t} = -u \frac{\partial \eta}{\partial x} - w \frac{\partial \eta}{\partial z} - f \frac{\partial v}{\partial z} + \frac{g}{\theta} \frac{\partial \theta'}{\partial x} + K_m \nabla^2 \eta .$$

It will be further assumed that  $K_m = K_H = K$  as a first approximation. Following Malkus and Witt (1959), Ogura (1963), and Orville (1964),

the eddy coefficients are estimated by Richardson's empirical formula  $K = 0.2 \ell^{4/3}$  (Richardson, 1926; see also Sutton, 1953; Pasquill, 1962), where  $\ell$  is the distance between grid points. For a vertical grid interval of 250 m this gives a value of about  $15 \text{ m}^2 \text{ sec}^{-1}$ . Since turbulent exchange is the link over the 10 m distance between the surface heating and the lowest grid points (see below), a value of  $K (= K')$  must also be specified there. An initial value of  $K' = 0.2 \text{ m}^2 \text{ sec}^{-1}$  was determined for the surface transfer term similarly estimated from Richardson's formula.

A significant diurnal variation in the exchange coefficient at low levels has been observed by such studies as Jehn and Gerhardt (1950) and Wong and Brundidge (1966). Quite an abrupt change in the coefficient is noted near sunrise and sunset with only slight mean variations during the intervening periods. In general the coefficient decreases by about an order of magnitude between day and night. This variation was included in the model by reducing the surface exchange coefficient ( $K'$ ) to  $0.02 \text{ m}^2 \text{ sec}^{-1}$  during periods of surface cooling (see below).

The use of non-zero eddy transfer coefficients has also been found to act as a smoothing device which prevents rapid development of numerical errors when advective terms dominate (Malkus and Witt, 1959).

#### Insolation Heating at the Surface

The driving agent of this circulation is the insolation heating and radiational cooling of a sloping surface. In this model (following Estoque, 1961; Fisher, 1961; Orville, 1964) this effect is specified as a diurnal potential temperature oscillation which is applied at the surface. This potential temperature variation at the mountain slope gives rise to a horizontal potential temperature gradient which in turn creates vorticity and initiates fluid motion.

More complex methods of introducing insolation heating have been employed--e. g. , the computation of a heat balance at the earth's surface, Magata (1965)--however, the level of sophistication in other aspects of this model gives little justification for using a more refined technique.

The surface temperature change is specified by the equation

$$\theta_s' = \bar{\theta}'(z) + C(z) \sin \frac{\pi t}{12 \times 3600}$$

where  $\bar{\theta}'(z)$  represents the initial thermal stratification of the atmosphere,  $C(z)$  represents the amplitude of the surface temperature oscillation as a function of height, and  $t$  equals time in seconds along the diurnal sine curve.

Following the findings of Orville (1964) that air which is warmed and creates vorticity through horizontal temperature gradients must be permitted to participate in the motion if realistic results are to be obtained, the surface potential temperature is propagated upward by diffusion a distance of 10 m to the lowest grid points of the model (cf. Fisher, 1961) and is then permitted to move parallel to the surface with a velocity given by a non-centered differencing of the stream function. Thus, both turbulent heating and advective cooling can occur at the lowest grid points.

The surface temperature amplitude function  $C(z)$  was estimated from a combination of data sources. Summer thermograph traces at stations in northeast Colorado (provided by the Colorado State University Hail Project) and at Berthoud Pass (provided by A. Judson of the Forest Service), studies in the Bavarian Alps reported by Geiger (1959), observations in the Santa Cataline Mountains of Arizona reported by Braham and Draginis (1960) and Silverman (1960), and comparisons of free air and mountain slope observations in the Rocky Mountains by Samson (1965) and on Brocken Mountain in Germany by Hänsel (1962) were all

included in the evaluation. On the basis of these data a surface heating function was introduced having a diurnal temperature amplitude of  $9^{\circ}\text{C}$  on the plain and decreasing to  $5^{\circ}\text{C}$  at the peak of the ridge.

### Boundary Conditions

In order to obtain a solution to the set of equations, the values of dependent variables must be specified at the boundaries. The upper boundary ( $z = M$ ) is treated as a rigid top (approximating the tropopause). The dependent variables are held constant at the upper boundary and no flow is permitted to cross it.

The two lateral boundaries are treated in different ways. Under initial conditions in which the atmosphere is at rest no flow is permitted to cross the left-hand boundary (over the mountain peak), however tangential flow is permitted at this boundary. We may thus write  $u = 0$  at  $x = 0$  and  $w = 0$  at  $z = M$ . The right-hand boundary (over the plain) does not represent a physical barrier of any type since the plain is assumed to extend indefinitely in this direction. Therefore, finite velocities normal to this boundary are permitted. Values of the dependent variables at this boundary are linearly extrapolated from the most recent values at two internal points. This procedure has been shown by Nitta (1962) to be stable for long wave disturbances with only slight noise formation at high wave numbers. In this way nearly flat gradients of the variables are maintained at the boundary so that fictitious disturbances do not propagate into the grid while disturbances originating in the interior of the grid are allowed to propagate out of the grid without reflection back into the region. At the lowest grid points tangential flow is also the restriction. These velocities are obtained by non-centered differences of the stream function.

To satisfy the given velocity boundary conditions, corresponding boundary conditions must be imposed on the stream function  $\psi$ . All of these conditions can be met by putting  $\psi = \text{constant}$  at the slope surface,

at the upper boundary, and on the vertical plane through the mountain ridge (left-hand boundary). Since  $\psi$  occurs in the equations only in its derivatives, the constant is arbitrary and is readily made zero. At the right boundary  $\psi$  is linearly extrapolated from two internal points.

Values of vorticity are similarly assigned to all boundaries. Certainly vorticities at the lower grid points may affect the vorticity values one grid interval into the interior through advection and turbulent terms. However, Malkus and Witt (1959) found their results to be rather insensitive to various assumptions regarding boundary values of vorticity and velocity. Although the vorticity will generally not be zero at the surface due to large shears in this region, the complexity of computing a value of vorticity here and the apparent negligible effect this has at interior grid points (as evidenced by the models of Fisher (1961) and Orville (1967)) justifies using  $\eta = 0$  at the lowest grid points.

The thermodynamic variable  $\phi$  is held constant at the upper boundary. At the right-hand boundary  $\phi$  is also linearly extrapolated from two internal points. At the left-hand boundary the variation of  $\phi$  is computed from the thermodynamic equation assuming reflective symmetry. At the lower grid points heating is accomplished by diffusion from the heated surface 10 m below. This diffusion term is given by

$$K' \nabla^2 \phi$$

and is computed in the following numerical form (see Figure 4.1).

$$K' \left[ \frac{(\phi_1 + \phi_2 - 2\phi_0)}{(\Delta x)^2} + \frac{(\phi_3 + \phi_4 - 2\phi_0)}{(\Delta z)^2} \right]$$

or assuming  $\phi_0 = \phi_2 = \phi_4$  and  $\phi_1 = \phi_3$

this reduces to

$$K' \left[ \frac{\phi_1 - \phi_0}{(\Delta x)^2} + \frac{\phi_1 - \phi_0}{(\Delta z)^2} \right]$$

where  $\Delta z$  is 10 m and  $\Delta x$  is given as 200 m on the mountain slope.

Advection parallel to the slope is permitted at the lower grid points.

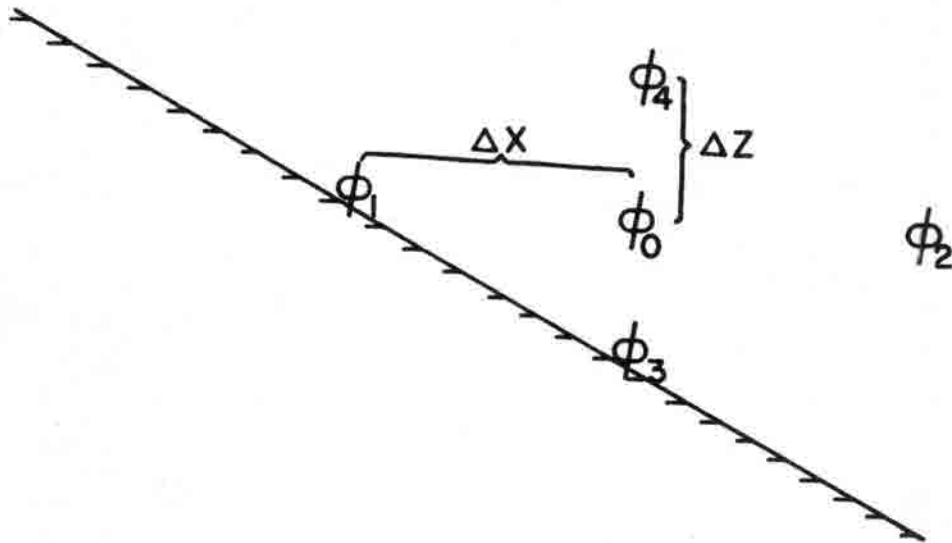


Figure 4. 1. Scheme for computing diffusion at lower boundary grid points.  $\phi_0$  represents the actual grid point.  $\phi_1$  and  $\phi_3$  are located on the surface.

### Computational Instability

The solution of differential equations by numerical integration yields small computational errors which arise from finite differencing approximations to derivatives and from round-off. In order that these

errors do not grow without bounds and rapidly destroy the validity of the calculation, the length of the time step in the integration must be restricted relative to the grid interval and certain other physical parameters in the equations. It was first shown by Courant et al. (1928) that simply decreasing the size of finite space and time increments would not guarantee a convergence of the finite-difference equation solution to that of the corresponding differential equation. For equations of the hyperbolic type the time increment must be such that neither fluid nor energy can propagate across a grid interval in a single time step. The existence of computational instability also depends on the particular finite-difference approximation being used.

For cases where the meteorological equations are linear these conditions are well-known (Charney, 1949; Gates, 1959; Thompson, 1961), as given by the Courant-Friedrichs-Lewy linear stability condition,  $(u + c) \frac{\Delta t}{\Delta x} \leq 1$ . For the case of the linearized heat-diffusion equation in which advective terms are omitted and the eddy coefficient  $K$  is treated as a constant, the forward explicit extrapolation system stability criterion is also well-known (e. g. , Richtmyer, 1957) and is given by  $\frac{2K\Delta t}{(\Delta z)^2} \leq 1$ . The non-linear cases are much more difficult to handle and not well understood. Richtmyer (1957) suggests that for cases of fluid flow in the presence of heat flow, by intuition the heat-flow equation would dominate in the limit if both equations are treated explicitly. Thus the heat-diffusion condition should be used. This stability criteria has been used for this computational method by Fisher (1961) and Orville (1964). Magata (1965; Magata and Ogura, 1967) requires that both of the above conditions be met. Deardorff (1967) also discusses the simultaneous application of both linear stability criteria.

Since the model equations above eliminate sound waves (incompressible) and the boundary conditions exclude external gravity waves (rigid lid), the maximum disturbance velocity will be given by the

representative velocity of internal gravity waves  $\sim 50 \text{ m sec}^{-1}$  (Thompson, 1961; cf. Sasaki, 1959).

If it is required that both of the above stability criteria are simultaneously satisfied for the smallest  $\Delta x$  and  $\Delta z$ , the choice of  $\Delta t$  can be simply estimated. Assuming only moderate winds ( $\sim 10 \text{ m sec}^{-1}$ ) are generated by the slope circulation, a time step of one minute is well within limits of the stability criteria. Baer and Simons (1968) point out that using a time increment substantially less than the critical one determined from linear analysis considerably reduces truncation errors.

### Numerical Method

A number of finite difference approximations to the hyperbolic equations of fluid dynamics have been described in the literature (Richtmyer, 1963) each having its theoretical and computational advantages and disadvantages. Orville (1964) in modeling mountain slope winds ran into serious problems using the flux form of the equations and the Lax-Wendroff differencing scheme (Lax and Wendroff, 1960). Similar problems were encountered by Fisher (1961); also Thyer and Buettner (1962) developed early instabilities using a center differencing technique. Orville was able to trace the irregularities in his work to the use of centered space differencing in the advective terms and alleviated the problem by upstream differencing of the advective form of the equations. In later versions of his model Orville (1967, 1968a) used upstream differencing of the advective terms only and centered space differences in other terms combined with non-centered time differences. Similar differencing procedures have been used by Fisher (1961), Magata (1965), and Lavoie (1968). The upstream differencing technique has been treated rigorously by Courant et al. (1952). This scheme is computationally stable under

the conditions previously defined and is frequently used because of its simplicity.

Other differencing schemes, especially higher order types, would no doubt be useful, e. g., Arakawa's method (Arakawa, 1966; Lilly, 1964, 1965; Fosberg, 1967) or the Roberts-Weiss method (Roberts and Weiss, 1966; Molenkamp, 1968). The Leap-Frog scheme (Richtmyer, 1963) has also been used in small-scale circulation problems by Malkus and Witt (1959), Lilly (1962) and Nickerson (1965). An evaluation of the accuracy of the various finite-difference methods as applied to the advection equation has been made by Molenkamp (1968). Molenkamp examined the accuracy of the upstream differencing technique for the case of a steady velocity field where the problem becomes linear and comparisons can be made with the analytically correct solution. He found that this differencing scheme introduces a pseudo-diffusive effect which is a function of the grid spacing, time increment, and velocity. Crowley (1968) similarly shows that inaccuracies caused by the implicit diffusion occur when upstream differencing is applied to pure advection equations. The significance of this error in the more complex turbulence-plus-advection problem has not been ascertained unless it can be assumed that turbulent diffusion and advection are physically distinct processes which are mathematically separable. Orville (1968b) suggests that the truncation error is not serious and that higher order finite difference schemes are not necessary for local-scale models at the present level of sophistication.

Based on present knowledge and economic expediency in terms of computational time, the uncentered differencing scheme will be employed for the advective terms. Fosberg (1969) has recently also found this scheme to be computationally most efficient.

The importance of time differencing techniques in studying long-term fluctuations has been pointed out by Lilly (1965) and Young (1968).

More than a dozen methods have been used or suggested with various degrees of complexity and yielding various orders of accuracy. Initially the simple Euler (forward) method was employed as in most of the previously discussed experiments. This method retains only one time level in the arrays and gives first order accuracy. In later versions of the model the second order Adams-Bashforth scheme (Lilly, 1965) was adopted in which two time levels are retained. Lilly showed this technique to be highly stable and accurate while retaining computational efficiency. Where comparisons were made the Adams-Bashforth scheme gave results generally comparable to the simple forward time differencing after integrations of several hours.

The solution of the stream function field from the vorticity field was carried out by the extrapolated Liebmann process (Thompson, 1961) using an over-relaxation coefficient of 0.65. The stream function was determined to an accuracy of  $\pm 0.1$  which corresponds to a wind field accuracy of  $\pm 0.04 \text{ cm sec}^{-1}$  in the u component and  $\pm 0.002 \text{ cm sec}^{-1}$  in the w component. The relaxation procedure took from 20 to 30 passes depending on the initial conditions being studied and used 70 to 75 per cent of the 2.2 to 3.0 seconds required for one time integration.

### Grid Scheme

The problem suggests a fairly large horizontal extent while still retaining a reasonable amount of grid detail over the mountain slope. To keep the total number of calculations within reasonable limits in terms of computation time, an expanding horizontal grid was used over the plain surface where a coarse resolution was felt to be adequate. The horizontal grid increment of 5 km over the mountain was expanded by 5 km each increment away from the slope to a maximum of 40 km. In this way details of the circulation near

the slope are resolved while at the same time gross features of the circulation are evaluated at considerable distances from the mountain slope (see Figure 4.2). Comparable differencing methods have been used in the horizontal by Estoque (1961) and in both horizontal and vertical coordinates by Fisher (1961) for sea breeze models, apparently without any computational difficulties.

A vertical grid increment of 250 m was used up to one level above the mountain peak and then expanded to 500 m up to the upper boundary. A 16 x 22 grid system was employed.

The mountain slope has a width of 35 km and a vertical extent of 1.75 km from base to peak (as approximated from contour maps of the northern Colorado Front Range). The plain surface extends 180 km eastward from the base of the slope. Since the plain itself has a slight slope (typically  $\sim 1/400$ ) a parameterization of this effect was included by extending the distance between the actual surface and the bottom row of grid points in such a way that the heat diffusion produced a linear variation in the horizontal temperature gradient. The effect of this was to produce upslope velocity components at all lower boundary grid points during periods of heating, which was not the case for a horizontal plain surface.

#### Initial Conditions

A flow chart of the numerical program is given in Figure 4.3. Potential temperature and ambient wind fields are specified initially. A reference-state potential temperature of  $296^{\circ}\text{C}$  is used. When stable conditions are specified, a potential temperature increase of  $1.0^{\circ}\text{C km}^{-1}$  is normally used which is supported by morning (1200 GMT) Denver soundings during summer. The ambient wind field used similarly corresponds to upper wind conditions commonly found at Denver during summer. More specific conditions will be described in the individual cases discussed in the next chapter.

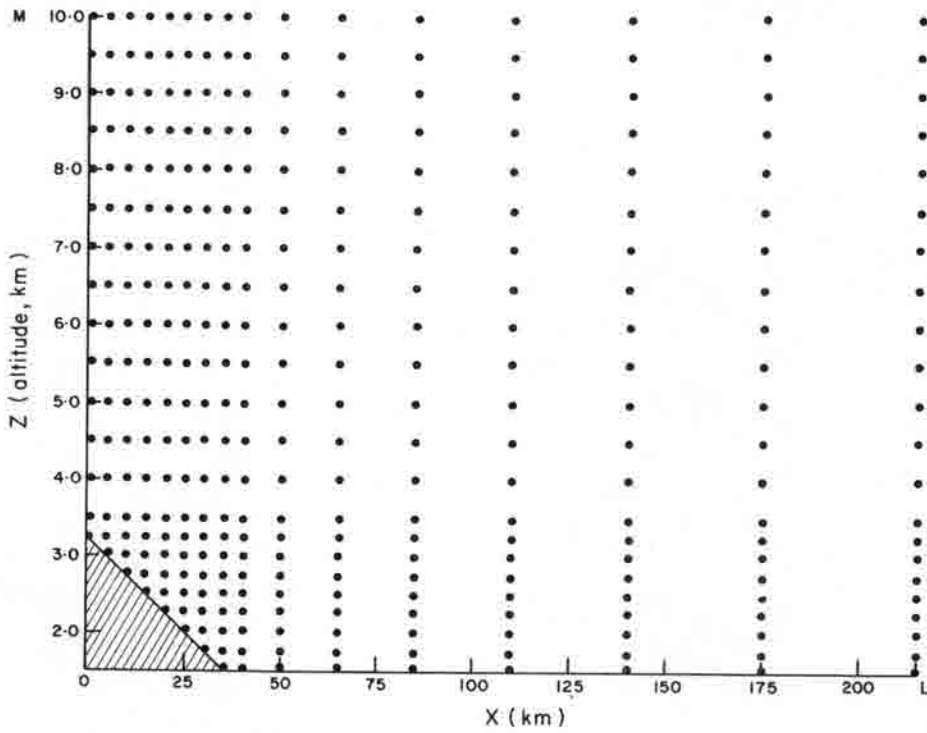


Figure 4.2. Computational grid mesh.

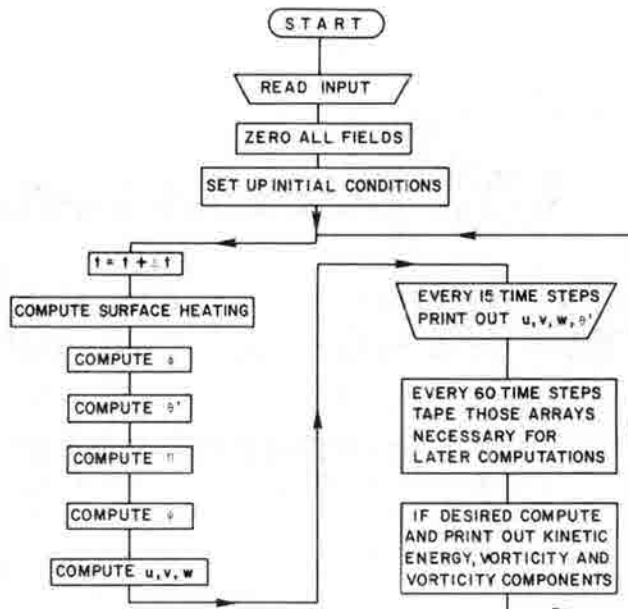


Figure 4.3. Flow chart of the numerical program. Symbols are defined in Preface.

## V. MODEL RESULTS

In all of the daytime cases the circulation was initiated four hours prior to the time of maximum surface temperature. A careful check of a number of thermograph traces for northeast Colorado indicated that minimum and maximum temperatures normally occurred between 0400 to 0600 MST and 1600 to 1800 MST, respectively. Thus, the time span tested in the model corresponds to early afternoon development. Most integrations were carried out over a period of two hours using a time step of one minute. This period of time appeared to be sufficient to permit an evaluation of the development of most of the circulation features.

Since moisture effects were not included in the formulation of the model, the role of condensation in the release of latent heat aloft and in the reduction of heating at the surface could not exert its proper controls in later stages of the circulation development. (Typically cumulus formation over the mountain ridge is quite extensive by 1200 LT.) Extending the integration to four hours--the time of maximum surface heating--led to the generation of large upslope wind vectors ( $\sim 20 \text{ m sec}^{-1}$ ) near the upper mountain slope. The reduction in surface radiation due to cloud cover as well as low level frictional drag due to the extremely irregular terrain over the mountain slope would seem to act as a control on this development.

### Case A-Adiabatic

The first application of the circulation model was to an adiabatically stratified atmosphere initially at rest. Evolution of the stream function is shown in Figure 5.1 after 30 minutes, 60 minutes, and 120 minutes of real time. Displacement of the stream function center at 15 minute time intervals is seen in Figure 5.2. A rapid development

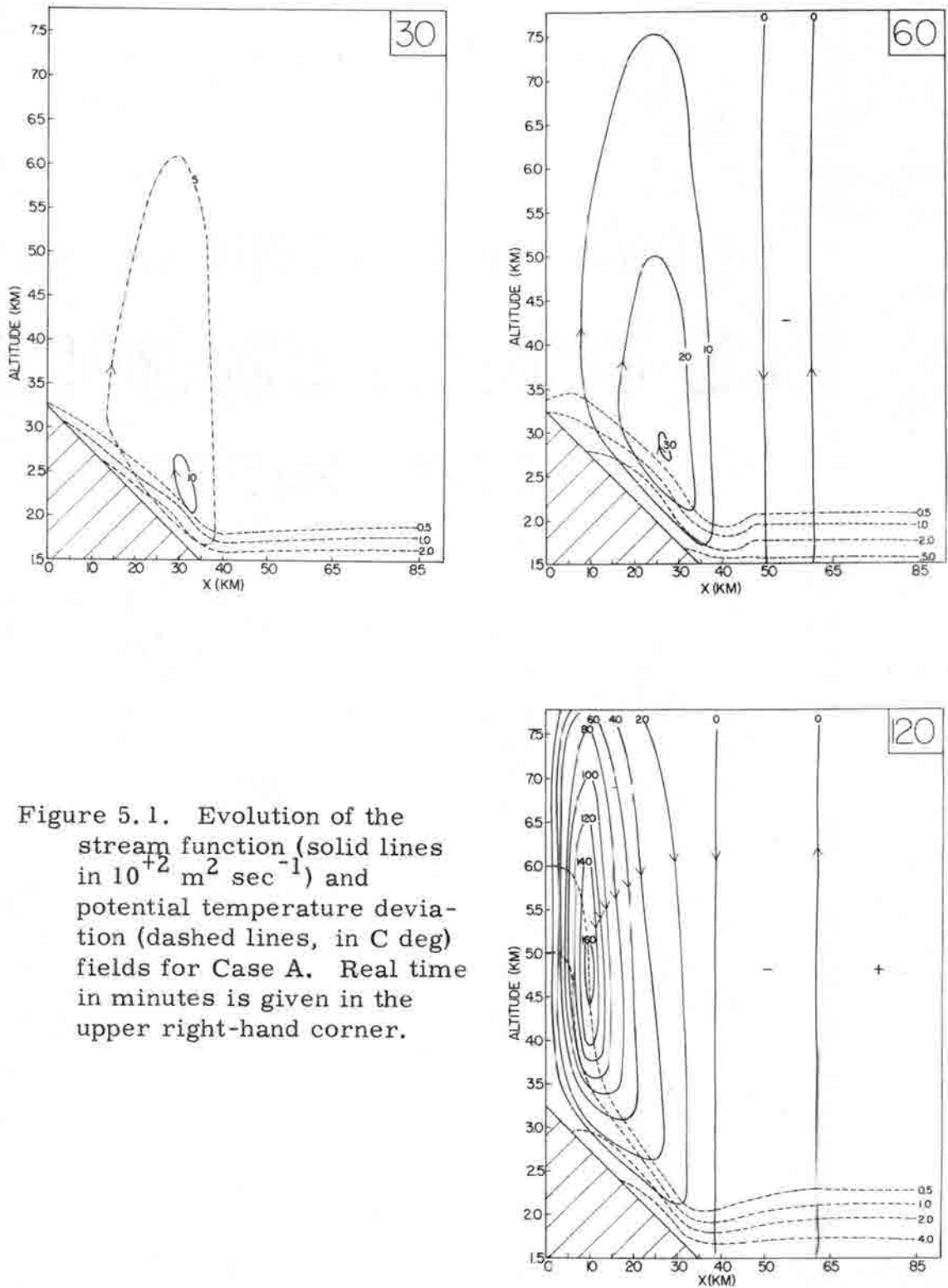


Figure 5.1. Evolution of the stream function (solid lines in  $10^{+2} \text{ m}^2 \text{ sec}^{-1}$ ) and potential temperature deviation (dashed lines, in C deg) fields for Case A. Real time in minutes is given in the upper right-hand corner.

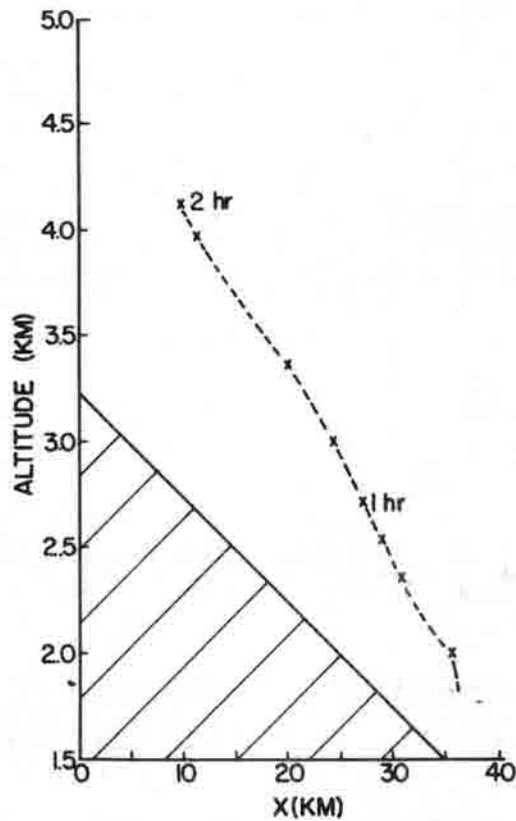


Figure 5.2. Trajectory of the stream function center for Case A shown at 15 minute positions.

with time is observed with the stream function center forming near the slope-plain intersection and then moving up and away from the slope surface. The development is similar to that described by Orville (1964) on a smaller scale. This smaller scale would appear as local variations in the problem under study, produced by individual peaks and ridges.

The potential temperature field (Figure 5.1) changes slowly during the first hour and then undergoes a more rapid development during the second hour when advective changes become large. A "convective chimney" is barely visible after one hour and at the end

of two hours it is seen to reach a level several kilometers above the ridge. The dominance of advective terms may also be observed in the compression of isotherms above the lower half of the slope and in the near lee where the descending branch of the circulation is strong. This descending flow extends 15 to 20 km into the plain. After about an hour a series of weak cells appears beyond the primary mountain slope circulation. These cells seem to be characteristic of an unstably stratified atmosphere and have been explained in terms of inertia-gravity wave theory (Lilly, 1960; cf. Magata and Ogura, 1967). The scale of these disturbances in numerical experiments is determined by the grid interval.

The condition of neutral stability is not characteristic even of the troposphere during summer and thus provides only a first look at the modeling procedure. Evening soundings (0000 GMT) over the Great Plains will frequently show a near adiabatic layer extending as high as 3 km above the surface, however, morning soundings typically reveal weak stability up to this level.

#### Case B--Weak Stability

Typical 1200 GMT soundings during summer at Denver indicate a potential temperature lapse rate of about  $1^{\circ}\text{C}$  per kilometer in the lower troposphere above the nocturnal inversion. This provides the more realistic initial conditions for the second case study.

Development of the stream function under conditions of weak stability is shown in Figure 5.3 and displacement of the circulation center is plotted in Figure 5.4. The vertical damping effect of the stability is quite apparent and is especially strong during later times in the development as seen from a comparison of Figures 5.2 and 5.4 between 1 hour and 2 hours. The strength of the circulation near the slope remained about the same as in the neutral case (Case A) and the circulation center remained closer to the slope.

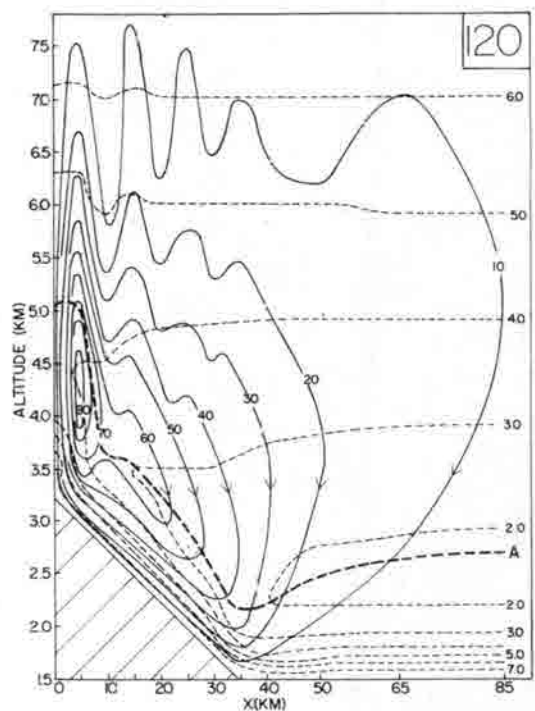
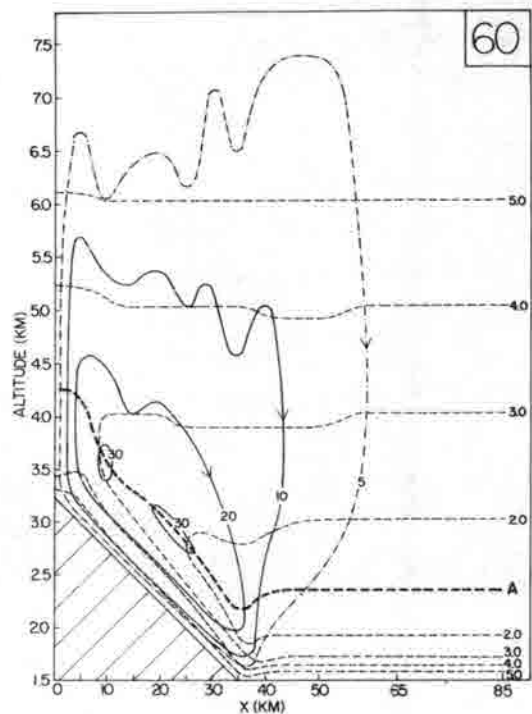
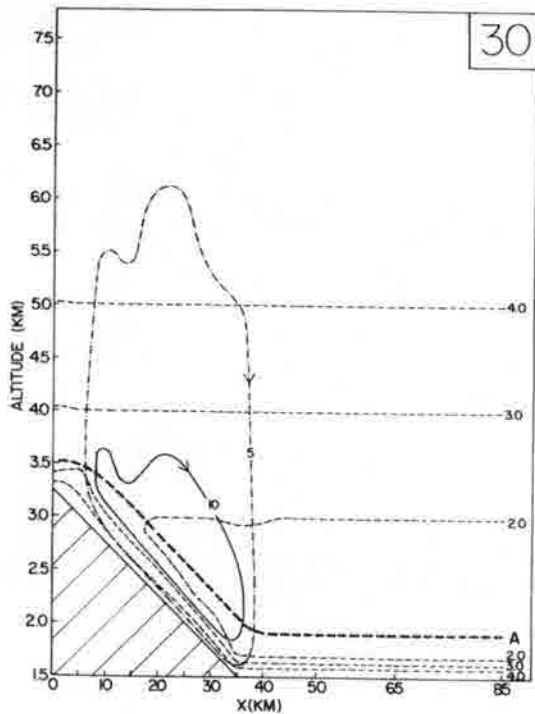


Figure 5.3. Evolution of the stream function (solid lines in  $10^2 \text{ m}^2 \text{ sec}^{-1}$ ) and potential temperature deviation (dashed lines in C deg) fields for Case B. Top of superadiabatic region is shown by heavy dashed line (A).

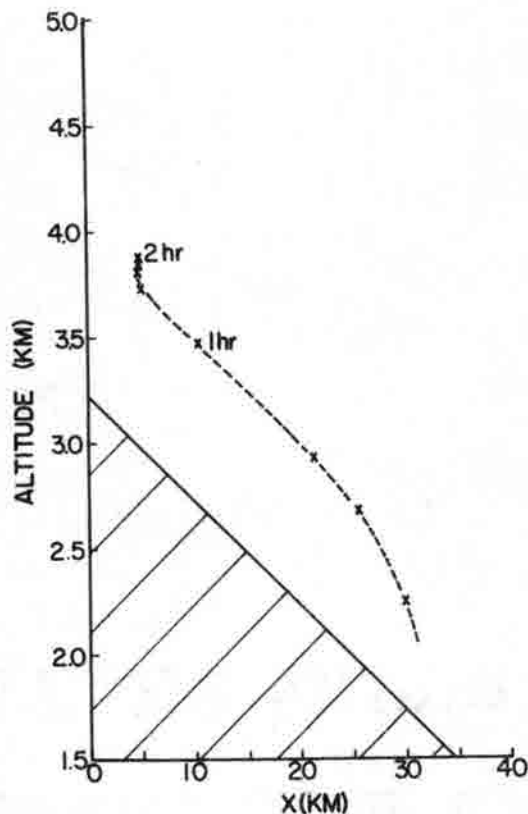


Figure 5.4. Trajectory of the stream function center for Case B shown at 15 minute positions.

The thermal pattern was similarly suppressed at later times although a well-defined "chimney" is evident after two hours. Static stability decreased in regions of ascent as a result of non-adiabatic heating advected up the slope while adiabatic heating increased the stability in the descending current. Forced lifting at upper levels overlying regions of ascent resulted in small potential temperature deficits at these levels. The superadiabatic layer reached a depth of about one kilometer over the plain after two hours and remained somewhat shallower over the mountain slope (Figure 5.3). At the top of the slope the depth increased substantially, while at earlier

times (see Figure 5.3 at 30 minutes) the unstable layer was very shallow at the top of the ridge. These developments are very similar to observations reported by Fosberg (1967).

A continuous upslope flow was present up to heights of 1 to 2 km above the plain. The depth of the flow increased near the mountain base. Over the mountain incline the depth of the upslope wind was about 1 km with a weaker anti-wind evident 1.5 to 2.0 km above it (Figure 5.5).

Vertical velocity components (Figure 5.5) were reduced considerably in the stable environment and the descending branch of the circulation extended 50 to 75 km eastward from the slope. Even at early times in the integration, a region of weak ascending flow formed 75 to 100 km from the slope (see Figure 5.6). This ascending flow persisted throughout the two-hour period with a slow eastward displacement and a reduction in vertical extent at later times.

After about an hour weak gravity waves appeared at upper levels above the mountains, moving slowly eastward. The wind speeds associated with these waves were very small and they appeared to have little effect on the circulation at lower levels. Ogura (1963) and Orville (1964) describe similar gravitational oscillations in cases of a stable environment.

The various terms in the vorticity equation (equation 5a in Chapter IV) were examined at a number of grid points in order to evaluate the contribution of individual components. Generation by the horizontal temperature gradient dominated during most of the first hour. Then as horizontal velocities approached  $1 \text{ m sec}^{-1}$  advection and dissipation terms attained the same magnitude as the generation, both terms usually opposing the generation. The Coriolis contribution was generally an order of magnitude smaller than the other effects.

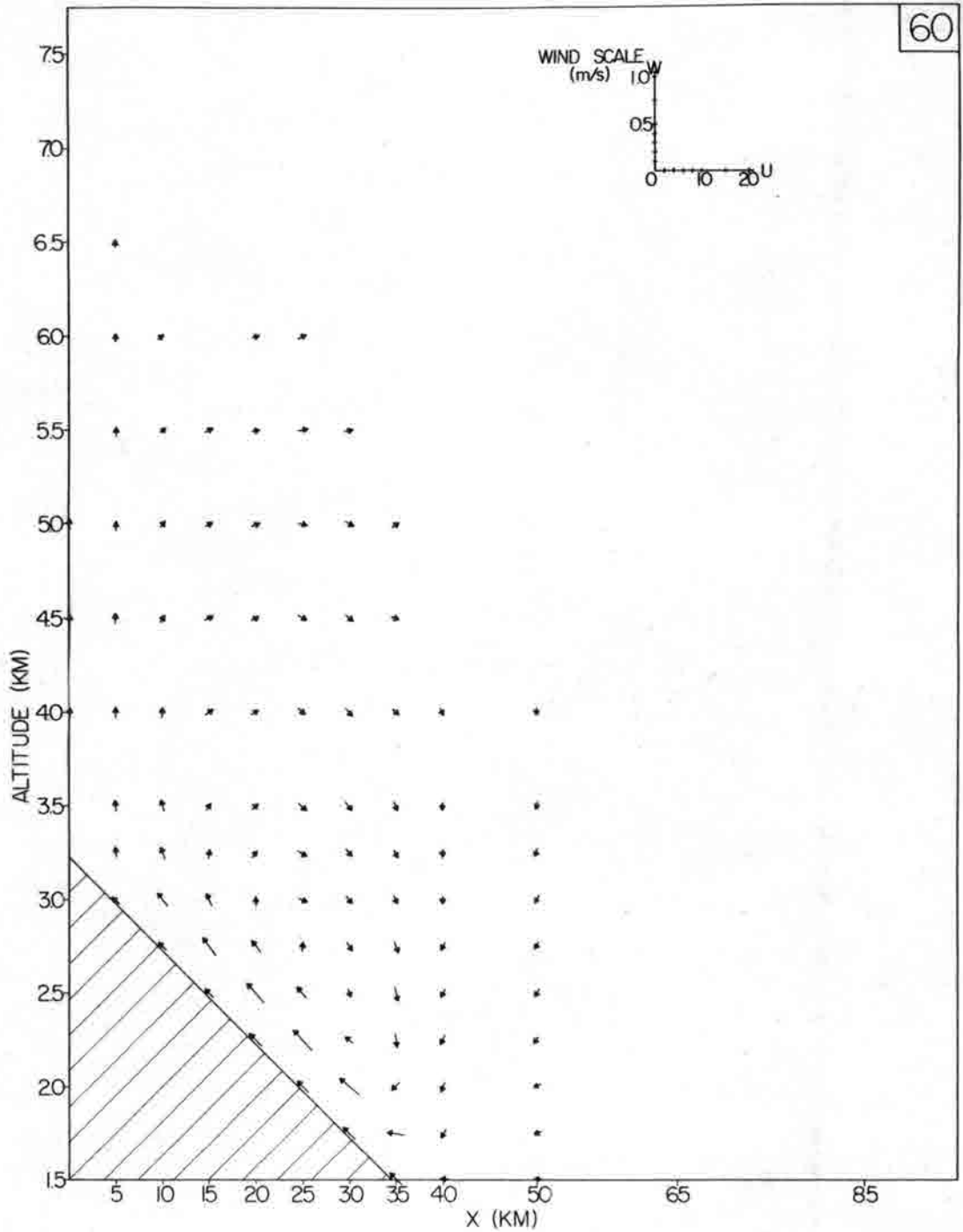


Figure 5.5. The computed wind field after 60 minutes of real time for Case B.

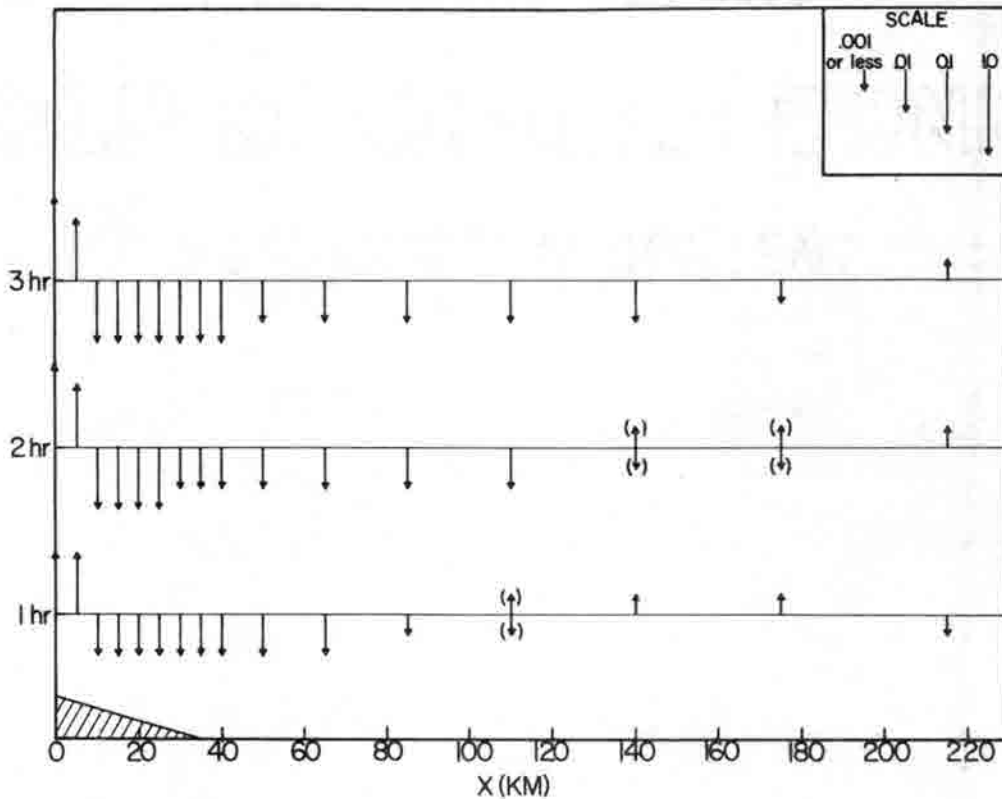


Figure 5. 6. Characteristic vertical motion components ( $\text{m sec}^{-1}$ , scaled by order of magnitude) in the lower troposphere for Case B. Vectors in parentheses indicate ascent at lowest levels with subsidence above.

Evolution of the vorticity field after one and two hours is seen in Figure 5.7. The buoyancy force exerted by surface heating results in the upslope flow of warm air creating both negative and positive vorticities. Positive vorticities are created by forced lifting of adiabatically cooling air. Near the slope maximum vorticities of  $-10^{-2} \text{ sec}^{-1}$  are attained after only one hour.

The kinetic energy generated by the circulation was computed for the entire field from the integral

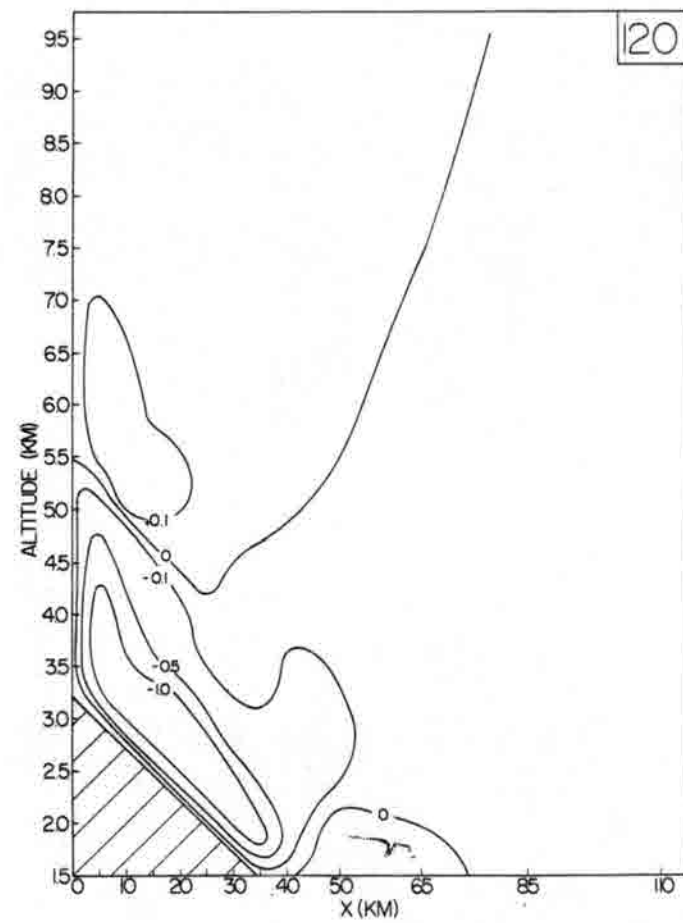
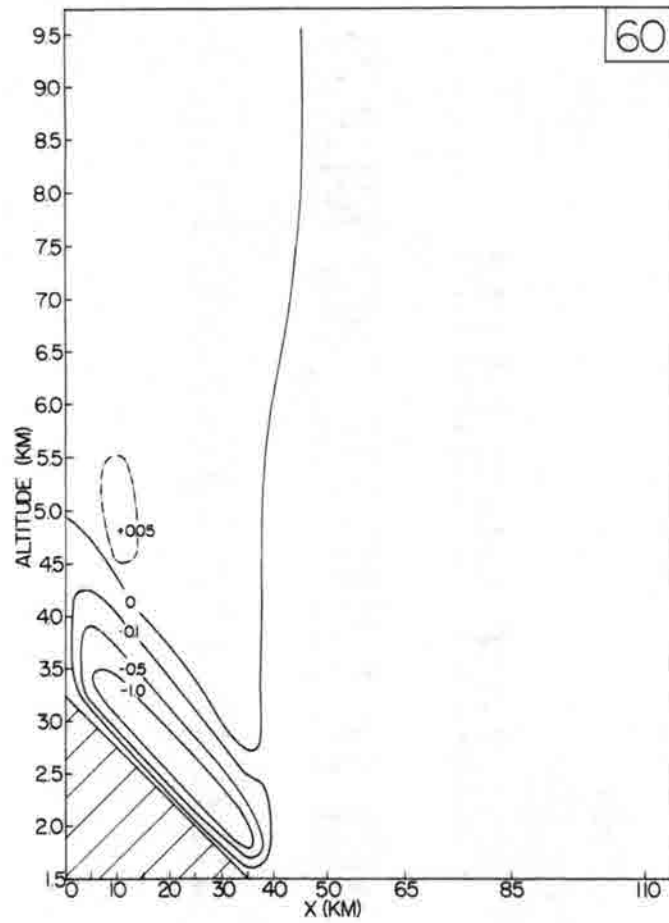


Figure 5.7. Evolution of the vorticity field (in  $10^2 \text{ sec}^{-1}$ ) for Case B.

$$E_K = \iiint \bar{\rho} \frac{(u^2 + v^2 + w^2)}{2} dx dy dz$$

where  $\bar{\rho}$  was assumed to be  $1.0 \text{ kg m}^{-3}$  and  $dy$  was assigned a value of 1 km. Figure 5.8 illustrates the changing kinetic energy of the system with a slow increase at early stages of development and more rapid changes at later times when strong vertical motions affect the release of potential energy created by the slope heating.

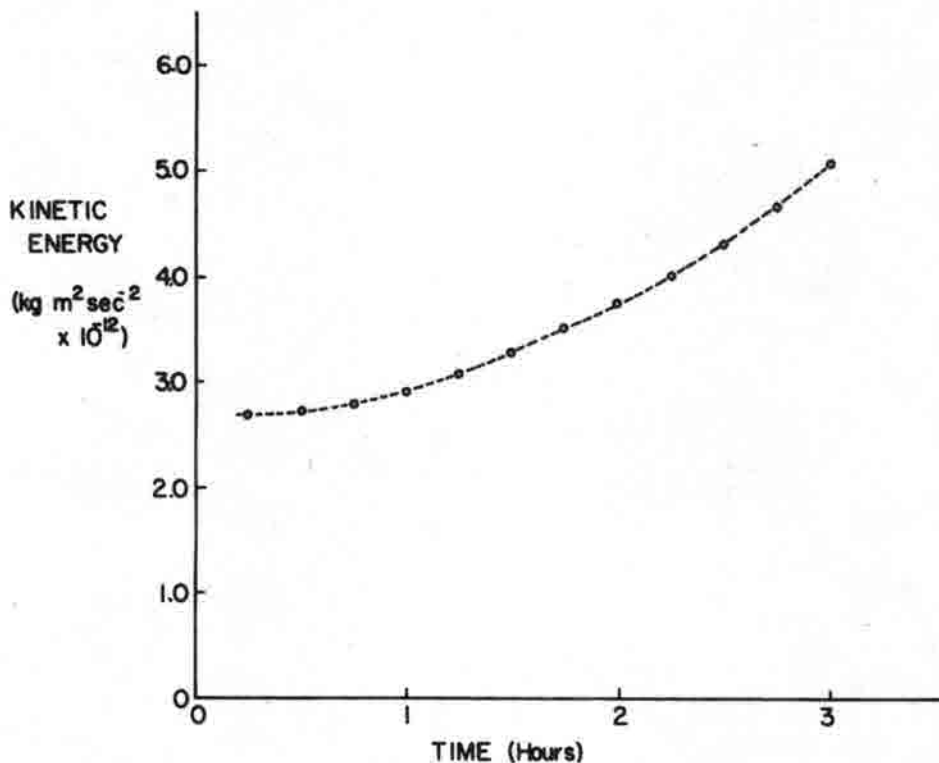


Figure 5.8. Time variation of kinetic energy as generated by the circulation for Case B.

Case C--Moderate Stability

In an effort to evaluate the effect of stability another experiment was performed using a potential temperature stratification of  $2.5^{\circ}\text{C}$  per kilometer--a value more applicable to wintertime conditions. The displacement of the circulation center in Figure 5.9 shows the stronger vertical retardation of the flow as compared to Figures 5.2 and 5.4. The intensity of the circulation at low levels remained comparable to the less stable case while stronger gravitational oscillations appeared at upper levels. An early zone of upward motion about 75 km from the slope was quickly eliminated and quite strong descent ( $\sim \text{cm sec}^{-1}$ ) occurred throughout the plain area.

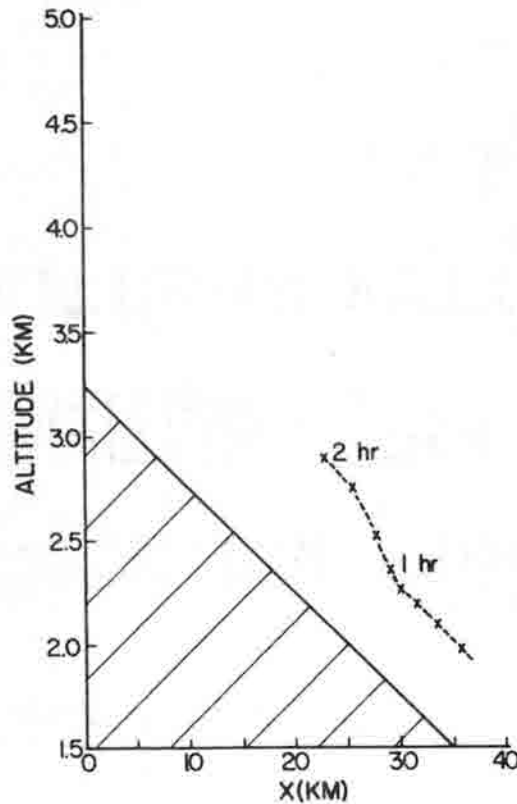


Figure 5.9. Trajectory of the stream function center for Case C shown at 15 minute positions.

### Case D--Shearing Wind

Although large scale weather systems may be weak during the summer, they still exert an influence due to a mean ambient pattern on which the local thermally driven circulation is superimposed. In the case of cumulus convection, it has been found that vertical shear may be favorable for convective development and that the convective motion interacts with the prevailing wind (Asai, 1964; Chao and Cheng, 1966; Orville, 1967). On the other hand, linear theory (Chao, 1962; Kuo, 1963) has shown that vertical shear tends to suppress convection. The strength of the sea breeze circulation in numerical studies has also been found to be dependent on the prevailing synoptic flow (Estoque, 1962; Magata, 1965).

Typical winds aloft profiles at Denver indicate that, particularly above the level of the mountain ridge, a mean westerly flow is coupled with an oscillatory wind field. A shearing wind of  $2 \text{ m sec}^{-1}$  per km gave a good approximation to the flow on a large number of days. This ambient flow pattern was combined with the initial condition of weak stability.

The evolving perturbation stream function field is shown in Figure 5.10 and the displacement of the slope circulation cell appears in Figure 5.11. The effect of the prevailing mean wind was to enhance the vertical development--e. g., as shown by a comparison of Figures 5.3 and 5.10 after 60 minutes. The shear gave a pronounced tilt to the circulation cell above the slope (Figure 5.10 at 60 minutes) so that part of the cell appeared to break off and form a much larger circulation cell out over the plain (Figure 5.10 at 120 minutes). A well-defined "chimney" again developed above the upper mountain slope which withstood the tilting forces of the ambient wind. Thermal fields were comparable to Case B. The gravity wave disturbances seemed to be somewhat reduced by the ambient shearing flow.

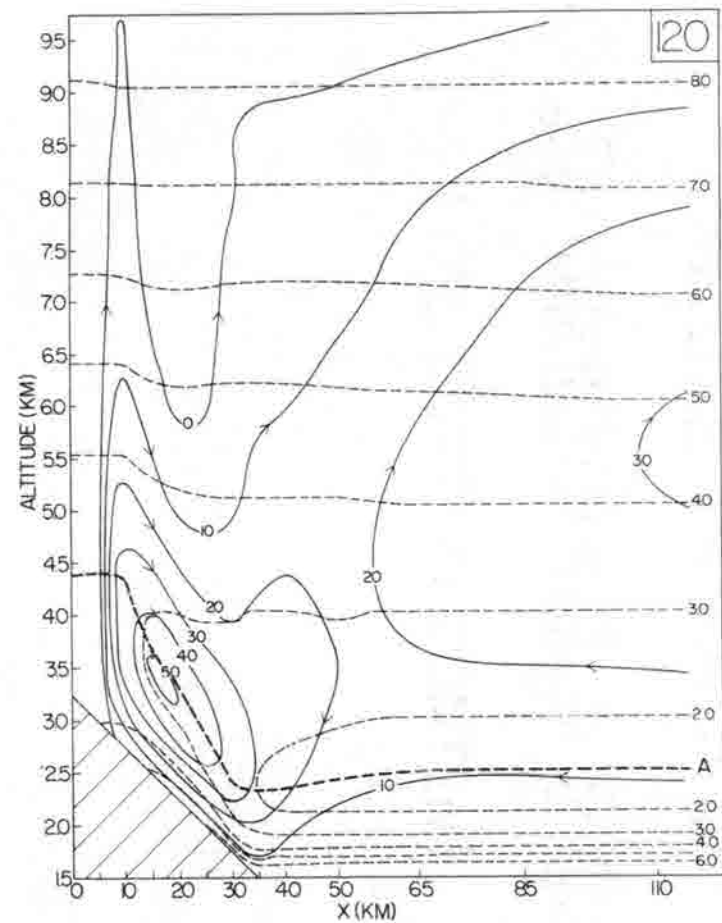
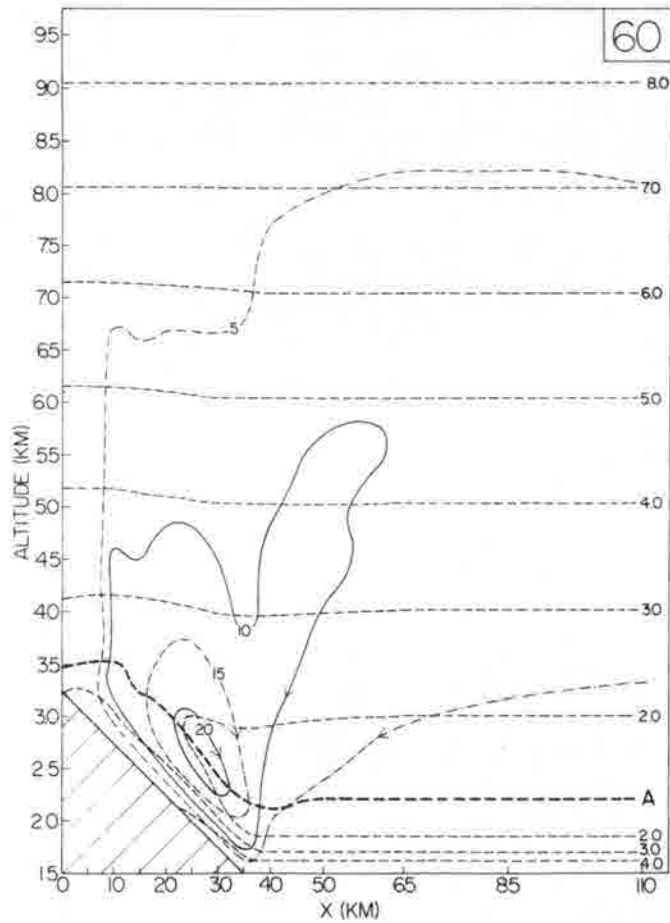


Figure 5.10. Evolution of the deviation stream function (solid lines in  $10^2 \text{ m}^2 \text{ sec}^{-1}$ ) and potential temperature deviation (dashed lines in C deg) fields for Case D. Top of superadiabatic region is shown by heavy dashed line (A).

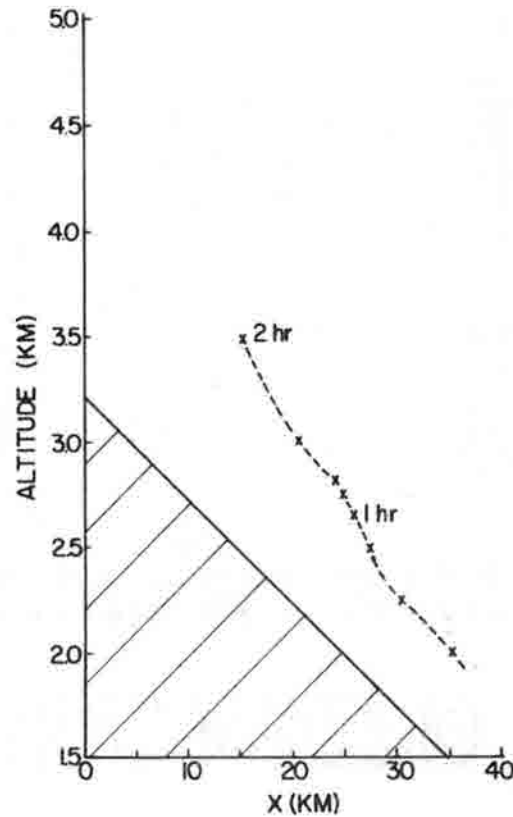


Figure 5.11. Trajectory of the solenoidal cell center for Case D shown at 15 minute intervals.

The "chimney" region over the mountain peak narrows and the vertical motions increase with time (Figure 5.12). A region of ascending motion was evident 50 to 100 km leeward of the slope with vertical velocities reaching several centimeters per second after two hours. This region of ascent over the plain became more extensive and developed somewhat larger vertical velocities than in Case B with no ambient wind (cf. Figure 5.6). Descending flow again occurred at the grid points farthest east. (The implications of these vertical motion fields to differential convective development are readily seen and will be discussed further in Chapter VI.)

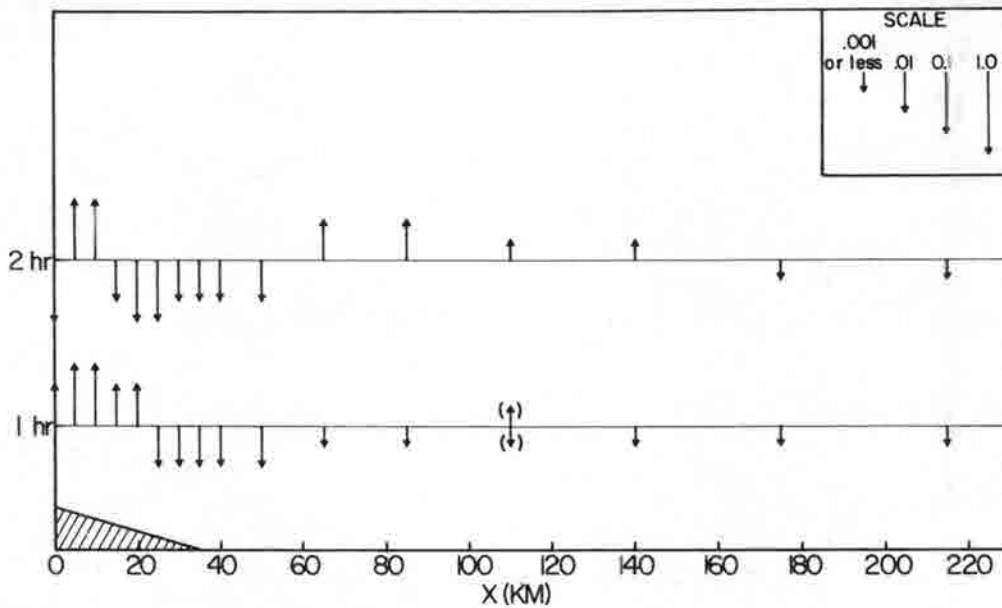


Figure 5.12. Characteristic vertical motion components ( $\text{m sec}^{-1}$ , scaled by order of magnitude) in the lower troposphere for Case D. Vectors in parentheses indicate ascent at lowest levels with subsidence above.

The perturbed shearing wind field after two hours is shown in Figure 5.13. The shearing wind introduced at upper levels acted to increase the upslope component above the plain where, after two hours, the easterly velocity exceeded  $1.0 \text{ m sec}^{-1}$  as compared to less than  $0.5 \text{ m sec}^{-1}$  for Case B without the ambient wind. The depth of the easterly flow was also found to extend to the base of the ambient wind field.

An interesting result of this integration was the apparent transfer of momentum from the convective system into the mean shear flow. This is clearly seen in the increased velocity vectors at mid-tropospheric heights where little return flow was observed in Case B. A similar transfer of momentum has been noted by Asai (1964) for a numerical simulation of two-dimensional convection under mean shear conditions. This "cascade" of energy toward larger scales in the case

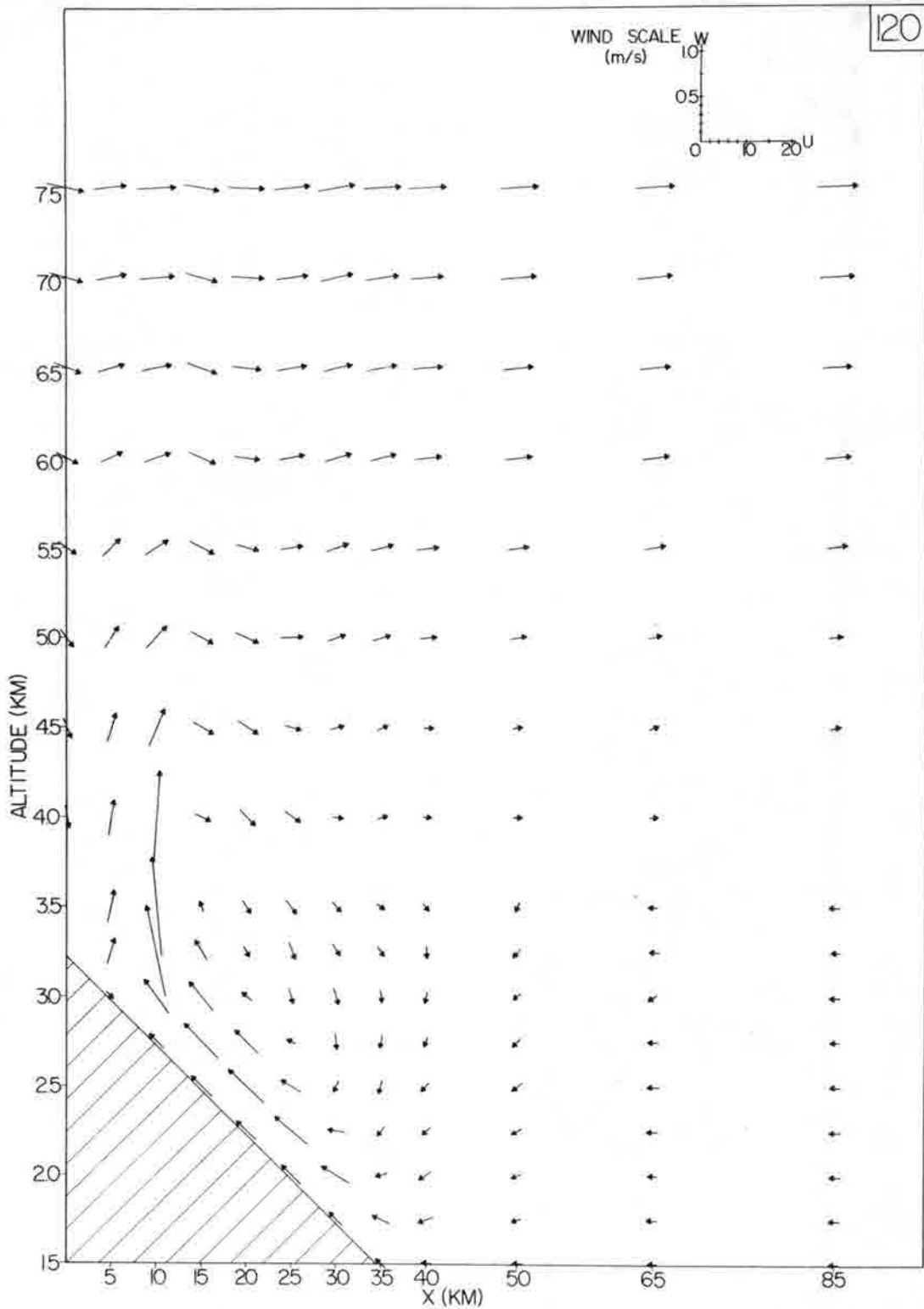


Figure 5.13. The total wind field after 120 minutes of real time for Case D.

of two-dimensional turbulence has been discussed by Fjörtoft (1953) and Kraichnan (1967) and is attributed to the condition that mean-square vorticity and kinetic energy per unit mass are inviscid constants in two-dimensional incompressible flow.

The results of this case suggest that an ambient shearing current aids in the development of the solenoidal field, so the evacuation concept discussed in Chapter II is supported by the numerical simulation. Whether the flow similarly enhances the formation of convective precipitation systems cannot be ascertained from this model. Orville (1967) found that winds and the convective cell developed more rapidly under shearing wind conditions but cloud formation was retarded.

#### Case E--Nocturnal Conditions

An extended run was carried out in an effort to determine the nocturnal features of the slope circulation and to examine long-term flow properties such as the time of flow reversal over the slope and the plain. The flow and thermal fields of Case D (shearing wind) after two hours of development were introduced as initial conditions at a time two hours before the descending node of the surface temperature wave ("sunset") and integrated for six hours.

Evolution of the perturbation stream function is seen in Figure 5.14 beginning at the onset of surface cooling. The solenoidal cell over the slope weakened rapidly and moved downslope as the surface heating was reduced. Downslope flow began on the upper slope shortly before "sunset" and within one-half hour after surface cooling was initiated the downslope flow had spread over the entire mountain slope. Two hours later a westerly current had developed along the entire plain surface. In terms of the relationship between local time and the temperature wave this would put the slope wind reversal in the mountains

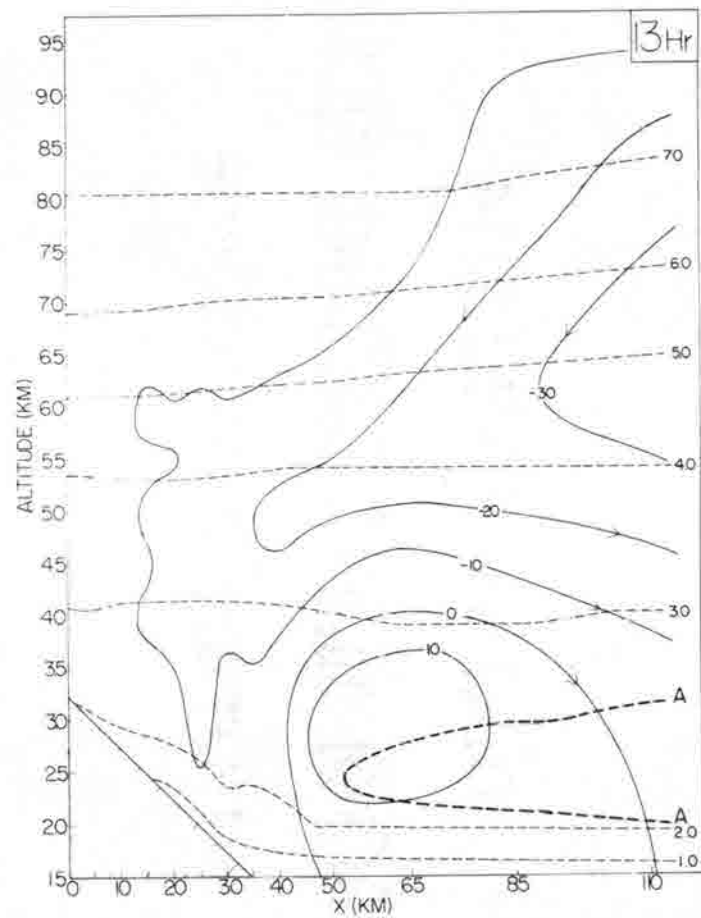
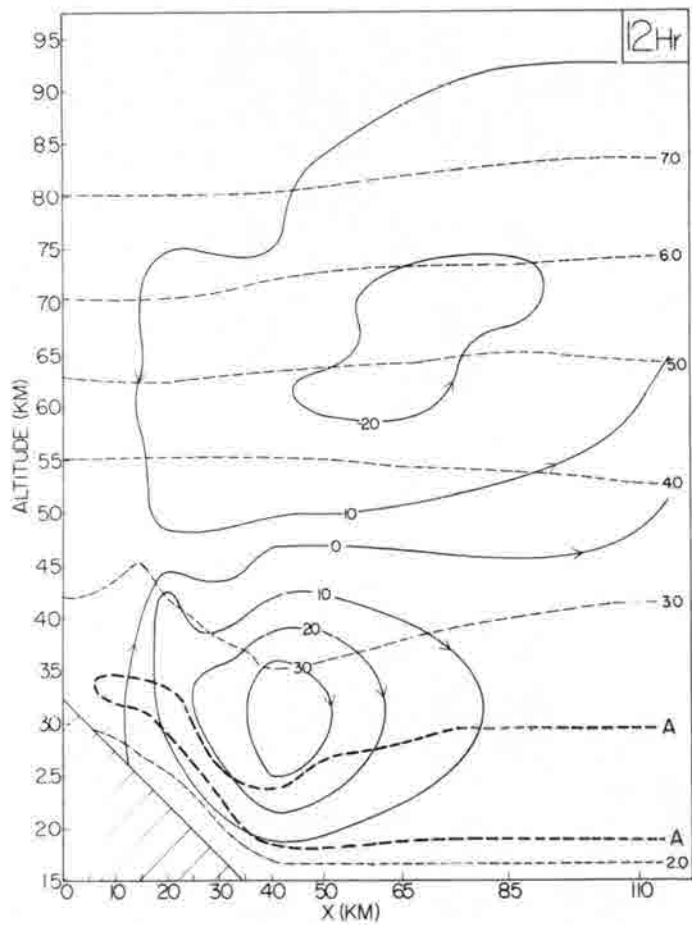


Figure 5.14. Evolution of the deviation stream function (solid lines in  $10^2 \text{ m}^2 \text{ sec}^{-1}$ ) and potential temperature deviation (dashed lines in C deg) fields for Case E. Time is in hours past start of diurnal sine wave.

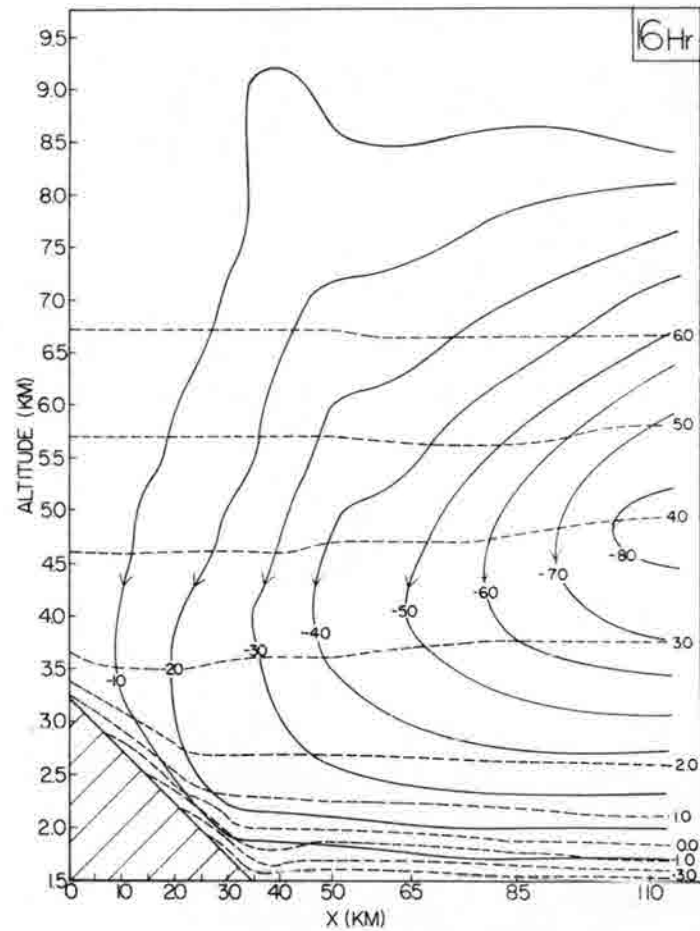
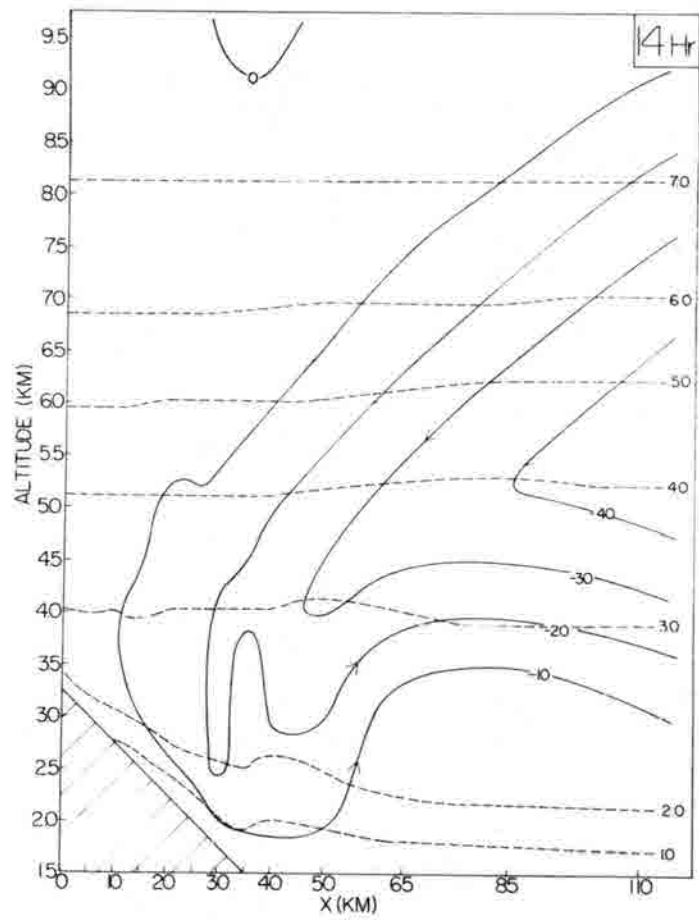


Figure 5.14. Continued.

around 2200 LT and the reversal over the plains to the lee around 2400 LT to 0100 LT. (Comparisons to observations will be made in Chapter VI.)

The thermal field is nearly isothermal in the lower one kilometer layer during the hour prior to "sunset". At that time the inversion begins to appear at the lowest grid points. About two hours later the isothermal layer is entirely removed and a strong inversion 250 m deep is present. After four hours of surface cooling the inversion extends 500 m upward with a potential temperature change of  $5^{\circ}\text{C}$ .

Ascending flow appears in the vertical component over the lower mountain slope a half hour before surface cooling is initiated and slowly extends itself eastward to 40 km at "sunset" and 50 km two hours later (Figure 5.15); after that it is rapidly eliminated. Vertical velocities are on the order of  $15\text{ cm sec}^{-1}$  at "sunset" and diminish to less than  $5\text{ cm sec}^{-1}$  two hours later. This would correspond to a possible enhancement of convection over the lower slope and adjacent plain during the evening hours.

#### Evaluation of Model Features

The strong upslope winds generated above the mountain slope somewhat exceed available observations of this wind component. Efforts to reduce this flow included varying the eddy viscosity coefficient (K) by as much as an order of magnitude and substantially reducing the heating with height along the mountain slope surface. Neither procedure appreciably changed the upslope velocity while, on the other hand, both resulted in unrealistic distortion of the flow above the slope so that the "chimney" was displaced down to the middle of the slope and subsidence took place immediately above the ridge. As pointed out at the beginning of this chapter, moisture and cloud formation may contribute significant modifications to the development of the mountain

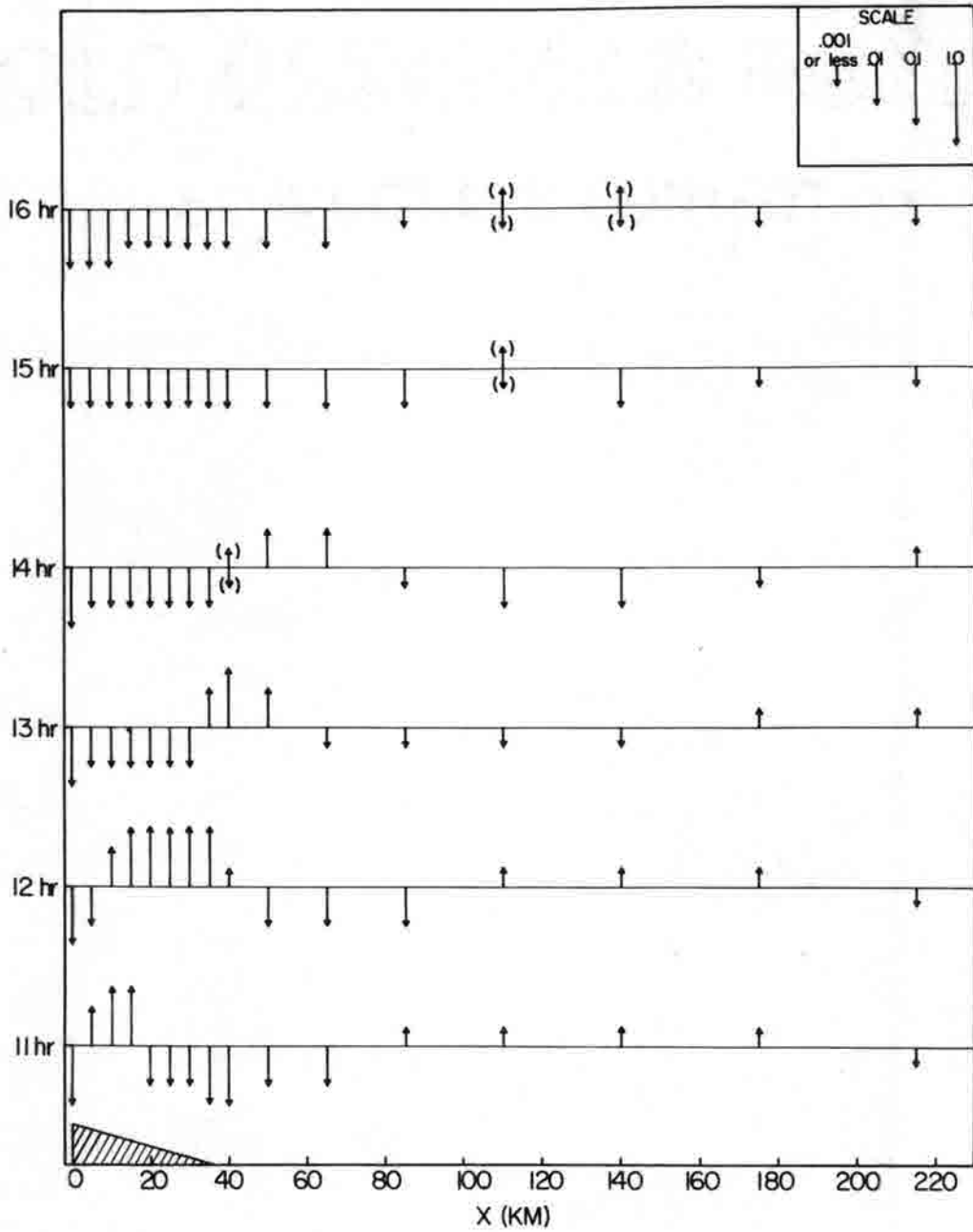


Figure 5.15. Characteristic vertical motion components ( $\text{m sec}^{-1}$ , scaled by order of magnitude) in the lower troposphere for Case E.

slope circulation, especially during the maximum heating phase. The effects of surface friction would also seem to be particularly large here due to the extremely irregular terrain.

A crude test of a somewhat more applicable Boussinesq system was carried out by using a constant vertical grid spacing of 250 m for the same grid scheme. The resulting 5 1/2 km deep layer could well approximate the "shallow convection" condition. A comparison of Figure 5.16 with Figure 5.3 after 60 minutes shows that, although the circulation is compressed, no major variations appear in the circulation pattern and the vertical motion fields are comparably developed.

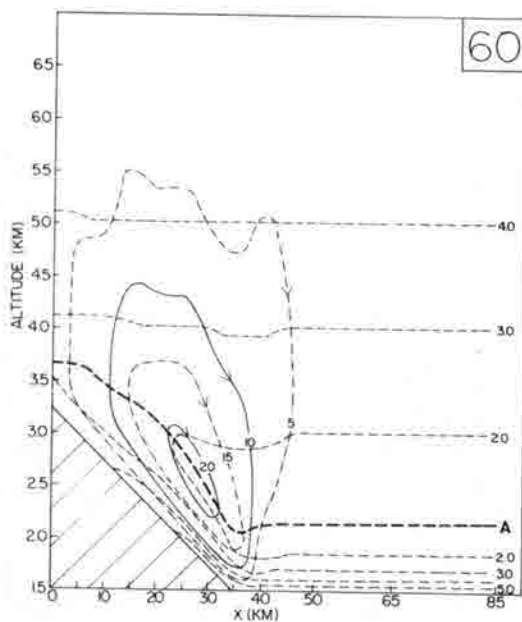


Figure 5.16. Streamline patterns for reduced vertical grid (stream function in  $10^2 \text{ m}^2 \text{ sec}^{-1}$ ) and potential temperature deviation field (dashed lines in C deg).

A very interesting feature of the modeling results was the region of ascending motion which appeared in Cases B and D at a distance around 75 to 100 km east of the mountain slope. This would provide a well-defined zone of preferred convective development and might be associated with the preferred regions of development found in Chapter II of this study. Because of its proximity to the right boundary of the model it was hypothesized that the feature was merely a result of the manner in which the boundary was treated. As a check the conditions of Case B (slightly stable) were integrated for 60 minutes using a one point linear extrapolation at this boundary. The region of ascent remained and no noticeable variations were evident interior of the boundary.

As a final check, the boundary was extended by six additional grid points ( $L = 560$  km). The ascending motion field again formed about 100 km eastward of the base of the mountain slope. In this case the upward motions extended further eastward with a maximum at about 300 km and diminishing beyond that. This variation may, at least in part, be due to the alteration in the plain slope which was necessary to perform this grid expansion. However, extending the boundary verified the reality of the zone of ascent in the modeling results.

The limitation on the plainward extent of the slope circulation due to Coriolis effects was also examined--in analogy to restrictions found in sea breeze circulations. Removal of the Coriolis term from the computations gave no significant variations and the vertical motion pattern remained without change even with the expanded grid with vertical shear.

As a final hypothesis, the effect of the plain slope was removed. Under these conditions the zone of ascending motion over the plain in Case B failed to appear. With a superimposed shearing wind

(Case D), removal of the plain slope removed the region of weak descent at large distances from the mountain slope (Figure 5.17) although the region of ascent nearer the mountains changed very little.

On the basis of these investigations, the zone of upward flow over the plain was demonstrated to be a property of the formulated model and resulted from the interaction of an intense circulation forming over a steep mountain slope and a weak circulation produced by an extensive slightly sloping plain. The plain slope was primarily important with no superimposed wind field. An ambient shearing wind greatly enhanced the vertical motions to the lee so that a well-defined zone of ascending flow appeared with or without the sloping plain.

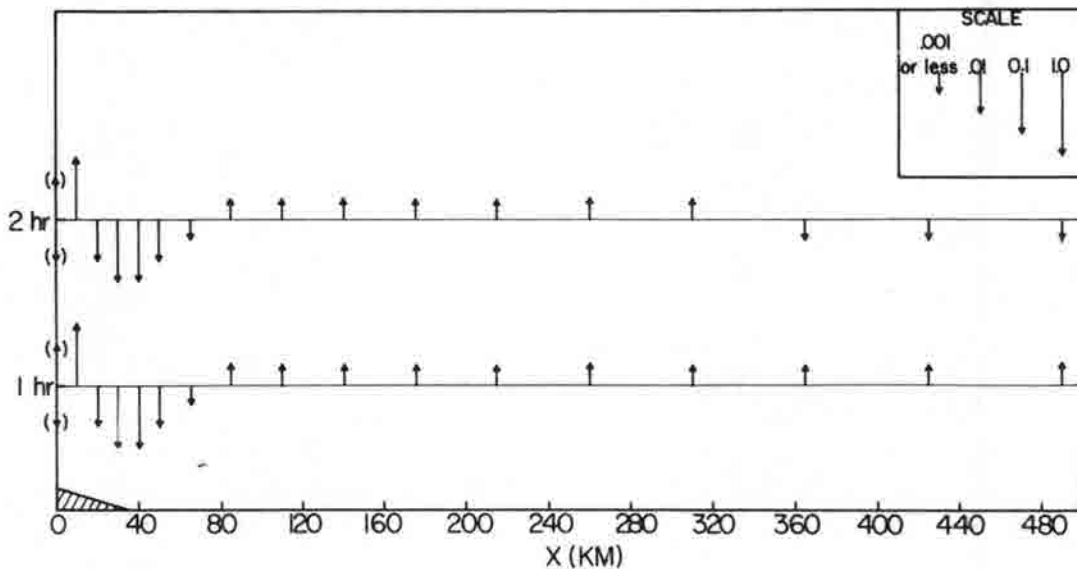


Figure 5.17. Characteristic vertical motion components ( $m \text{ sec}^{-1}$ , scaled by order of magnitude) in the lower troposphere after 60 minutes real time. Conditions correspond to Case D with an extended grid in the x direction, with (upper) and without (lower) plain slope.

Provided other flow characteristics of the model are in accord with observation (see next chapter), the simulation may well represent the existing situation in the lee of the Rockies. Furthermore, it would account for the enhancement of convective development 100 to 300 km to the lee of the mountains and could also be related to the high frequency of hailstorms in that area. A summary of the various cases and their main features is shown in Table 5.1.

TABLE 5.1. Summary of main conditions and results of various cases. Principal feature is underlined.

Case	Thermal Stability	Ambient Wind	Surface Input	Real Time Span	Principal Results
A	<u>adiabatic</u>	calm	heating	2 hr	Strong deep, mountain slope cell with inertia-gravity cells over the plain
B	<u>weak stability</u>	calm	heating	2 hr	Strong mountain slope cell with weak ascent beginning about 75 km out over the plain
C	<u>moderate stability</u>	calm	heating	2 hr	Mountain slope cell is reduced from Case B and ascent is suppressed over plain
D	weak stability	<u>linear shear</u>	heating	2 hr	Enhancement of mountain slope cell and increased ascent 50 to 100 km leeward of mountain
E	weak stability	linear shear	<u>cooling</u>	8 hr	Ascent over lower slope and near lee of mountain, flow reverses, inversion forms

## VI. A COMPARISON OF OBSERVED AND MODEL WINDS

A Rocky Mountains-Great Plains circulation was first inferred by Wagner (1939) from pilot-balloon observations made at eleven stations in the central United States. Bleeker and Andre (1951) examined the diurnal changes of horizontal divergence over six-hour intervals using wind observations at 4,000, 10,000 and 18,000 ft during the month of August. A pronounced decrease in divergence took place over the plain states during the principal night period (2200 to 0400 CST) while divergence increased over mountain areas during this time. Kinematic vertical velocity computations at 3 km described by Curtis and Panofsky (1958) similarly revealed a large decrease in divergence over much of the plains area between 0900 and 2100 CST. Sullivan and Severson (1966) computed the horizontal divergence at 700 mb over the Colorado Rockies during July and August using the Bellamy triangle method. These results indicated a definite mean diurnal variation with divergence at 0500 MST and convergence in the afternoon (1700 MST), thus implying general vertical motion fields over the entire mountain area rather than local mountain-valley influences.

A preliminary investigation was made to evaluate divergence patterns on an approximate mesoscale so that more detailed spatial and diurnal variations might be examined. Divergence was computed by the Bellamy triangulation method (Bellamy, 1949; Endlich and Clark, 1963) over the mountains of Colorado and northern New Mexico and the plains states eastward to Fort Worth and Omaha. Up to 23 observing stations were included using all available rawinsonde and pilot-balloon observations. The use of pibal winds gave much better resolution to the divergence fields, especially at 0600

and 1800 GMT, however, there appeared to be an accompanying loss in accuracy. These analyses further supported the large scale variations of divergence as shown by the example in Figure 6.1. The vertical continuity of divergence-convergence confirmed the large scale reliability of the data, but local and regional patterns were not defined and appeared to vary from day to day even though a time period was chosen when strong synoptic disturbances were absent. Although these results further support the concept of a regional scale mountain-plain circulation, they provide little information for verification of the numerical model.

### Wind Profiles

Profiles of the diurnal oscillations in winds aloft provided a more critical set of observations for evaluation of the circulation. These oscillations were first studied near the surface boundary layer (Blackadar, 1957; Buajitti and Blackadar, 1957; Bonner, 1965), but more recently they have been found to extend far into the stratosphere (Mantis, 1960; Hering and Borden, 1962; Wallace and Hartranft, 1969). For the purpose of this study only tropospheric oscillations will be examined.

Time-altitude sections of the westerly and southerly components of the mean deviation wind fields calculated by Hering and Borden (1962) are shown in Figure 6.2 for Fort Worth, Texas and in Figure 6.3 for Shreveport, Louisiana. These analyses were derived from averaged six-hourly rawin data for July 1958. Prominent peaks are found near 1 and 5 km. Comparable oscillations are noted on mean vertical profiles at Fort Worth obtained by Bonner (1965) on 16 summer days during which continuous low-level jet features were observed.

A recent paper by Wallace and Hartranft (1969) expanded the study of diurnal wind variations to include 14 years of twice daily radiosonde observations at 105 stations. Their results along with

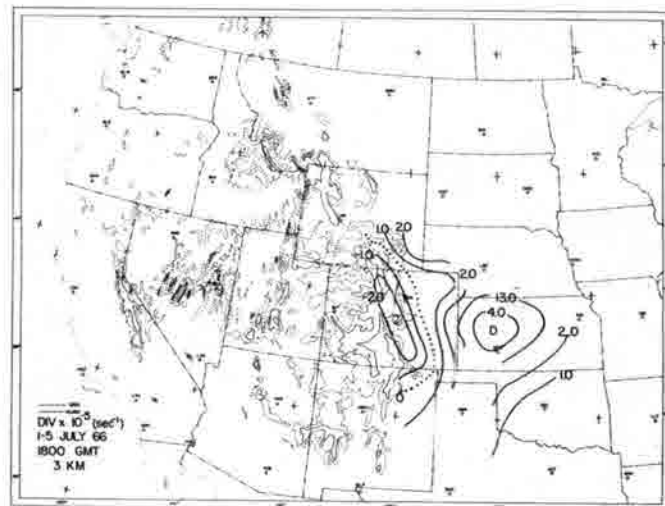
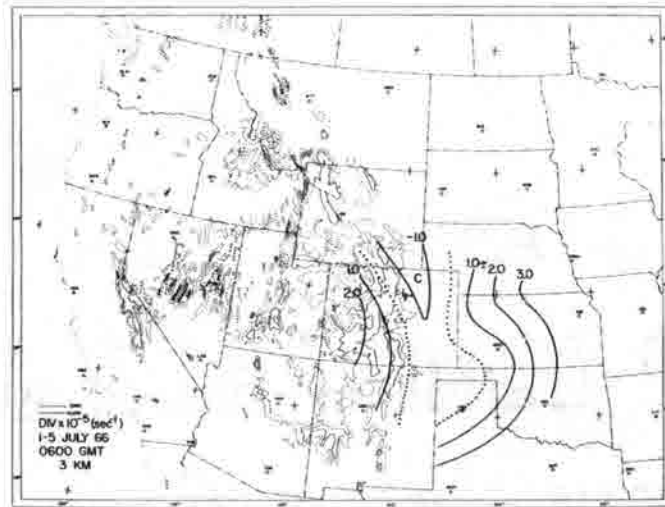


Figure 6.1. Average divergence (in  $\text{sec}^{-1}$ ) at 3 km for 0600 GMT (upper) and 1800 GMT (lower), 1 to 5 July 1966.

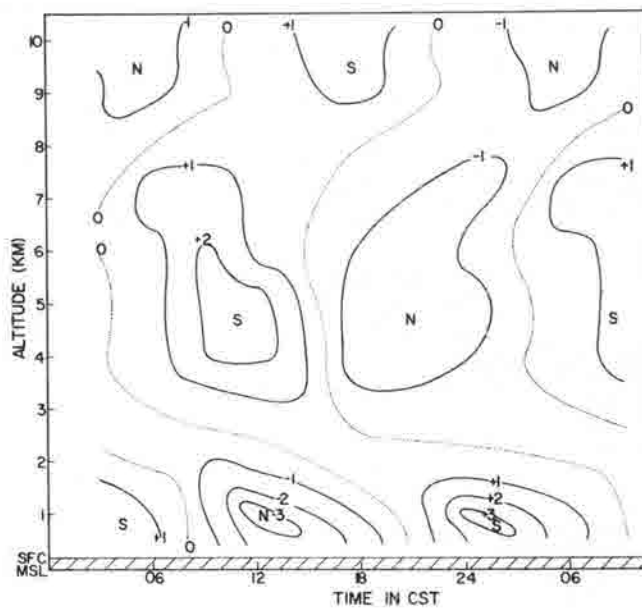
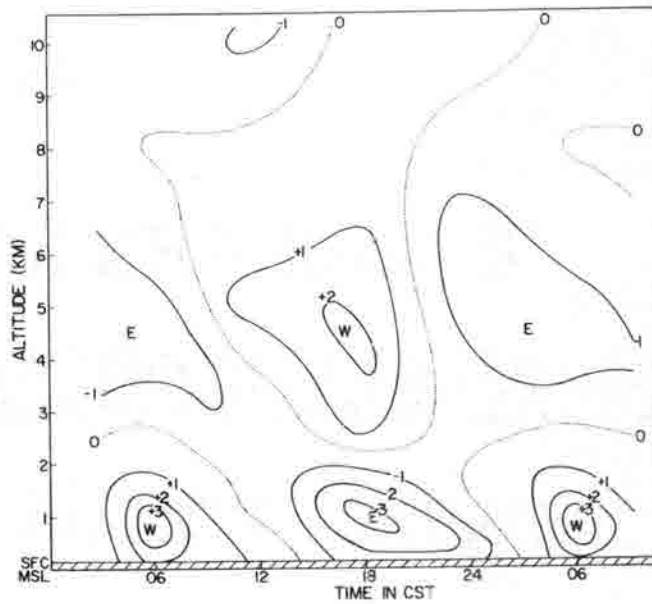


Figure 6.2. Westerly (upper) and southerly (lower) components of the mean departure vector as a function of altitude and time for July 1958 at Fort Worth, Texas (after Hering and Borden, 1962). Values are in  $\text{m sec}^{-1}$ .

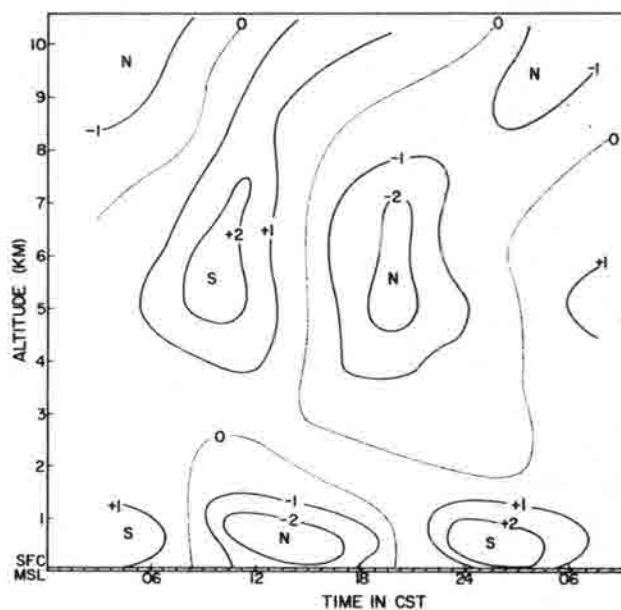
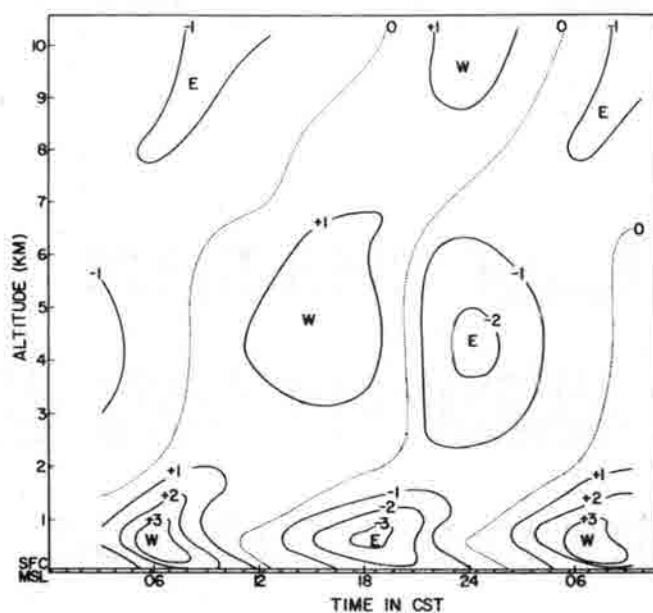


Figure 6. 3. Westerly (upper) and southerly (lower) components of the mean departure vector as a function of altitude and time for July 1958 at Shreveport, Louisiana (after Hering and Borden, 1962). Values are in  $m\ sec^{-1}$ .

those of Hering and Borden give good evidence of a major topographic influence on the diurnal tides throughout the troposphere. This includes effects of sloping terrain as well as land-sea differences. The dominance of the summer season contribution to the annual mean as found by Wallace and Hartranft for both the 900 mb and 500 mb levels lends further support to the important role of orography. They conclude that in view of the strong correspondence between the tidal wind field and heating patterns the time-varying frictional force, which results from the diurnal variation of eddy viscosity (cf. Buajitti and Blackadar, 1957), may be of only secondary importance in many regions.

Tropospheric sections were constructed for stations in and near the Rocky Mountains for 28 days selected during the summer of 1966 when no fronts or widespread overcast might obscure the regional scale mountain-plain circulation. Time-altitude sections of the westerly deviation wind component are shown for Amarillo (Figure 6.4), Dodge City (Figure 6.5), Albuquerque (Figure 6.6), and Denver (Figure 6.7). Upper regions ( $> 4$  km) at Dodge City and Albuquerque are estimated from 0000 and 1200 GMT data only since pilot-balloon observations are used at the alternate times and the upper level data are often missing. Amplitude peaks appear at 3 and 7 km at Denver, 2 and 5 km at Amarillo, and about 1.5 km at Dodge City. Only a weak peak in the  $u$  field at 2 km is observed for Albuquerque. The location of Albuquerque within the major ranges of the Rockies rather than on the eastern slope or the plains appears to result in a large reduction in the amplitude of the diurnal oscillation produced by the mountain-plain circulation.

An evaluation of the results presented by the model must necessarily be somewhat subjective since the model represents a mean idealized cross-section of the Colorado-New Mexico Rockies while the real data used for comparison are available for only a few stations, therefore, local influences are not easily removed. Since the

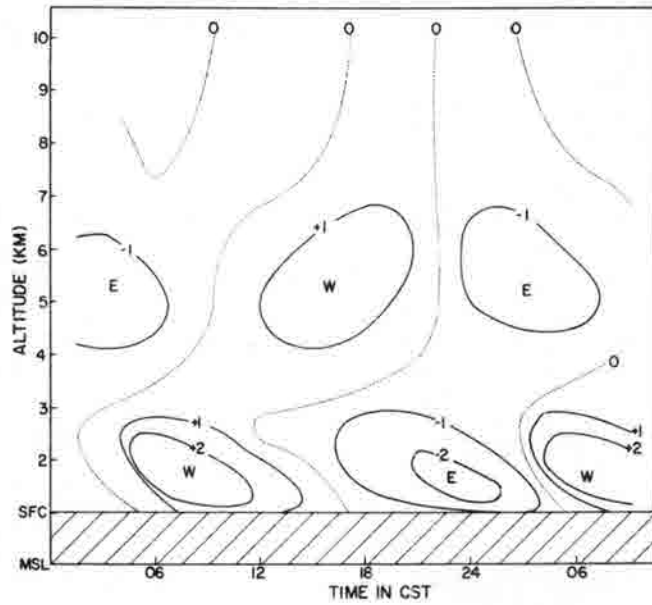


Figure 6.4. Westerly component of the mean departure vector as a function of altitude and time for 28 days selected during summer 1966 at Amarillo, Texas. Values are in  $\text{m sec}^{-1}$ .

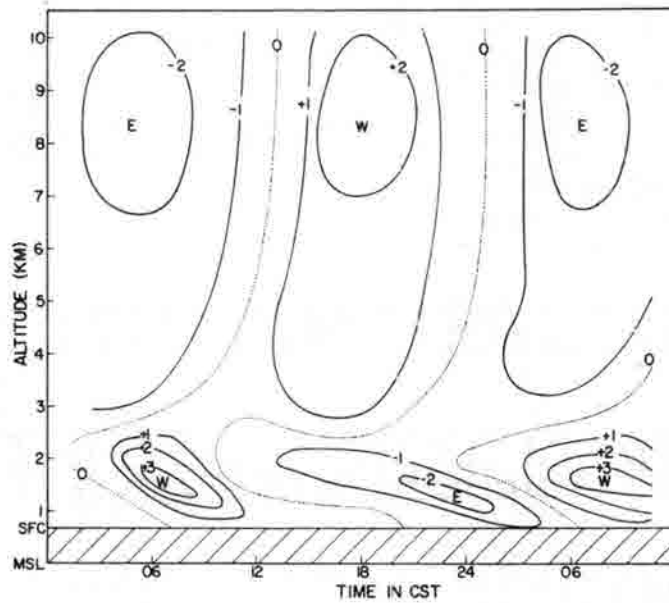


Figure 6.5. Westerly component of the mean departure vector as a function of altitude and time for 28 days selected during summer 1966 at Dodge City, Kansas. Values are in  $\text{m sec}^{-1}$ .

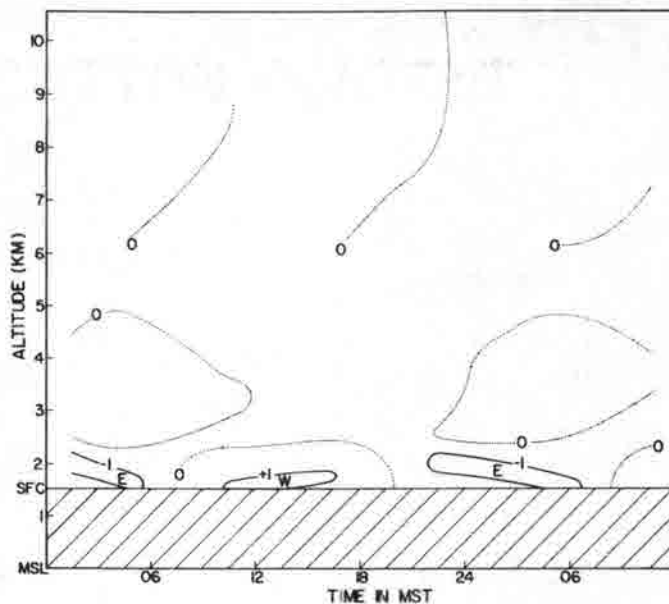


Figure 6.6. Westerly component of the mean departure vector as a function of altitude and time for 28 days selected during summer 1966 at Albuquerque, New Mexico. Values are in  $\text{m sec}^{-1}$ .

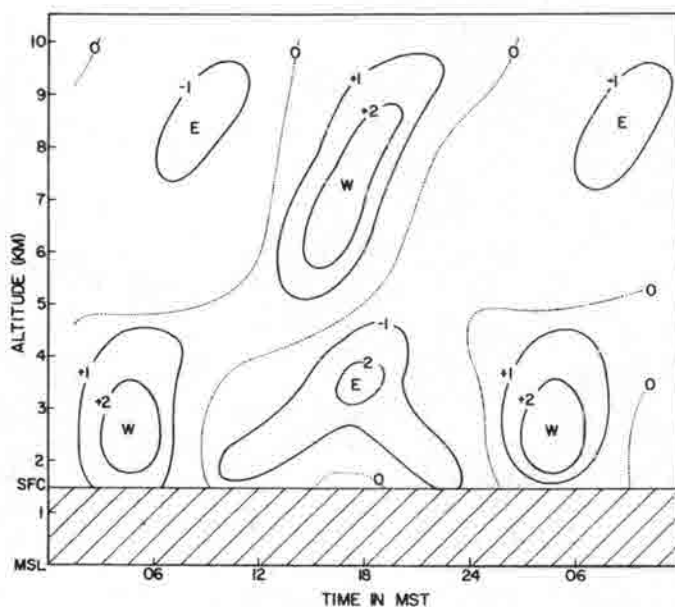


Figure 6.7. Westerly component of the mean departure vector as a function of altitude and time for 28 days selected during summer 1966 at Denver, Colorado. Values are in  $\text{m sec}^{-1}$ .

theoretical model is based on an east-west cross-section, the characteristics of the westerly wind fields over the plain will be examined and compared with those generated by the model. Unfortunately, data are not available directly over the mountain slope, however, this slope circulation cell has been described on a smaller scale by the work of Orville (1964, 1967) and Fosberg (1967).

Figure 6.8 illustrates the oscillating westerly wind component of the model at a distance 35 km from the base of the mountain slope corresponding to the approximate location of the Denver Weather Bureau. The conditions of Case E of the previous chapter are used which closely approximate mean summer conditions at Denver. In this case the integration was extended to eight hours. Even over this short time a good similarity is noted between model and observation (Figures 6.8 and 6.7). Model times are adjusted to approximate local times in terms of the phase of the surface temperature cycle as discussed previously. The time of reversal of the low level flow is nearly the same. (The early easterly current at Denver--1200 MST--seems to be caused by some local effect since corresponding features are not observed at other stations--see Figures 6.2 to 6.5.) Magnitudes of the deviation velocities at both upper and lower levels compare well, as does the depth of the low level flow (~4.5 km). Ideally a long-term integration of the model (> 30 hours) using an extended horizontal grid would provide a great deal of useful information here, however, the limitations on available computer time did not permit such a study.

Several other features were of interest in comparing the model with observations. The depth of the lower branch of the plain circulation appears to increase as the stations are located nearer the mountains, e. g. , 1.5 to 2.0 km at Fort Worth and Shreveport (Figures 6.2 and 6.3), 2.0 to 2.5 km at Amarillo and Dodge City (Figures 6.4 and 6.5), 3.5 km at Denver (Figure 6.7). The conditions of Case B with an extended horizontal grid also show an increasing depth in the upslope

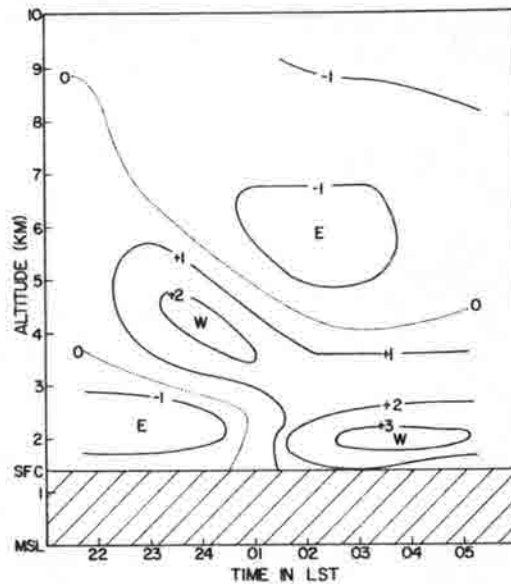


Figure 6. 8. Westerly component of the perturbation flow of the model as a function of altitude and time, taken at a point 35 km from the base of the mountain slope. Values are in  $m\ sec^{-1}$ .

flow from 2 km, at distances 300 to 500 km from the mountains, to 3 km at distances of 30 to 75 km. It is interesting to note that the maxima in the diurnal oscillations (and therefore also the reversals in flow) occur at approximately the same time at all stations. Thus there is no significant lag in adjustment of the flow in various regions. As has been discussed (Case E), the model also required only a very short time to undergo a complete reversal of the flow over the plain. This would seem to point to the effect of the plain slope itself rather than an extensive drainage from the mountain slope.

Several model assumptions are insufficiently precise to account for significant variations with observation. Among these are the non-sinusoidal shape of the surface temperature curve, the constant density and incompressibility assumptions, and the absence of water vapor and the accompanying effects of latent heat and cloud cover. The presence of the rigid lid at 10 km prevents the upward propagation of the

disturbances so the energy is trapped in the troposphere. Wallace and Hartranft (1969) found that, particularly in the Great Plains Region, vertically propagating modes of the diurnal tide are very evident. Yet in spite of these simplifications the numerical simulation appears to be quite appropriate.

Oscillations of the southerly flow component have not been discussed because the idealized east-west two-dimensional model does not account for variations in the north-south plane. There is a very small plain slope in this direction and, particularly in the southern Great Plains, land-sea contributions would have to be considered. Also there is a mean superimposed synoptic pattern producing southerly flow over the Plains at low levels, associated with the western extension of the circulation around the Bermuda High. In the model, diurnal oscillations of the southerly component were determined solely from the effects of the earth's rotation. Equation 2a of Chapter IV,

$$2a) \quad \frac{\partial v}{\partial t} = -u \frac{\partial v}{\partial x} - w \frac{\partial v}{\partial z} - fu + F_y$$

gives the generation of north-south velocities entirely in terms of the east-west velocity and the magnitude of the Coriolis parameter. If the viscous contribution is secondary this would give an acceleration in the v component as long as the u component did not change sign, thus respective maxima of u and v would be approximately six hours out of phase. Examination of the corresponding phase relationships at Fort Worth (Figure 6.2), Shreveport (Figure 6.3) and Denver clearly indicated that such a relationship existed and was probably the dominant factor. A direct comparison could not be made with the model since a mean southerly wind component was not determined. Examination of the relative magnitudes of the u and v components for Case B showed that in general these wind components were of the same

magnitude, corresponding to similar magnitudes of the departure components of the observed data.

It has been shown that the regional scale mountain-plain circulation is able to account for most of the characteristics of diurnal oscillations of the tropospheric wind field over the Great Plains during summer. The flow patterns produced by the numerical simulation are furthermore in good agreement with the observed features of the tropospheric wind field.

### Patterns of Convective Development

Based on the above verification of the numerical experiment, the preferred regions of convective development found in Chapter II of this report may then be compared with model results. In Case B (weak stability) a zone of ascending flow was noted 75 to 100 km east of the mountains (Figure 5.6). With the extended horizontal grid the upward motion appeared east of a point 100 km from the mountains with maximum uplift around 300 to 400 km. In Case D (shear with weak stability), the ascending flow appears 50 to 100 km from the slope (Figure 5.12) and with the extended grid from 50 to 300 km away (Figure 5.17), the greatest uplift occurring at 50 to 100 km. The differences in magnitude between the standard and extended grids are probably largely due to the variation in the parameterization used for the surface to lower boundary diffusion (see Chapter IV). The greater eastward extent of the ascending flow is probably due to the different parameterization and boundary conditions. Since the plain slope actually continues eastward another 1000 km, a precise description of the plain slope circulation cannot be expected. The results of the preceding numerical experiment, however, do verify the presence of a distinct region of ascending flow beginning 50 to 100 km leeward of the mountains and extending several hundred kilometers or more eastward. Maximum ascent occurs 50 to 300 km to the lee and appears to be highly dependent on thermal stability and wind shear.

The evaluation of preferred convective development regions over the Great Plains discussed in Chapter II shows that an area 100 to 500 km from the mountains is most favorable for early convection (Figure 2.7). Plains type squall lines and organized thunderstorm systems are most likely to form in that area and frontal zones will often show greater development there. Hailstorms also show a high frequency in that region (Figure 2.5). The vertical lifting provided by the model circulation, although small, when coupled with normal convective activity is sufficient to enhance the release of convective instability. Vertical motions on the order of several centimeters per second acting over a period of four or five hours would produce lifting of one-half kilometer. If the lifting condensation level is only 1 to 2 km above the surface, the resulting vertical motions are quite significant. The ascending flow also tends to destabilize the thermal structure thereby further enhancing the convective development locally. Very small changes in stability ( $\sim 0.1$  C deg per km) may be significant. On the other hand weak descent further out over the plain has exactly the reverse effects thereby suppressing early development in the plain further east by increasing the stability or at least retarding the effects of thermal convection. The strong descent over the lower mountain slope clearly accounts for the divergence zone commonly observed over the lower slope and immediately to the lee.

In the area east of the Rockies where warm moist southerly flow at low levels is frequently overridden by cooler westerly flow aloft, a stable layer or "cap" is often found between these air masses as described in Chapter II. The added lift provided by the mountain-plain circulation may be just sufficient to break through the "cap" while in other areas to the east the convection is not released.

Meridional organization (e. g. , as seen in Figure 2.11) of the convective systems can be directly explained by the model.

Implications of the growth of convective systems in the meridional direction (cf. Abdullah, 1954) can also be made.

The magnitude of the slope circulation effect relative to influences of atmospheric disturbances on other scales may be examined through a comparison of the corresponding fields of divergence of the horizontal wind. Computations from the modeled flow indicate divergences of the order of  $5 \times 10^{-4} \text{ sec}^{-1}$  at low levels in the zone at the base of the mountain slope. Such effects appear to be sufficiently strong to have a major influence on convective cells carried leeward of the mountain ridge and to generally suppress daytime convective development in the near-lee region. Summertime no-lift balloon tracks in the Denver vicinity (provided by Professor L. O. Grant, Colorado State University) indicate convergence and divergence maxima on the order of  $10^{-3} \text{ sec}^{-1}$  in the vicinity of cumuli and thunderstorms. Approximate mesoscale patterns from pilot balloon and rawinsonde data rarely exceed magnitudes of  $5 \times 10^{-5} \text{ sec}^{-1}$ .

In the late afternoon and possibly during periods of extensive cloudiness over the mountain slopes the strength of the circulation may be sufficiently reduced so that convection may persist in the near-lee. It is a matter of common observation that during late afternoon and early evening mountain thunderstorms are able to move into the near-lee and continue to develop. Also in some cases thunderstorms appear to "back into" the area from the east. This may be explained by the reversal of the slope circulation flow (Case E). When downslope flow begins over the mountains, it is coupled with an ascending branch near the base of the mountain slope providing an enhancement of convective cell development in that area.

The region of convergence further to the lee is not nearly as strong with magnitudes on the order of  $10^{-6} \text{ sec}^{-1}$ , however, this effect coupled with a comparable divergence field over the Middle

West may be closely related to the observed diurnal variability in convective activity over the Great Plains. The magnitude of the convergence is in fact of the same magnitude and opposite in sign to synoptic scale observations at 700 mb over the Middle West given by Curtis and Panofsky (1958).

Good agreement has been found between the flow features of the model and the observed regions of preferred convective development. The limited horizontal extent of the numerical model prevents a complete description of the Rocky Mountains-Great Plains circulation, however, the numerical formulation provides the flow features necessary to establish a zone of enhanced convective development.

## VII. AN EXAMINATION OF ATMOSPHERIC WAVES AND OTHER MECHANISMS FOR CONTROLLING CONVECTION

The modification of an existing air current by a mountain barrier may result in a wide range of wave-like perturbations in the airflow. In winter, when intense cyclonic systems dominate mid-latitude weather, anchoring of the planetary waves by the mountain barrier largely controls the storm tracks outside the tropics (Bolin, 1950). Leeward trough formation and cyclogenesis are commonly considered to be the result of vertical stretching of air columns as they move downslope under conservation of potential vorticity (Hess and Wagner, 1948; McClain, 1960). Newton (1956) further includes the effects of friction on a sloping surface in lee cyclogenesis. The dynamics associated with cyclone and planetary scale waves do not provide an explanation of summer convective systems which are of mesoscale dimension.

Various mechanisms in the atmosphere are capable of producing a wide spectral range of internal gravity waves. Of particular interest here is the flow over mountainous terrain (Queney, 1947, 1948; Scorer, 1949, 1953), as well as several convection-related mechanisms which have been considered. Townsend (1965) described the production of internal waves due to impulses at the base of a stably stratified layer by rising convective elements in an underlying turbulent boundary layer. Haurwitz (1947) showed that cloud patterns produced by convection and those produced by internal waves are closely related and may indeed be the same phenomenon since both modes of origin are usually present--unstable stratification and wind shear.

Recent observations of mesoscale phenomena in the upper atmosphere have been interpreted as the result of internal gravity waves (Kochanski, 1964; Newell et al., 1966; Hines, 1960, 1963)

and have led to quite elaborate evaluations of internal gravity wave properties, especially by Hines. Goldie (1925; more recently Potheary, 1954) discussed features of waves formed on a shear boundary between a shallow stable lower layer and a superimposed, infinitely deep layer in an incompressible fluid. The wave effects were interpreted on the basis of short-period fluctuations in wind and pressure and appeared to travel over quasi-stationary frontal surfaces. The same internal wave disturbances have been applied to fluctuations related to the sea breeze boundary (Gossard and Munk, 1954; McRae and McGann, 1965) and to pressure oscillations associated with a squall line (Ferguson, 1967). Wavelengths of these disturbances ranged from 5 to 200 km often varying with time.

Another approach to the application of internal gravity wave perturbations has been suggested by Tepper (1950, 1952). The gravitational wave appears as a pressure jump line as it travels along an inversion surface and is defined by analogy to a hydraulic jump in a liquid or shock waves in a gas. Acceleration of the air below the inversion or an elevation of the inversion surface-- particularly in relation to the acceleration of a cold front--could produce the pressure jump line. The lift produced by the traveling gravity wave is made responsible for the local release of convective instability and results in a propagating instability line.

Williams (1953) observed pressure wave occurrences in the central Midwest during 1952 and found that about one-third were not associated with cold fronts. Preferred times of occurrence (1900-0300 CST) and regions of occurrence (west-central Kansas, south-central Nebraska and east-central Kansas) suggested that diurnal and topographic forces are dominant in the genesis of pressure waves. "The occurrence of pressure waves in the central Midwest area is believed to be intimately related to the presence of the Rocky Mountains."

There is some question as to the nature of the pressure jump, whether it is a cause or effect of convective systems. Tepper (1952) showed that pressure jumps occur when no thunderstorm activity is observed which gives substance to the theory but it is not the usual case. Brunk (1949) described a case of widespread pressure pulsations occurring on both sides of the surface front and attributes the initiation of the large pulsations to the thunderstorm activity. Fujita (1955) pointed out that most "pressure jumps" are the result of the large thunderstorm high, i. e. , they are produced when high momentum air aloft is cooled and brought down by the downdraft. Fujita further gave an example in which tornado cyclone development preceded the organization of the pressure surge line. As pointed out in Chapter II , the apparent absence of a well-defined inversion layer in a large number of cases further excludes the pressure jump line as the general mechanism being sought.

Modification of convective systems by lee waves has been considered by Booker (1963; Hosler et al. , 1963) based on a detailed radar climatology and on no-lift balloon flights over the Allegheny Mountains of central Pennsylvania. He attributes a dry belt in the lee of the mountain ridge to dissipation of convective systems as they move into the lee wave region. It is pointed out that large wind shear aloft is favorable both for lee wave and severe thunderstorm development. It should, however, also be emphasized that lee waves occur more favorably if the stability decreases with height, a condition which is certainly not commonly characteristic of convective conditions. Scorer (1953) found that waves are possible with an adiabatic layer near the ground but the magnitude of the disturbances will be small at upper levels. Lee wave modification of convection does not seem to account for the extensive "dry zone" in the lee of the Rockies, nor does it provide for preferred convective development further east. Observation and theory ordinarily find lee wave wavelengths in the range of 2 to 30 km, however, there has been some evidence of a

longer wave mode ( $> 60$  km, e. g., Wooldridge and Lester, 1969) which is not accounted for by theory.

Other observations of mesoscale oscillations in the troposphere and stratosphere (Neiburger and Angell, 1956; Sawyer, 1961; DeMandel and Scoggins, 1967) reveal largely horizontal wave modes with periods of several hours and horizontal dimensions of several hundred kilometers. Theoretically these waves have been explained by an interaction of gravitational and Coriolis effects and have been called gravity-inertia waves (Queney, 1948) or gravity-Coriolis waves (Sawyer, 1959). Queney (1947, 1948) has shown theoretically that oscillations with periods of several hours can be set up by a mountain range whose half width is on the order of 100 km. A complex system of wave perturbations is obtained in frictionless flow of a stable atmosphere over such a barrier. Sufficient time is required in traversing this mountain range for the Coriolis acceleration to produce a significant horizontal displacement of the current and to form a system of lee side inertial waves with wavelength dimensions of several hundred kilometers. The stratification of the atmosphere and the rotation of the earth are controlling factors in the occurrence of these waves. There are several shortcomings in the applicability of this model. The theory does not extend to conditions of very weak or neutral stability which may be present throughout much of the lower troposphere during summer days. The condition for standing inertia waves is quite sensitive to variations in the mountain width and shape. This further limits the application of the theory to the present situation since the Rocky Mountains of Colorado and northern New Mexico represent a barrier with large variations in width and shape. Queney's theoretical model is also lacking in that it applies only to a barotropic current, neglecting the important temperature advection parallel to the mountains.

An admittedly crude analysis by Godske et al. (1957) attempted to determine a wavelength of maximum instability lying somewhere

between that of inertial and shearing waves, i. e., from the combination of shearing instability and rotational stability. A region from about 500 to 1000 km is found to be unstable, however, the method of analysis employed places serious doubt on the reality of the results obtained.

Satellite photograph investigations by Reiter et al. (1965) and Dirks et al. (1967) have shown the presence of orographically related cloud features in the lee of the Rockies having dimensions of several hundred kilometers. The latter report ascribed these features to an orographically induced mesoscale wave. Linear solution of the compressible hydrodynamic equations yielded sub-synoptic scale wavelengths ( $< 1000$  km) under conditions of low mean wind speed and small static stability. Several cases were presented in which observational evidence showed good agreement with theoretical wavelength calculations.

A further evaluation of the above model was carried out by application to cases selected from the summer of 1966. Ten cases were examined in which theoretical results were computed from several near-by radiosonde reports of atmospheric parameters and then compared to wavelength estimates determined independently from satellite and radar observations. The procedure and results are summarized in the Appendix. A few cases show reasonable agreement but in general the corresponding results were quite poor. The restricted application of the theoretical model to cases of low wind speeds and weak stability also excludes a large percentage of the meso-systems evaluated in Chapter II of this report. Therefore it is believed that this type of wave oscillation does not represent a general mechanism for the observed zones of reduced and enhanced convection.

Employing a development quite similar to Dirks et al. above, Sawyer (1961) proposed an oscillatory motion resulting from a balance of inertial, Coriolis, and thermodynamic effects to explain

short period oscillations ( $\sim$  hours) observed in the lower stratosphere. These oscillations had vertical dimensions  $\sim 1$  km and horizontal dimensions  $\sim 400$  km. This theory gave sub-synoptic wavelengths as long as  $(u - c)$  remained small ( $< 15 \text{ m sec}^{-1}$ ) or for stationary waves ( $c = 0$ ) as long as the mean wind speed remained small.

The evidence for an intermediate scale wave presented in Chapter II gives substance to some sort of orographically controlled wave. However, all of the theories proposed thus far are largely restricted to conditions which cover only a small part of the observations reported in Chapter II. It also seems somewhat doubtful that a single type of wave could be influential through such a large range of conditions, a limitation which need not be placed upon the thermally generated lee slope vortex. The wave-like perturbations described in Chapter II may in fact be effects of the regional circulation rather than of a dynamically induced wave phenomenon.

It may be reasonably concluded at this point that no known wave mechanism is generally applicable to the convective features under study. It is, of course, true that specific cases may be influenced by a particular wave phenomenon and that certain types of meso-scale convective systems may originate from wave-like perturbations-- e. g., pre-frontal squall lines.

For completeness, several other features might be briefly examined in regard to their feasibility as mechanisms for producing zones of enhanced and reduced convective development. Due to the barrier effect of the Rockies the moisture available over the Great Plains is largely the result of Gulf air advected by southerly flow at low levels (surface to 800 mb). A dew point front or dry-line is often evident over the western Great Plains along which mesosystem formation is favorable (Fujita, 1958; McGuire, 1962). The moisture availability itself does not appear to be the significant factor in the preferred formation because the moisture is often even more plentiful several hundred kilometers to the east, and

furthermore, an area further east receives the solar heating at an earlier time. The position of the dew point discontinuity is at least in part attributable to advection resulting from the mountain-plain circulation, which would result in a diurnal variation in the position of the "front". The moisture boundary is also significantly affected by the large scale low-level flow pattern around the Bermuda High. The Bermuda High is commonly centered off the southeastern coast of the United States during summer and the western branch of the flow around it is paramount in conveying moist Gulf air into the Great Plains. The superposition of transient synoptic-scale disturbances upon this low-level circulation often significantly alters the east-west pressure gradient over the Plains so that moisture is carried into the western limits of the Plains. It has been shown that these conditions are common when extensive thunderstorm activity and severe storms occur in northeast Colorado (Hodges, 1959; Renné, 1969).

An examination of 850 mb height gradients between North Platte and Denver and Dodge City and Denver for the summer of 1966. showed that on 15 days when extensive thunderstorm activity was observed in eastern Colorado the gradients were generally two to three times greater than the mean. Upon further examination, the gradients also indicated a mean 2 to 3 mb variation between early morning (1200 GMT) and late afternoon (0000 GMT). The mean early morning gradient from North Platte was reversed, i. e., directed from Denver to North Platte, as were the individual gradients between Dodge City and Denver on numerous occasions. The diurnal gradient is readily attributed to the mountain-plain circulation and is in fact of the same magnitude as that estimated from the model circulation. The diurnal pressure field is seen to be a major component of the total gradient at the 850 mb level ( $\sim 50\%$ ), and even in the cases of extensive thunderstorm activity it makes a significant contribution ( $\sim 25\%$ ). These results support the previous

conclusions regarding the major role of the mountain-plain circulation in controlling summer convective development on the high plains.

Frictional turning in the boundary layer over a sloping plain could enhance a cyclonic circulation and has been shown to be significant in lee cyclogenesis (Newton, 1956). It was pointed out by Charney and Eliassen (1949) that frictionally induced convergence in the planetary boundary layer could produce vertical velocities at the top of this layer as given by

$$w_o = \frac{1}{2} \sqrt{\frac{2A}{f}} \zeta_g \sin 2\epsilon$$

where A is the kinematic eddy viscosity coefficient,  $\epsilon$  is the angle between the surface geostrophic wind and the surface isobars, and  $\zeta_g$  is the vorticity of the surface geostrophic wind. More recently Charney and Eliassen (1964) have proposed that a frictionally induced convergence in boundary layer regions with cyclonic vorticity may result in a kind of secondary instability which transforms small-scale cumulus convection into cyclone-scale motions in the tropics (see also Gray, 1967). Over the Great Plains there is no persistent low-level shearing current which is capable of producing cyclonic vorticity in the boundary layer region of preferred convective development. The low-level jet, when present, could produce such an area to the left of the jet maxima, however, the low-level jet is often not present when meso-systems form and its location is quite variable throughout the Plains area (Dirks, 1969). Significant vertical wind shears in the vicinity of the low-level jet as well as strong directional shears at higher levels also tend to impair the effects of the Charney-Eliassen "secondary instability".

It follows from the above considerations that the low-level jet cannot provide a general mechanism for enhancing convection over the far western plains, although the dynamics of the jet have been shown to be especially important in the nocturnal maintenance of convective systems (Pitchford and London, 1962; Bonner, 1963). The jet itself is not well understood and it is possible that the dynamical influences controlling the convection also contribute to the intense low-level jet over the Great Plains.

Each of the mechanisms described above may well contribute to the formation of mesoscale convective systems in particular situations, however, not one of them provides general application to the variety of conditions found in Chapter II. Only the slope circulation appears to apply in a general sense.

## VIII. SUMMARY AND CONCLUSIONS

Climatological studies and case studies of the development of Great Plains mesoscale convective systems have pointed out certain features regarding preferred activity. There appeared to be a preference for early convective development several hundred kilometers to the lee of the Rockies while organized convection was suppressed farther east. Convection is also subdued in the first 100 km in the immediate lee of the mountains. Convective activity occurred during a variety of synoptic conditions. The only conditions consistently necessary were convective instability and a tongue of warm, moist air at low levels. A short wave was frequently in evidence at mid-tropospheric levels.

Numerical simulation of the Rocky Mountains-Great Plains flow field was performed by a two-dimensional model in a vertical cross section. Characteristics of the flow produced in this model were found to correspond to climatological wind observations at stations on the western Plains. An idealized daytime flow pattern derived from the numerical experiment is shown in Figure 8.1 for a cross section extending from the ridge of the Rocky Mountains to the Mississippi River. A strong circulation cell forms over the mountain slope with large ascending motions over the upper slope and strong downward motions over the lower slope and extending 50 km or more out over the plain. A weaker larger scale cell forms over the plain as a result of the plain slope and a coupling with the cell over the mountain slope. The resulting circulation advects air from the plain into the mountain slope circulation and also creates a zone of ascending flow from 50 to several hundred kilometers east of the mountains. The air carried upward in this flow advects moisture from low levels over the plain so that the formation of convective systems should be highly correlated with this weak ascending current. The position and magnitude of the

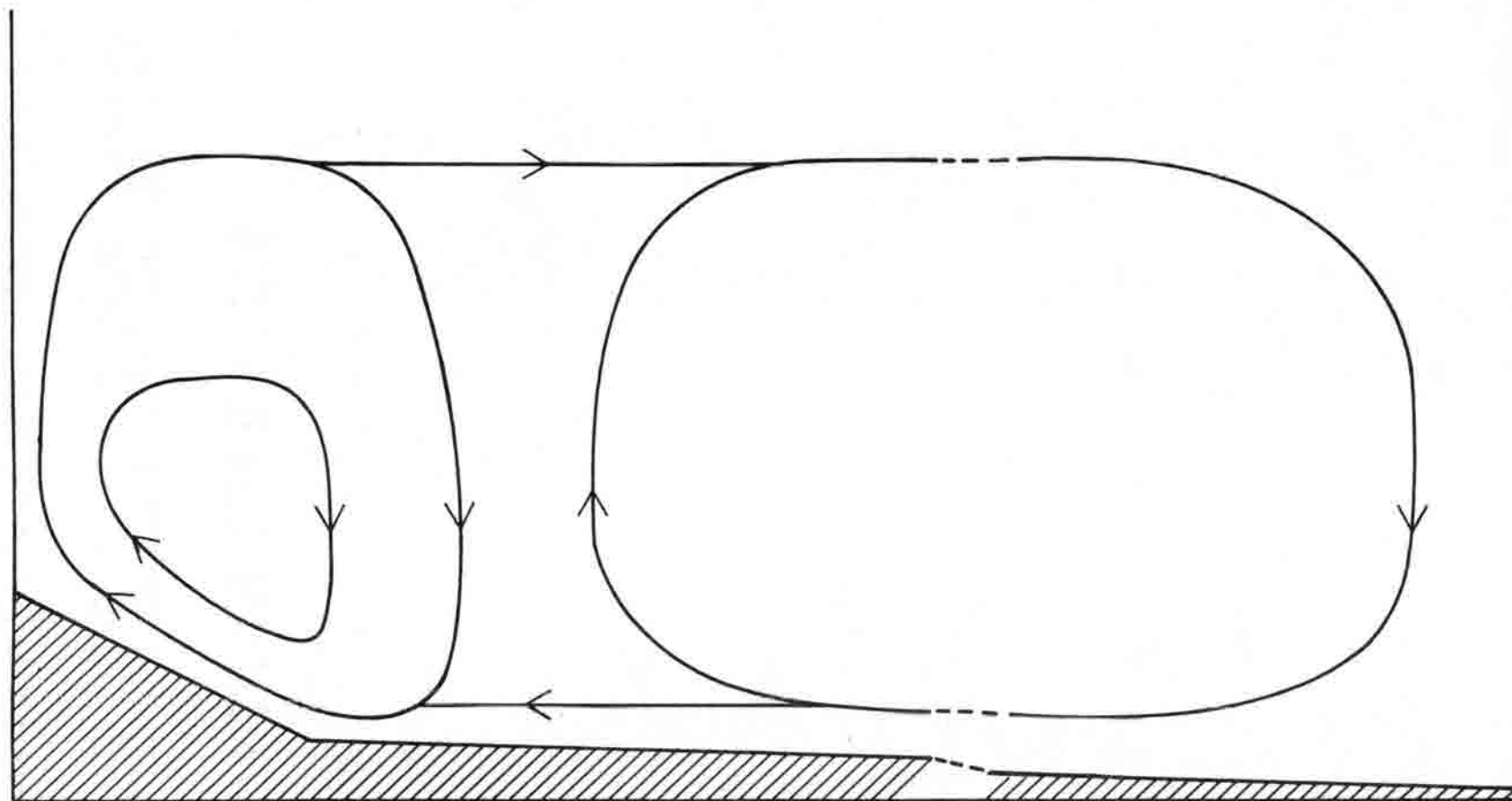


Figure 8.1. Schematic illustration of the idealized Rocky Mountains-Great Plains daytime circulation.

ascending flow was found to be a function of the thermal stability and the ambient wind field. The entire circulation pattern is essentially reversed during the night.

The mountain-plain regional circulation has provided a satisfactory explanation of the zones of enhanced and reduced convection while at the same time providing general applicability throughout a wide range of synoptic conditions. This general applicability was not true of lee wave perturbations and various other mechanisms which were examined. The dearth of observational data on the mesoscale in both space and time limits the direct quantitative verification of this circulation system, however, vertical profiles of the diurnal oscillatory wind fields show reasonably good agreement. The results of weather satellite and radar observations begin to fill the mesoscale data gap and in this case present qualitative evidence for the circulation model.

The further application of this model to other areas is of interest and should serve to evaluate the role of particular topographic and geographic factors. The Rocky Mountains-Plains region of southern Canada provides similar orographic conditions with variations in solar heating and other geographic factors. Hailstorms are common in this area but not tornadoes. The Andes Mountains and the Pampas of Argentina also offer a somewhat similar topographic situation. In both of these cases an extensive sloping plain is coupled with a well-defined longitudinally oriented mountain ridge.

Various modifications of the model are plausible such as extending the mountain ridge to include a broad plateau or a modification to represent more detailed terrain and plain slope features. A major improvement of the model could be made by treating the boundary layer separately with more resolution, possibly in a manner comparable to that used by Estoque (1963), and then

coupling this layer with the larger scale numerical procedure which has been used in Chapter IV.

Numerical simulations of slope circulations in two-dimensional cross sections have been used successfully on the local and convective scale to investigate convective cloud development over mountain peaks. On a somewhat larger scale numerical sea-breeze experiments have also corresponded well with observation. In this study it has been shown that a similar modeling procedure, which couples the effects of a large mountain slope with an extensive slightly sloping plain, may be employed on a regional mountain-plain scale and that this circulation is capable of explaining observed patterns of convective development on this scale.

OLD DEPARTMENT BOND

LITERATURE CITED

- Abdullah, A. J., 1954: The meridional growth of squall lines. Journal of Meteorology, 11, 301-308.
- Arakawa, A., 1966: Computational design for long-term numerical integration of the equations of fluid motion: Two-dimensional incompressible flow. Part I. Journal of Computational Physics, 1, 119-143.
- Asai, T., 1964: Cumulus convection in the atmosphere with vertical wind shear: Numerical experiment. Journal of the Meteorological Society of Japan, 42, 245-259.
- Baer, F., and T. J. Simons, 1968: Computational stability and time truncation of coupled nonlinear equations with exact solutions. Atmospheric Science Paper No. 131, Colorado State University, 43 pp.
- Bates, F. C., 1962: Tornadoes in the central United States. Transactions, Kansas Academy of Science, 65, 215-246.
- \_\_\_\_\_, and C. W. Newton, 1965: The forms of updrafts and downdrafts in cumulonimbus in a sheared environment. Text of talk at National AMS on Cloud Physics and Severe Local Storms, October 1965, Reno, Nevada, 15 pp.
- Beebe, R. G., and F. C. Bates, 1955: A mechanism for assisting in the release of convective instability. Monthly Weather Review, 83, 1-10.
- Bellamy, J. C., 1949: Objective calculations of divergence, vertical velocity and vorticity. Bulletin of the American Meteorological Society, 30, 45-49.
- Blackadar, A. K., 1957: Boundary layer wind maxima and their significance for the growth of nocturnal inversions. Bulletin of the American Meteorological Society, 38, 283-290.
- Bleeker, W., and M. J. Andre, 1951: On the diurnal variation of precipitation, particularly over central U. S. A., and its relation to large-scale orographic circulation systems. Quarterly Journal of the Royal Meteorological Society, 77, 260-271.
- Bolin, B., 1950: On the influence of the earth's orography on the general character of the westerlies. Tellus, 2, 184-195.

- Bonner, W. D., 1963: Thunderstorms and the low-level jet. Meso-meteorology Research Paper No. 22, University of Chicago, 21 pp.
- \_\_\_\_\_, 1965: Statistical and kinematical properties of the low-level jet stream. SMRP Research Paper No. 38, University of Chicago, 55 pp.
- Booker, D. R., 1963: Modification of convective storms by lee waves. Meteorological Monographs, 5(27), Severe Local Storms, American Meteorological Society, Boston, 129-140.
- Braham, R. R., and M. Draginis, 1960: Roots of orographic cumuli. Journal of Meteorology, 17, 214-226.
- Breiland, J. G., 1958: Meteorological conditions associated with the development of instability lines. Journal of Meteorology, 15, 297-302.
- Brunk, I. W., 1949: The pressure pulsation of 11 April 1944. Journal of Meteorology, 6, 181-187.
- \_\_\_\_\_, 1953: Squall lines. Bulletin of the American Meteorological Society, 34, 1-9.
- Buajitti, K., and A. K. Blackadar, 1957: Theoretical studies of diurnal wind structure variations in the planetary boundary layer. Quarterly Journal of the Royal Meteorological Society, 83, 486-500.
- Buettner, K. J. K., and N. Thyer, 1965: Valley winds in the Mount Rainier area. Archiv für Meteorologie, Geophysik und Bioklimatologie, B14, 125-147.
- Burger, A., and E. Ekhardt, 1937: Über die tägliche Zirkulation der Atmosphäre im Bereiche der Alpen. Gerlands Beiträge zur Geophysik, 49, 341-367.
- Chao Jih-Ping, 1962: On the effects of stratification and prevailing wind on the development of small-scale disturbances. Scientia Sinica, 11, 859-872.
- \_\_\_\_\_, and Cheng Li-Shoo, 1966: On the effects of the vertical wind shear on the development and structure of convection. Paper No. 3683, Douglas Aircraft Company, Inc., Santa Monica, California (translated by J. C. Wu and F. W. Murray), 21 pp.

- Charney, J. G. , 1949: On a physical basis for numerical prediction of large-scale motions in the atmosphere. Journal of Meteorology, 6, 371-385.
- \_\_\_\_\_, and A. Eliassen, 1949: A numerical method for predicting the perturbations of the middle latitude westerlies. Tellus, 1, 38-54.
- \_\_\_\_\_, and \_\_\_\_\_, 1964: On the growth of the hurricane depression. Journal of the Atmospheric Sciences, 21, 68-75.
- Courant, R. , K.O. Friedrichs, and H. Lewy, 1928: Über die partiellen Differenzgleichungen der mathematischen Physik. Mathematische Annalen, 100, 32-74.
- \_\_\_\_\_, E. Isaacson, and M. Rees, 1952: On the solution of non-linear hyperbolic differential equations by finite differences. Communications on Pure and Applied Mathematics, 5, 243-255.
- Crow, L. W. , 1969: Relationships between hail and rain in Kansas, Nebraska and Eastern Colorado. Final Report, Contract NSF C-522, 34 pp.
- Crowley, W. P. , 1968: Numerical advection experiments. Monthly Weather Review, 96, 1-11.
- Curtis, R. C. , and H. A. Panofsky, 1958: The relation between large-scale vertical motion and weather in summer. Bulletin of the American Meteorological Society, 39, 521-531.
- Davidson, B. , and S. Jaffe, 1960: Observation and theory of local wind systems. New York University, College of Engineering, Final Report, Contract DA-36-039-sc-78127, 57 pp.
- \_\_\_\_\_, and P. K. Rao, 1958: Preliminary report on valley wind studies in Vermont, 1957. New York University, College of Engineering, Final Report, Contract AF 19(604) 1971, 54 pp.
- Deardorff, J. W. , 1965: A numerical study of pseudo three-dimensional parallel-plate convection. Journal of the Atmospheric Sciences, 22, 419-435.
- \_\_\_\_\_, 1967: Numerical methods for solving the Navier-Stokes and heat conduction equations. Thermal Convection: A Colloquium, NCAR-TN-24, National Center for Atmospheric Research, Boulder, Colorado, 215-226.

- Defant, F. , 1949: Zur Theorie der Hangwinde, nebst Bemerkungen zur Theorie der Berg und Talwinde. Archiv für Meteorologie, Geophysik und Bioklimatologie, A1, 421-450.
- \_\_\_\_\_, 1951: Local winds. Compendium of Meteorology, T. F. Malone, ed. , American Meteorological Society, Boston, 655-672.
- DeMandel, R. E. , and J. R. Scoggins, 1967: Mesoscale wave motions as revealed by improved wind profile measurements. Journal of Applied Meteorology, 6, 617-620.
- Dessens, H. , 1960: Severe hailstorms are associated with very strong winds between 6,000 and 12,000 meters. Physics of Precipitation, Geophysical Monographs No. 5, 333-338.
- Dirks, R. A. , 1969: A climatology of Central Great Plains mesoscale convective systems. Technical Report, Contract E-10-68G, Colorado State University, 60 pp.
- \_\_\_\_\_, J. D. Mahlman, and E. R. Reiter, 1967: Evidence of a mesoscale wave phenomenon in the lee of the Rocky Mountains. Atmospheric Science Paper No. 115, Colorado State University, 50 pp.
- Dutton, J. A. , and G. H. Fichtl, 1969: Approximate equations of motion for gases and liquids. Journal of the Atmospheric Sciences, 26, 241-254.
- Ekhart, E. , 1940: Zum Klima der freien Atmosphäre über USA (I, II, and III). Beiträge zur Physik der freien Atmosphäre, 26, 50-66, 77-106, 210-242.
- Endlich, R. M. , and J. R. Clark, 1963: Objective computation of some meteorological quantities. Journal of Applied Meteorology, 2, 66-81.
- Estoque, M. A. , 1961: A theoretical investigation of the sea breeze. Quarterly Journal of the Royal Meteorological Society, 87, 136-146.
- \_\_\_\_\_, 1962: The sea breeze as a function of the prevailing synoptic situation. Journal of Meteorology, 19, 244-250.
- \_\_\_\_\_, 1963: A numerical model of the atmospheric boundary layer. Journal of Geophysical Research, 68, 1103-1113.

- Fawbush, E. J. , R. C. Miller, and L. G. Starrett, 1951: An empirical method of forecasting tornado development. Bulletin of the American Meteorological Society, 32, 1-9.
- Ferguson, H. L. , 1967: Mathematical and synoptic aspects of a small-scale wave disturbance over the lower Great Lakes area. Journal of Applied Meteorology, 6, 523-529.
- Fisher, E. L. , 1961: A theoretical study of the sea breeze. Journal of Meteorology, 18, 216-233.
- Fjørtoft, R. , 1953: On the changes in the spectral distribution of kinetic energy for two-dimensional nondivergent flow. Tellus, 5, 225-230.
- Fleagle, R. G. , 1950: A theory of air drainage. Journal of Meteorology, 7, 227-232.
- Flohn, H. , 1955: Zur vergleichenden Meteorologie der Hochgebirge. Archiv für Meteorologie, Geophysik und Bioklimatologie, B6, 193-206.
- \_\_\_\_\_, 1968: Contributions to a meteorology of the Tibetan Highlands. Atmospheric Science Paper No. 130, Colorado State University, 120 pp.
- Fosberg, M. A. , 1967: Numerical analysis of convective motions over a mountain ridge. Journal of Applied Meteorology, 6, 889-904.
- \_\_\_\_\_, 1969: An interface model between cloud physics and cloud dynamics--cold orographic clouds. Unpublished Manuscript, 15 pp.
- Fournet, M. J. , 1840: Des brises de jour et de nuit autour des montagnes. Annales de Chimie et de Physique, 74, 337-401.
- Freeman, J. C. , 1948: An analogy between the equatorial easterlies and supersonic gas flows. Journal of Meteorology, 5, 138-146.
- Fujita, T. , 1955: Results of detailed synoptic studies of squall lines. Tellus, 7, 405-436.
- \_\_\_\_\_, 1958: Structure and movement of a dry front. Bulletin of the American Meteorological Society, 39, 574-582.

- Fujita, T., and H. A. Brown, 1958: A study of mesosystems and their radar echoes. Bulletin of the American Meteorological Society, 39, 338-354.
- Fulks, J. R., 1951: The instability line. Compendium of Meteorology, T. F. Malone, ed., American Meteorological Society, Boston, 647-652.
- Gates, W. L., 1959: On the truncation error, stability and convergence of difference solutions of the barotropic vorticity equation. Journal of Meteorology, 16, 556-568.
- Geiger, R., 1959: The Climate Near the Ground. Harvard University Press, Cambridge, 494 pp.
- Godske, C. L., T. Bergeron, J. Bjerknes, and R. C. Bundgaard, 1957: Dynamic Meteorology and Weather Forecasting. American Meteorological Society, Boston, and Carnegie Institution, Washington, D. C., 800 pp.
- Goldie, A. H. R., 1925: Waves at an approximately horizontal surface in the atmosphere. Quarterly Journal of the Royal Meteorological Society, 51, 239-246.
- Gossard, E., and W. Munk, 1954: On gravity waves in the atmosphere. Journal of Meteorology, 11, 259-269.
- Gray, W. M., 1967: Global view of the origin of tropical disturbances and storms. Atmospheric Science Paper No. 114, Colorado State University, 105 pp.
- Hann, J. v., 1879: Zur Theorie der Berg- und Thalwinde. Zeitschrift öst. Ges. Meteorologie, 14, 444-448.
- \_\_\_\_\_, 1919: Über die Theorie der Berg- und Talwinde. Meteorologische Zeitschrift, 36, 287-289.
- Hänsel, C., 1962: Die Unterschiede von Temperatur und Relativer Feuchtigkeit zwischen Brocken und umgebender freier Atmosphäre. Zeitschrift für Meteorologie, 16, 248-252.
- Haurwitz, B., 1947: Internal waves in the atmosphere and convection patterns. Annals of the New York Academy of Sciences, 48, 727-748.
- \_\_\_\_\_, 1962: Thermally driven circulations. Beiträge zur Physik der Atmosphäre, 35, 145-159.

- Hering, W. S. , and T. R. Borden, Jr. , 1962: Diurnal variations in the summer wind field over the central United States. Journal of the Atmospheric Sciences, 19, 81-86.
- Hess, S. L. , and H. Wagner, 1948: Atmospheric waves in the north-western United States. Journal of Meteorology, 5, 1-19.
- Hines, C. O. , 1960: Internal atmospheric gravity waves at ionospheric heights. Canadian Journal of Physics, 38, 1441-1481.
- \_\_\_\_\_, 1963: The upper atmosphere in motion. Quarterly Journal of the Royal Meteorological Society, 89, 1-42.
- Hodges, H. , 1959: Synoptic patterns associated with hail occurrence in northeastern Colorado. National Science Foundation Research Participation Report (unpublished). CER59HH29, Colorado State University, 77 pp.
- Holton, J. R. , 1967: The diurnal boundary layer wind oscillation above sloping terrain. Tellus, 19, 199-205.
- Hosler, C. L. , L. G. Davis, and D. R. Booker, 1963: Modification of convective systems by terrain with local relief of several hundred meters. Journal of Applied Mathematics and Physics, 14, 410-419.
- Hydrometeorological Report, 1947: Thunderstorm Rainfall. Report No. 5.
- Jeffreys, H. , 1922: On the dynamics of wind. Quarterly Journal of the Royal Meteorological Society, 48, 29-47.
- Jehn, K. H. , and J. R. Gerhardt, 1950: A preliminary study of the eddy transfer of heat near the earth's surface. Journal of Meteorology, 7, 343-346.
- Kochanski, A. , 1964: Atmospheric motions from sodium cloud drifts. Journal of Geophysical Research, 69, 3651-3662.
- Kraichnan, R. H. , 1967: Inertial ranges in two-dimensional turbulence. The Physics of Fluids, 10, 1417-1423.
- Kuo, H. L. , 1963: Perturbations of plane couette flow in stratified fluid and origin of cloud streets. The Physics of Fluids, 6, 195-211.

- Lavoie, R. L., 1968: A mesoscale numerical model and lake-effect storms. Ph. D. Dissertation, The Pennsylvania State University, 102 pp.
- Lax, P. D., and B. Wendroff, 1960: Systems of conservation laws. Communications on Pure and Applied Mathematics, 13, 217-237.
- Lettau, H. H., 1966: A case study of katabatic flow on the South Polar plateau. Studies in Antarctic Meteorology, Antarctic Research Series Vol. 9, American Geophysical Union, 1-11.
- \_\_\_\_\_, 1967: Small to large-scale features of boundary layer structure over mountain slopes. Atmospheric Science Paper No. 122, (Proceedings of the Symposium on Mountain Meteorology, edited by E. R. Reiter and J. L. Rasmussen), Colorado State University, 1-74.
- \_\_\_\_\_, and W. Schwerdtfeger, 1967: Dynamics of the surface-wind regime over the interior of Antarctica. Antarctic Journal, 2, 155-158.
- Lilly, D. K., 1960: On the theory of disturbances in a conditionally unstable atmosphere. Monthly Weather Review, 88, 1-17.
- \_\_\_\_\_, 1962: On the numerical simulation of buoyant convection. Tellus, 14, 148-172.
- \_\_\_\_\_, 1964: Numerical solution of the shape-preserving two-dimensional thermal convective element. Journal of the Atmospheric Sciences, 21, 83-98.
- \_\_\_\_\_, 1965: On the computational stability of numerical solutions of time-dependent non-linear geophysical fluid dynamics problems. Monthly Weather Review, 93, 11-25.
- McClain, E. P., 1960: Some effects of the western cordillera of North America on cyclonic activity. Journal of Meteorology, 17, 104-115.
- McGuire, E. L., 1962: The vertical structure of three dry lines as revealed by aircraft traverses. National Severe Storms Project Report No. 7, 10 pp.
- McRae, J. N., and J. J. McGann, 1965: Periodic fluctuations in wind, pressure and temperature at Port Hedland. Australian Meteorological Magazine, 48, 1-7.

- Magata, M., 1965: A study of the sea breeze by the numerical experiment. Papers in Meteorology and Geophysics, 16, 23-37.
- \_\_\_\_\_, and S. Ogura, 1967: On the airflow over mountains under the influence of heating and cooling. Journal of the Meteorological Society of Japan, 45, 83-95.
- Malkus, J. S., 1955: The effects of a large island upon the trade wind air stream. Quarterly Journal of the Royal Meteorological Society, 81, 538-550.
- \_\_\_\_\_, and G. Witt, 1959: The evolution of a convective element: A numerical calculation. The Atmosphere and the Sea in Motion, The Rockefeller Institute Press, New York, 425-439.
- Mantis, H. T., 1960: On a diurnal variation of stratospheric winds. Journal of Meteorology, 17, 465-468.
- Means, L. L., 1952: On thunderstorm forecasting in the central United States. Monthly Weather Review, 80, 165-189.
- Molenkamp, C. R., 1968: Accuracy of finite-difference methods applied to the advection equation. Journal of Applied Meteorology, 7, 160-167.
- Murakami, T., R. V. Godbole, and R. R. Kelkar, 1969: Numerical simulation of the monsoon along 80°E. Unpublished Manuscript, 24 pp.
- Musil, D. J., and A. S. Dennis, 1968: Convective storms of 1966 and 1967 in western Nebraska. Report 68-7, Institute of Atmospheric Sciences, South Dakota School of Mines and Technology, 27 pp.
- Neiburger, M., and J. K. Angell, 1956: Meteorological applications of constant-pressure balloon trajectories. Journal of Meteorology, 13, 166-194.
- Newell, R. E., J. R. Mahoney, and R. W. Lenhard, 1966: A pilot study of small scale wind variations in the stratosphere and mesosphere. Quarterly Journal of the Royal Meteorological Society, 92, 41-54.
- Newton, C. W., 1956: Mechanisms of circulation change during a lee cyclogenesis. Journal of Meteorology, 13, 528-539.
- \_\_\_\_\_, 1963: Dynamics of severe convective storms. Meteorological Monographs, 5(27), Severe Local Storms, American Meteorological Society, Boston, 33-58.

- Newton, C.W., and H.R. Newton, 1959: Dynamical interactions between large convective clouds and environment with vertical shear. Journal of Meteorology, 16, 483-496.
- Nickerson, E. C., 1965: A numerical experiment in buoyant convection involving the use of a heat source. Journal of the Atmospheric Sciences, 22, 412-418.
- Nitta, T., 1962: The outflow boundary condition in numerical time integration of advective equations. Journal of the Meteorological Society of Japan, 40, 13-24.
- Ogura, Y., 1963: The evolution of a moist convective element in a shallow, conditionally unstable atmosphere: A numerical calculation. Journal of the Atmospheric Sciences, 20, 407-424.
- \_\_\_\_\_, and J. G. Charney, 1962: A numerical model of thermal convection in the atmosphere. Proceedings of the International Symposium on Numerical Weather Prediction in Tokyo, Meteorological Society of Japan, 431-451.
- \_\_\_\_\_, and N. A. Phillips, 1962: Scale analysis of deep and shallow convection in the atmosphere. Journal of the Atmospheric Sciences, 19, 173-179.
- Orville, H. D., 1964: On mountain upslope winds. Journal of the Atmospheric Sciences, 21, 622-633.
- \_\_\_\_\_, 1965: A numerical study of the initiation of cumulus clouds over mountainous terrain. Journal of the Atmospheric Sciences, 22, 684-699.
- \_\_\_\_\_, 1967: The numerical modeling of mountain upslope winds and cumulus clouds. Report 67-2, Institute of Atmospheric Sciences, South Dakota School of Mines and Technology, 66 pp.
- \_\_\_\_\_, 1968a: Ambient wind effects on the initiation and development of cumulus clouds over mountains. Journal of the Atmospheric Sciences, 25, 385-403.
- \_\_\_\_\_, 1968b: Notes and correspondence. Journal of Applied Meteorology, 7, 938.
- Pasquill, F., 1962: Atmospheric Diffusion. Van Nostrand, Princeton, New Jersey, 297 pp.

- Pearce, R. P. , 1955: The calculation of the sea breeze circulation in terms of the differential heating across the coast line. Quarterly Journal of the Royal Meteorological Society, 81, 351-331.
- Phillips, N. A. , 1967: The Boussinesq approximation. Thermal Convection: A Colloquium, NCAR-TN-24, National Center for Atmospheric Research, Boulder, Colorado, 23-36.
- Pitchford, K. L. , and J. London, 1962: The low-level jet as related to nocturnal thunderstorms over midwest United States. Journal of Applied Meteorology, 1, 43-47.
- Porter, J. M. , L. L. Means, J. E. Hovde and W. B. Chappell, 1955: A synoptic study on the formation of squall lines in the north central United States. Bulletin of the American Meteorological Society, 36, 390-396.
- Pothecary, J. J. W. , 1954: Short-period variations in surface pressure and wind. Quarterly Journal of the Royal Meteorological Society, 80, 395-401.
- Prandtl, L. , 1942: Führer durch die Strömungslehre. Vieweg und Sohn, Braunschweig, 382 pp.
- Queney, P. , 1947: Theory of perturbations in stratified currents with applications to airflow over mountain barriers. Miscellaneous Reports No. 23, The University of Chicago Press, 81 pp.
- \_\_\_\_\_, 1948: The problem of air flow over mountains: A summary of theoretical studies. Bulletin of the American Meteorological Society, 29, 16-26.
- Ratner, B. , 1961: Do high-speed winds aloft influence the occurrence of hail? Bulletin of the American Meteorological Society, 42, 443-446.
- Reiter, E. R. , D. W. Beran, J. D. Mahlman, and G. Wooldridge, 1965: Effect of large mountain ranges on atmospheric flow patterns as seen from TIROS satellites. Atmospheric Science Technical Paper No. 69, Colorado State University, 1-86.
- Renné, D. S. , 1969: Stability and dynamic processes in the formation of high plains hailstorms. Atmospheric Science Paper No. 136, Colorado State University, 53 pp.
- Richardson, L. F. , 1926: Atmospheric diffusion shown on a distance-neighbour graph. Proceedings of the Royal Society, A, 110, 709-737.

- Richtmyer, R. D. , 1957: Difference Methods for Initial Value Problems. Interscience Tracts in Pure and Applied Mathematics, No. 4, Wiley (Interscience), New York, 238 pp.
- \_\_\_\_\_, 1963: A survey of difference methods for non-steady fluid dynamics. NCAR Technical Notes 63-2, National Center for Atmospheric Research, Boulder, Colorado, 25 pp.
- Roberts, K. V. , and N. O. Weiss, 1966: Convective difference schemes. Mathematics of Computations, 20, 272-299.
- Samson, C. A. , 1965: A comparison of mountain slope and radiosonde observations. Monthly Weather Review, 93, 327-330.
- Sangster, W. E. , 1967: Diurnal surface geostrophic wind variations over the Great Plains. Central Region Technical Memorandum 13, U. S. Weather Bureau, Kansas City, Missouri, 16 pp.
- Sasaki, Y. , 1959: A numerical experiment of squall-line formation. Journal of Meteorology, 16, 347-353.
- Sawyer, J. S. , 1959: The introduction of the effects of topography into methods of numerical forecasting. Quarterly Journal of the Royal Meteorological Society, 85, 31-43.
- \_\_\_\_\_, 1961: Quasi-periodic wind variations with height in the lower stratosphere. Quarterly Journal of the Royal Meteorological Society, 87, 24-33.
- Scorer, R. S. , 1949: Theory of airflow over mountains. Quarterly Journal of the Royal Meteorological Society, 75, 41-56. ✓
- \_\_\_\_\_, 1953: Theory of airflow over mountains: II. The flow over a ridge. Quarterly Journal of the Royal Meteorological Society, 79, 70-83. ✓
- \_\_\_\_\_, 1955: Theory of airflow over mountains: IV. Separation of flow from the surface. Quarterly Journal of the Royal Meteorological Society, 81, 340-350. ✓
- Silverman, B. A. , 1960: The effect of a mountain on convection. Cumulus Dynamics, C. E. Anderson, ed. , Pergamon Press, New York, 4-27. ✓
- Skaggs, R. H. , 1967: On the association between tornadoes and 500 mb indicators of jet streams. Monthly Weather Review, 95, 107-110.

- Spiegel, E. A. , and G. Veronis, 1960: On the Boussinesq approximation for a compressible fluid. The Astrophysical Journal, 131, 442-447.
- Sterten, A. K. , and J. Knudsen, 1961: Local and synoptic meteorological investigations of the mountain and valley wind system. Final Report, Forsvarets Forskningsinstitut, Agreement N-03-MWP-A-59, Kjeller-Lillestrøm, Norway, 139 pp.
- Sullivan, W. G. , Jr. , and J. O. Severson, 1966: A study of summer showers over the Colorado mountains. Central Region Technical Memoranda 2 and 3, U. S. Weather Bureau, Kansas City, Missouri, 7 pp.
- Sutton, O. G. , 1953: Micrometeorology. McGraw-Hill Book Company, Inc. , New York, 333 pp.
- Tepper, M. , 1950: A proposed mechanism of squall lines: The pressure jump line. Journal of Meteorology, 7, 21-29.
- \_\_\_\_\_ , 1952: The application of the hydraulic analogy to certain atmospheric flow problems. Research Paper No. 35, U. S. Weather Bureau, Washington, D. C. , 50 pp.
- Thompson, P. D. , 1961: Numerical Weather Analysis and Prediction. The MacMillan Company, New York, 170 pp.
- Thyer, N. H. , 1966: A theoretical explanation of mountain and valley winds by a numerical method. Archiv für Meteorologie, Geophysik und Bioklimatologie, A15, 318-348.
- \_\_\_\_\_ , and K. J. K. Buettner, 1962: Part A: On valley and mountain winds III; Part B: Valley wind theory. University of Washington, Final Report, Contract AF 19(604)-7201, 203 pp.
- Townsend, A. A. , 1965: Excitation of internal waves by a turbulent boundary layer. Journal of Fluid Mechanics, 22, 241-252.
- U. S. Department of Commerce, Weather Bureau: Colorado map of normal May-September precipitation, 1931-1960. Available from Colorado Water Conservation Board, Denver, Colorado.
- Vulfson, N. I. , 1964: Convective Motions in a Free Atmosphere. Translated from Russian, Israel Program for Scientific Translations, Jerusalem, 188 pp.

- Wagner, A., 1932: Neue Theorie des Berg- und Talwindes. Meteorologische Zeitschrift, 49, 329-341.
- \_\_\_\_\_, 1938: Theorie und Beobachtung der periodischen Gebirgswinde. Gerlands Beiträge zur Geophysik, 52, 408-449.
- \_\_\_\_\_, 1939: Über die Tageswinde in der freien Atmosphäre. Beiträge zur Physik der freien Atmosphäre, 25, 145-170.
- Wallace, J. M., and F. R. Hartranft, 1969: Diurnal wind variations, surface to 30 kilometers. Monthly Weather Review, 97, 446-455.
- Wenger, R., 1923: Zur Theorie der Berg- und Talwinde. Meteorologische Zeitschrift, 40, 193-204.
- Williams, D. T., 1953: Pressure wave observations in the central midwest, 1952: Monthly Weather Review, 81, 278-289
- Wong, E. Y. J., and K. C. Brundidge, 1966: Vertical and temporal distributions of the heat conductivity and flux. Journal of the Atmospheric Sciences, 23, 167-178.
- Wooldridge, G., and P. F. Lester, 1969: Detailed observations of mountain lee waves and a comparison with theory. Atmospheric Science Paper No. 138, Colorado State University, 87 pp.
- Young, J. A., 1968: Comparative properties of some time differencing schemes for linear and nonlinear oscillations. Monthly Weather Review, 96, 357-364.

APPENDIX: MESOSCALE WAVE APPLICATION

The theoretical formulation for a mesoscale wave phenomenon has been developed in a previous publication (Dirks et al., 1967) and will not be repeated here. By employing linearization methods an equation is obtained for the stationary wavelength (L),

$$L = \frac{2\pi}{f} \left[ \frac{\bar{u} [\bar{u}^{-2} n (n + \frac{\partial \bar{\ell} n \rho}{\partial z}) - \bar{u} n \frac{\partial \bar{u}}{\partial z} + \frac{g}{T} (\frac{\partial \bar{T}}{\partial z} + \frac{g}{c_p})]}{(n + \frac{\partial \bar{\ell} n \rho}{\partial z}) (\bar{u} n - \frac{\partial \bar{u}}{\partial z}) - \frac{\bar{u} n}{T} (\frac{\partial \bar{T}}{\partial z} + \frac{g}{c_p})} \right]^{1/2}$$

where n is a vertical damping coefficient for which a value of  $-3 \times 10^{-4} \text{ m}^{-1}$  has been estimated and all other symbols have their standard meaning. The term  $\frac{\partial \bar{\ell} n \rho}{\partial z}$  arises from the retention of vertical density advection in the continuity equation; a value of  $-1 \times 10^{-4} \text{ m}^{-1}$  was estimated for this term.

Data from soundings prior to (1200 GMT) and following (0000 GMT) the formation of meso-systems were substituted into the above wavelength equation at select stations over the Western Plains. The various input parameters were determined between the surface (or top of the surface inversion) and a mid-tropospheric level which was frequently at the base of the temperature inversion observed between 500 and 600 mb (or arbitrarily at 500 mb when no inversion was present). Only the westerly component of the wind was used ( $\bar{u}$ ), and vertical wind shears ( $\partial \bar{u} / \partial z$ ) and temperature lapse rates ( $\partial \bar{T} / \partial z$ ) were estimated by the best linear fit for the entire layer. Results of the stationary wavelength computations are shown in the table which follows.

TABLE A. 1. Estimated theoretical and observed mesoscale wavelengths (in kilometers) for select days during summer 1966. (Observed estimates were made from satellite photographs and radar observations.)

Date	Time (GMT)	Theoretical Wavelength (by station)						Observed Wavelength	
6 June	1200	DEN	1700	DDC	1900	LBF	1000	500, 700	
7 June	0000								1300
7 June	1200	DEN	1050	DDC	1200	ABQ	1600	1700	650
8 June	0000								
18 June	1200	DEN	1100	DDC	1600	ABQ	1400	1800	450
19 June	0000								
21 June	1200	DEN	1100	ABQ	1250	AMA	2300	450	
22 June	0000								1100
27 June	1200	DEN	4600	DDC	1600	AMA	7250	350, 600	
28 June	0000								1700
1 July	1200	DEN	1450	DDC	2250	LBF	2000	500	
2 July	0000								1500
2 July	1200	DEN	1700	LBF	1700	ABQ	1100	2700	400, 550
3 July	0000								
26 July	1200	DEN	1100	DDC	1900	LBF	800	750	
27 July	0000								
5 Aug.	1200	DEN	1600	DDC	2250	ABQ	1300	5600	600
6 Aug.	0000								
20 Aug.	1200	DEN	1200	DDC	2900	ABQ	2000	3000	400, 600
21 Aug.	0000								